ResearchOnline@JCU

JAMES COOK UNIVERSITY AUSTRALIA

This file is part of the following work:

Campbell, Graeme Robert (2007) ***A rheological study of ammonium phosphate slurries.*** **PhD Thesis, James Cook University.**

Access to this file is available from:

https://doi.org/10.25903/hynf%2Dw138

Copyright © 2007 Graeme Robert Campbell

The author has certified to JCU that they have made a reasonable effort to gain permission and acknowledge the owners of any third party copyright material included in this document. If you believe that this is not the case, please email researchonline@jcu.edu.au

A RHEOLOGICAL STUDY OF AMMONIUM PHOSPHATE SLURRIES

Thesis Submitted by
Graeme Robert CAMPBELL
In August 2007

For the Degree of Doctor of Philosophy
In the School of Engineering
James Cook University

STATEMENT OF ACCESS

I, the undersigned, author of this work, understand that James Cook University will make this thesis available for use within the University Library and, via the Australian Digital Theses network, for use elsewhere.

I understand that, as an unpublished work, a thesis has significant protection under the Copyright Act and I do not wish to place any further restriction on access to this work.

_____ _____

Graeme Campbell Date

STATEMENT OF SOURCES

DECLARATION

I declare that this thesis is my own work and has not been submitted in any form for another degree or diploma at any university or other institution of tertiary education. Information derived from the published or unpublished work of others has been acknowledged in the text and a list of references is given.

_____ _____

Graeme Campbell Date

ACKNOWLEDGEMENTS

I would like to express my gratitude to the following people who have contributed to the completion of this thesis:

- Dr Yee Kwong Leong, for his role as primary supervisor. Dr Leong has been a generous source of knowledge, expertise and support. He has been instrumental in guiding and assisting me to complete this project.

- Dr Jong-Leng Liow and Gerrie Du Plessis for their roles as secondary supervisors. Dr Liow assisted with the CFD section of this document and also took over the role of primary supervisor after Dr Leong's departure.

- Dr Madoc Sheehan who took on primary supervisor responsibilities at the end of the project. Dr Sheehan provided valuable assistance in editing the final version of the document.

- Dr Chris Berndt who has assisted in the formulation of the thesis document and provided guidance and motivation towards its completion.

- Danielle Garner, Steve Thatcher, Daina Tamasauskas, Nick Olsen, Kobus Kirsten and Pieter Haverkamp, all of whom held, in succession, the position of Technical Superintendent at Phosphate Hill. Also, the various members of the laboratory staff, operations and technical team at Phosphate Hill that assisted me over the years.

- WMC and the ARC for providing research funding as well as a generous scholarship.

Most importantly, to my wife, Rachael, I owe you the most in helping me complete this document. You have spent countless hours supporting me in the times I needed it most and I will always be grateful to you.

PUBLICATIONS

The following publications have been produced during the course of this work:

Campbell G.R., Leong Y.K. and Yeow Y.L., "Obtaining The Shear Stress Shear Rate Relationship and Yield Stress of Liquid Foods from Parallel Disk Data." *J. Food Sci.* **70** (2005) E50-55.

Campbell G.R., Leong Y.K., Berndt C.C. and Liow J.L., "Ammonium Phosphate Slurry Rheology and Particle Properties - The influence of Fe(III) and Al(III) impurities, solid concentration and degree of neutralization", *Chem Eng Sci*, **61** (2006) 5856-5866.

Leong YK, Sganzerla M, Berndt CC and Campbell GR, "Metal ions Solubility in Plant Phosphoric acid – degree of ammonia neutralization and temperature effects", *Ind. Eng. Chem. Res.* (2008) – in press.

ABSTRACT

Phosphate Hill is a mine site located in North West Queensland. At the site, mined phosphoric rock is reacted with sulphuric acid to produce phosphoric acid. The phosphoric acid is combined with ammonia in a reactor known as the pre-neutraliser. The reaction forms a very hot and viscous slurry which is later further ammoniated in a cylindrical vessel known as a granulator, to produce solid fertiliser granules of mono-ammonium phosphate (MAP) or di-ammonium phosphate (DAP). Two important parameters used in the processing of ammonium phosphate slurries are the nitrogen to phosphorous mole ratio (MR) and the specific gravity (SG). Both of these parameters can affect the rheology of the slurry produced inside the reactor. The impurities carried over in the phosphoric acid from the reaction with the phosphate rock can also have significant effects on the rheology of the slurry. The objective of this study was to examine the rheological characteristics of the ammonium phosphate slurries formed in the pre-neutraliser (PN) and determine how the viscosity changes with mole ratio, impurity composition and specific gravity.

There is a lot of variability in the literature on the rheology of ammonium phosphate slurries. Previous work did not take into account the non-Newtonian nature of the slurry, whilst also basing their findings on plant based measurements, where proper control of the slurry properties would have been difficult. A bulk quantity of phosphoric acid was collected from Phosphate Hill and used as a baseline for testing the effect of adding impurities. Laboratory grade $FePO_4$, $AlPO_4$ and $Mg_3(PO_4)_2$ were added to the plant acid to form acids of varying impurity content. Further to the viscosity experiments, work was conducted to determine the slurry particle size, chemical composition (by XRD/XRF analysis), solubility of precipitates and physical characteristics, in an attempt to explain the mechanisms behind the observed viscosity changes. Testing the viscosity of ammonium phosphate slurry was found to be very time consuming and problematic. The experimental work was complicated by a multitude of factors, including high temperatures, slow reaction and evaporation times, the precipitation of impurities and the solidification of the slurry.

The trend in the viscosity with mole ratio for the as-received acid was similar to that seen in the literature. The addition of both aluminium and iron caused an increase in the viscosity around the MAP minimum solubility point of 0.9 MR. In both cases, the formation of hydrolysis products were shown to have reduced the particle size of the precipitating ammonium phosphate crystals, thus increasing the viscosity. As the mole ratio is increased, mono-ammonium phosphate combines with the additional ammonia to form di-ammonium phosphate. The hydrolysis products for iron also changed at the same time and the resultant slurry formed particles with high interparticle attractive forces which in turn formed a flocculated suspension. Increasing the iron content not only increased the viscosity in this region, but also lowered the mole ratio whereby the increase in viscosity is seen to occur. An increase in the aluminium content had no effect on the viscosity at higher mole ratios. Based on the findings, it is recommended that slurries containing high iron be preferentially processed to make mono-ammonium phosphate and slurries with high aluminium be preferentially processed to make di-ammonium phosphate.

Computational Fluid Dynamics (CFD) modelling was conducted on the mixing dynamics of the PN vessel. The CFD model showed that the upper region of the vessel was the least well mixed. The potential for stagnation of the flow field and subsequent solidification increases when the viscosity of the slurry also increases. To counteract this threat, the volume of slurry in the reactor must be decreased, or the agitation speed increased. The most effective method to ensure proper mixing dynamics in the vessel was to lower the viscosity, by preferentially processing each slurry by its impurity content as mentioned above.

SUMMARY

Phosphate Hill is a mine site located 180km south-east of Mt Isa in a remote area of North West Queensland. Situated on a large deposit of high quality phosphate rock, the mine combines ammonia, which it produces from natural gas, with phosphoric acid to produce ammonium phosphate fertiliser. The ammonium and the phosphoric acid are first mixed together in a vessel known as the pre-neutraliser (PN). Neutralisation is the term used to describe when enough ammonia is reacted with the phosphoric acid to produce and solidify out mono-ammonium phosphate (MAP) or di-ammonium phosphate (DAP), the two main fertiliser products of the mine. This study is concerned with characterising the rheological properties of the slurry produced within the PN, so as to determine methods to enhance the mixing dynamics of the vessel and increase product throughput.

The literature survey revealed that phosphoric acid impurities such as iron, aluminium, magnesium and fluorine were primarily thought to be responsible for changes in the pre-neutraliser slurry viscosity. Ando and Akiyama (1972) claimed that high $F:R_2O_3$ (where R is Al or Fe) ratios led to the formation of small colloidal crystals that increased the viscosity. However, Achorn et al. (1980) claimed that crystals formed in a slurry with high $F:R_2O_3$ ratio were coarser than those with lower levels of fluorine. Handley (1984) stated that fluorine was beneficial to lowering slurry viscosity, but did not compare his results to the R_2O_3 content. All three had differing opinions in respect to the extent that iron, aluminium and magnesium had in altering the slurry viscosity. Other literature focused on single viscosity measures using plant, or pilot plant based experiments, where accurately determining specific gravity and mole ratio would have been difficult. Leong (2002) demonstrated that large changes in the viscosity could occur with small changes in specific gravity or temperature. Making conclusions about the effects of impurities on viscosity is difficult without controlled and documented conditions. In order to properly characterise the rheological behaviour of ammonium phosphate slurries, comprehensive laboratory controlled experiments are required.

Laboratory testing of the viscosity of ammonium phosphate slurry appears to be a straight forward process. However, it has been found to be very time consuming and problematic as there was no previously established procedure for conducting such a test. The experimental work was complicated by a multitude of factors. These included high temperatures, slow reaction and evaporation times, the precipitation of impurities and the solidification of the slurry, as well as delays in determining the mole ratio of the slurry.

The phosphoric acid used was collected from the 40% acid tanks at the plant and contained some suspended solids. The as-received acid was designated DAP1 and all samples were collected at the same time from the same sample location in the plant. $FePO_4$, $AlPO_4$ and $Mg_3(PO_4)_2$ were dissolved in DAP1 to produce acids with different impurity contents. The DAP1 acid was used as a baseline to compare the changes in viscosity with varying impurity content.

Ammonia gas was bubbled through a continuously stirred solution of phosphoric acid in an 800 ml beaker until the desired mole ratio is reached. A sub-sample was then poured into a test tube, which was weighed to determine the specific gravity. The slurry was heated on a hot plate with stirring to evaporate water, increasing the specific gravity. The specific gravity of slurry is directly related to the free moisture content in the slurry at given mole ratio. Sub-samples were taken from the beaker periodically in clean test tubes until the slurry became too viscous to pour into the test tube. The reaction was highly exothermic, so the ammonia addition rate was controlled to ensure that the reaction stayed close to the boiling point of the liquid (110-120^{o}C). Sub-samples were placed in a hot oil bath for several minutes, until the temperature was maintained at 110^{o}C, ensuring that the viscosity was always measured at the same temperature. The rheology of the slurry was measured with a Brookfield LVDV-II+ viscometer using a concentric cylinder geometry with the cylindrical test-tube being the outer cylinder.

At low specific gravity (1.4), the flow behaviour was observed to be Newtonian in the range of shear rate characterised (10-100 s^{-1}). The slurry displayed non-Newtonian shear thinning behaviour at higher specific gravity (1.6). This was reflected by a

decreasing viscosity with increasing shear rate. The viscosity versus shear rate plot on a log-log scale was found to be linear, so the flow behaviour was reasonably well represented by a power law model. The viscosity was found to increase exponentially with increasing slurry specific gravity (or decreasing water content of the slurry).

The DAP1 plant acid slurry viscosity versus mole ratio trend compared favourably to the literature. Both Ando and Akiyama (1972) and Tang et al. (2004) showed trends with a peak in the viscosity occurring at 0.8-0.9 MR as with the DAP1 data. This was unexpected because the minimum solubility point of MAP occurs at 1.0 MR. Maximum solids content should coincide with the maximum viscosity. Compared to DAP1, the slurries containing additional iron showed increases in the maximum viscosity of the peak occurring at 0.9 MR and also increased viscosity above 1.2 MR. It was concluded that iron has a more significant effect on the viscosity during the production of di-ammonium phosphate, where the mole ratio in the pre-neutraliser is typically 1.55-1.60. During production of mono-ammonium phosphate, where the slurry mole ratio is typically 0.65-0.7, the iron content does appear to have an influence on the viscosity; however the measured viscosity was around an order of magnitude lower for the same specific gravity and shear rate, compared to that during di-ammonium phosphate production. In conclusion, ore with high iron content can be more effectively processed under MAP conditions than under DAP conditions.

The slurries containing additional aluminium showed an increase in the measured viscosity across all mole ratios below 1.3 MR. Above 1.4 MR the viscosity shows no significant change and may in fact decrease with increased aluminium content. This observation would lead us to believe that slurries containing high aluminium content should not be processed under MAP conditions. Under DAP conditions the aluminium content appears to have no effect on the viscosity. The measured viscosity of slurries containing the additional magnesium was irregular and trends were inconclusive with respect to viscosity and mole ratio.

Interestingly, the shape of the viscosity versus mole ratio curves were different for aluminium and iron. In the literature, aluminium and iron are commonly referred to together as R_2O_3, where R can be either Fe or Al. Therefore, it was assumed that the

effect of altering the concentration of either would be similar. Instead, the effects of these impurities were found to be significantly different. Iron increased the peak of the viscosity at 0.9 MR, while aluminium had a significant affect on broadening the peak, particularly above 0.9 MR. Iron increased the viscosity in the higher mole ratio range, above 1.4 MR, whilst aluminium had no real effect in this range. This suggests that combined high iron and high aluminium ores will be problematic to process at any mole ratio.

The titration method used to determine the mole ratio was found to be erroneous. The sulphate content of the acid affects the titration calculation, reporting a lower N:P mole ratio. The titration method was found to return the N:(P + 2S) mole ratio below 1.0 MR and the N:(P + S) mole ratio at higher mole ratios. Therefore, the peak in the viscosity that was observed at 0.8-0.9 MR instead occurred at closer to 1.0 N:P MR. The viscosity increase results from the precipitation of mono-ammonium phosphate.

The precipitation of ammonium phosphate solids, for slurries made from pure phosphoric acid with added metal ions, began at MR ~0.6 (pH ~2) for Fe(III), 0.85 (pH~3.5) for Al (III) and 1.3 (pH~7) for Mg(II). At the same mole ratio, the respective metal ions also formed hydrolysis products (Baes and Mesmer 1986), indicating that hydrolysis products are required to initiate solids formation. The hydrolysis products formed very small particles that act as nucleation sites for crystallization and have been shown to hinder crystal size growth. Aluminium based slurries had the smallest particle size, followed by iron and magnesium. Ammonium phosphate slurry made from pure phosphoric acid had large soluble particles (1-2 mm in size). Aluminium and iron based slurries did not have any of these large inter-dispersed ammonium phosphate crystals, whilst magnesium slurries did. However, magnesium did not form hydrolysis products below 1.25 MR and so large ammonium phosphate crystals were able to form.

Adsorbed hydrolysis products may give rise to a range of interparticle forces in slurry such as bridging, charged patch and enhanced van der Waals attraction (Leong 2005). These forces will have a significant effect on slurry rheology. Slurries containing iron were observed to form strong interparticle forces above 1.4 MR, at the same time as

the viscosity increased. The interparticle forces are demonstrated by adding 30 ml of the slurry to 500 ml of water. Slurries below 1.4 MR settled to the base of the beaker. Slurries above 1.4 MR formed a flocculated suspension that occupied almost all of the 500 ml solution. Ammonium phosphate slurries were generally white in colour. The increased interparticle forces for slurries with high iron content above 1.4 MR corresponded to a change in the slurry colour to yellow. The principle iron hydrolysis products in solution change between 1.3-1.5 MR, indicating that the viscosity increase is related to the hydrolysis products.

Computational Fluid Dynamics (CFD) modelling was conducted on the mixing dynamics of the PN vessel. The CFD model was validated by injecting a LiCl tracer into the PN vessel and comparing the residence time distribution of the simulated and experimental results. The focus of the research was on the rheological characterisation rather than the optimisation of the reactor geometry and as such, the modelling and model validation appears in the appendix only. Validation of the model was inhibited as the level in the PN vessel at the time of testing was unable to be determined. The CFD model showed that the upper region of the vessel was the least well mixed. The potential for stagnation of the flow field and subsequent solidification increases when the viscosity of the slurry also increases. To counteract this threat, the volume of slurry in the reactor must be decreased, or the agitation speed increased. The most effective method to ensure proper mixing dynamics in the vessel was to lower the viscosity, by preferentially processing each slurry by its impurity content.

TABLE OF CONTENTS

LIST OF FIGURES

LIST OF TABLES

1.0 INTRODUCTION

1.1 Background

Phosphate Hill is a mine site located 180 km South-south-east of Mt Isa in a remote area of North West Queensland. Situated on a large deposit of high quality phosphate rock, the mine combines ammonia, which it produces from natural gas, with phosphoric acid to produce ammonium phosphate fertiliser. The phosphoric acid is produced through the reaction of the phosphate rock with sulphuric acid. The mine site has a planned output of 1 million tonnes of fertiliser per year and is expected to last for 30 years (WMC 2001).

The ammonia and the phosphoric acid are first mixed together in a vessel known as the pre-neutraliser. Neutralisation is the term used to describe when enough ammonia is reacted with the phosphoric acid to produce and solidify out mono-ammonium phosphate or di-ammonium phosphate, the two main fertiliser products of the mine. The pre-neutraliser (PN) mixes together enough of the two components to form a thick, but fluid, slurry that is pumped into a rotating cylinder known as the granulator. Inside the granulator further ammonia is added to solidify the required product. This study is concerned primarily with the rheological properties of the slurry produced within the PN.

1.2 Overview

The PN is essentially a cylindrical vessel with four evenly spaced baffles, stirred by a four-blade impeller (WMC 2000). Spargers close to the base of the tank feed ammonia into the vessel and phosphoric acid is pumped in from above. The reaction between these two reactants is highly exothermic, and the heat liberated results in typical operating temperatures of 120°C (Garner 2003). A computational fluid dynamics model will be made of the PN in an effort to determine the mixing

dynamics of the slurry within it. In order to conduct a CFD model of the PN, it is important to understand the rheological properties of the slurry. The PN slurry has been shown to be a non-Newtonian fluid (Leong 2000), which means the viscosity changes with shear rate. The degree of non-Newtonian behaviour and the viscosity of the slurry has been shown to change with several factors (Ando and Akiyama 1972; Handley 1984; Barbera 1988; Leong 2000; Datsun 2002). These can include:

- Temperature
- Ammonia to phosphoric acid, or N:P mole ratio (MR)
- Moisture content
- Impurities (such as Fe, Al; carried over from the phosphate rock)

The effects of some of these factors on the rheological behaviour of ammonium phosphate slurry will be studied in detail. A good understanding of these effects will help optimise slurry processing or allow the operator to develop an appropriate processing strategy for the more rheologically difficult slurry. Potentially, this could lead to increased throughput of product and reduced downtime caused by process blockages.

1.3 Aims of Project

The aims of this project are:

- To develop an in depth understanding of and to measure the rheological properties of the ammonium phosphate slurries as a function of composition, impurities, solids loading, and colouring agents such as biodunder.
- To determine if any of the properties of the ammonium phosphate slurry can be easily manipulated to allow better control of the process to be achieved.

In addition, preliminary computational fluid dynamics (CFD) modelling was conducted on the PN vessel. Moreover, the focus of the research was on the

rheological characterisation rather than the optimisation of the reactor geometry and as such, the modelling and model validation appears in the appendix only.

1.4 Outline

This thesis is set out in the following manner:

Chapter 1: Introduction

Chapter 2: Literature Survey

This chapter features an analysis of the relevant literature regarding previous rheological studies of ammonium phosphate slurries, plant data from Phosphate Hill and the chemistry of the process.

Chapter 3: Rheological Characterisation of Ammonium Phosphate Slurries

Chapter three contains a qualitative assessment of how the viscosity of an ammonium phosphate slurry changes with mole ratio, specific gravity, shear rate and impurity composition.

Chapter 4: Properties of Ammonium Phosphate Slurries

The properties of ammonium phosphate slurries are examined in order to understand the mechanisms behind the viscosity changes observed in chapter three. The chapter covers crystal composition, slurry particle size, solubility of solids & impurities and physical observations.

Chapter 5: Conclusions and Recommendations

The conclusion presents an assessment of the effects of impurities on the viscosity of ammonium phosphate slurries and outlines their associated causes. Recommendations are made on the preferred processing route of impurities and further work that could be undertaken as a result of this thesis.

Appendix I: CFD Modelling

Appendix I contains the computational fluid dynamics component of the project, including the design, set-up and validation of the model as well as several model scenarios and assessments.

Appendix II: Viscosity Graphs

The viscosity vs shear rate graphs are presented here for reference.

2.0 LITERATURE SURVEY

In this chapter, the following is presented:

- An overview of the fertiliser manufacture process at Phosphate Hill
- Generic trends used by the fertiliser industry to control the process
- A review on the viscosity of ammonium phosphate slurries and its relationship with N:P mole ratio, specific gravity, temperature, impurity composition and shear rate
- The hydrolysis curves for aluminium and iron

2.1 Phosphate Hill Operations

2.1.1 Production Process Overview

At Phosphate Hill, phosphate rock deposits are mined, washed and then mixed with water to form a slurry. The phosphate rock slurry is reacted with sulphuric acid to produce phosphoric acid and calcium sulphate (WMC 1999) (gypsum). Most of the gypsum is removed in the process and the resultant acid is evaporated to the required concentrations of 20, 40 and 52% P_2O_5. The acid also contains impurities from the ore and some leftover gypsum from the acid leach stage.

40% acid is mixed with ammonia in a vessel known as the pre-neutraliser. Ammonia is made on site from catalytic conversion of natural gas with air. The acid is ammoniated to produce a slurry at an intermediate mole ratio before being sent to the granulator for final ammoniation. The reaction is highly exothermic; hence the temperature is typically 120°C. A large amount of water is evaporated off during this stage due to the exothermic reaction.

In the granulator, the slurry is sprayed or poured onto a bed of seed fertiliser and further ammoniated until it hardens into the product fertiliser. The product fertiliser is

dried in a rotary drum and then screened for size with the undersize particles sent back as seed in a recycle stream.

2.1.2 Pre-Neutraliser Operating Parameters

The granulation technicians at Phosphate Hill use the following parameters to control the PN reactor:

- Specific Gravity (SG)
- Mole ratio of NH_3:P_2O_5 (MR)
- Temperature
- pH (to a lesser extent)

The specific gravity (SG) is in reference to water at 20°C and is measured to 0.01 unit accuracy. It is controlled through the acid addition, whereby changing the input ratio of 40% and 52% P_2O_5 acid alters the water input. A small change in SG can represent a significant change in the suspended solids concentration. For example, a 0.01 unit change in SG can be equivalent to a 1.2% change in water content. At typical operating conditions with 15% H_2O, the suspended solids content is about 36%, while at 14% H_2O the solids content is 40.5%, an 11% increase (Schnetler 2003).

The mole ratio is the stoichiometric ratio between NH_3 and P_2O_5 in the slurry or product fertiliser. Mono-ammonium phosphate (MAP) has a mole ratio of 1; Di-ammonium phosphate (DAP) has a mole ratio of 2. Typical product fertiliser is lower than these values due to the presence of impurities and the precipitation of the slurry. The pre-neutraliser has a lower mole ratio than the product as the slurry is hardened within the granulator with further ammoniation. The mole ratio can be controlled by the rate of acid or ammonia addition.

The slurry is usually kept close to its boiling point. The evaporation of water vapour in the slurry is the primary mechanism for removing heat from the reaction. The slurry is less viscous at higher temperatures. The boiling point of the slurry increases with decreasing water content (Shengwei, Hui et al. 2004).

The pH is related to the mole ratio in the slurry. A higher pH indicates a higher mole ratio. The pH is used as a rapid way to estimate the mole ratio.

2.1.3 Typical Plant Conditions

Table 1 indicates the typical plant conditions and slurry properties employed in the production of MAP or DAP fertiliser.

Table 1: Typical Operating Conditions And Slurry Properties For Fertiliser Manufacture (Garner 2003).

	MAP	DAP
Temperature	115°C	118°C
Mole Ratio	0.65	1.55
Specific Gravity	1.60	1.57
P2O5 Content	43%	48%
Moisture	16%	18%

Naturally, there are some slight fluctuations in these plant conditions and slurry properties during fertiliser manufacture.

2.1.4 Plant Based Trends

WMC's operations manual contains several graphs showing trends and information of interest. It is important to realise that these are generalised graphs based on plant data. As the slurry changes with composition, mole ratio, temperature and specific gravity, these trends or results can change.

Figure 1 shows the solubility of ammonium phosphate slurries at various temperatures. As expected, the solubility appears to be lowest at the mole ratios 1.0 and 2.0, where mono-ammonium phosphate and di-ammonium phosphate are formed, respectively. The solubility increases with increasing temperature and reaches a maximum close to a mole ratio of 1.5.

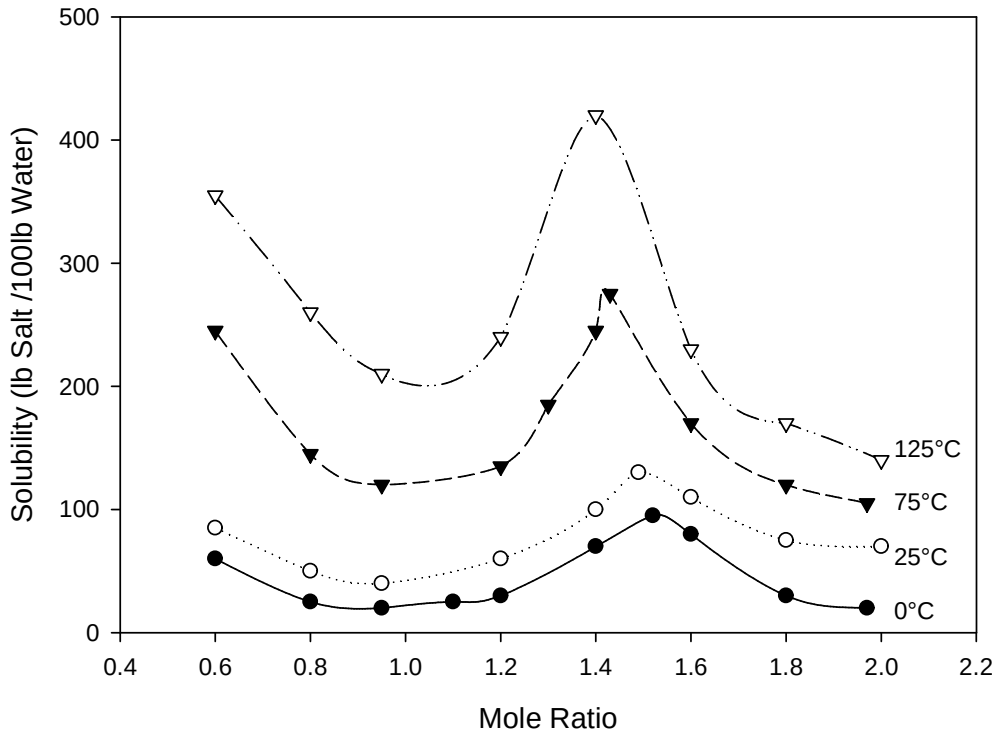

Figure 1: Solubility of Ammonium Phosphate Slurries at Various Temperatures. Reproduced From (WMC 1999).

Figure 2 shows that there is an inversely linear relationship between the specific gravity of the slurry and the moisture content, for a given mole ratio. The specific gravity increases as the moisture content falls due to more solids coming out of solution as the water is evaporated. The specific gravities for pure mono-ammonium phosphate (1.0 mole ratio) and pure di-ammonium phosphate (2.0 mole ratio) are 1.8 and 1.62 respectively (Online Source 2005b). Pure phosphoric acid (0.0 mole ratio) has a specific gravity of approximately 1.83. Slurries with higher mole ratios have lower specific gravities for a given moisture content due to the ammonia molecule attaching to the phosphoric acid.

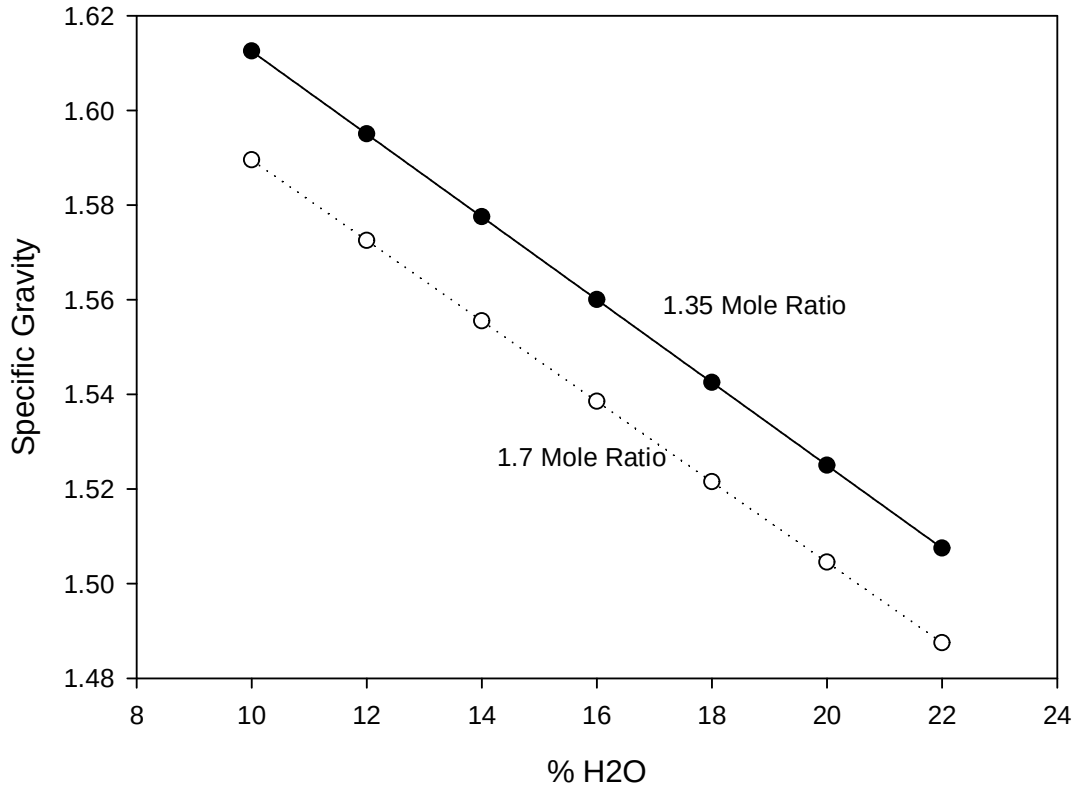

Figure 2: Specific Gravity Vs Moisture Content for a 1.35 and 1.7 MR Slurry. Reproduced From (WMC 1999).

Figure 3 shows the relationship between mole ratio and the pH (in a 10% solution with water) of the slurry. This information is useful as it can provide a quick estimate of the mole ratio using a pH probe. The equivalence point for this titration is close to a mole ratio of 1, or a pH of 4. The low pH at the equivalence point indicates that the mono ammonium phosphate is slightly acidic. As the pH will continue to increase with the addition of ammonia, di-ammonium phosphate will be slightly alkaline.

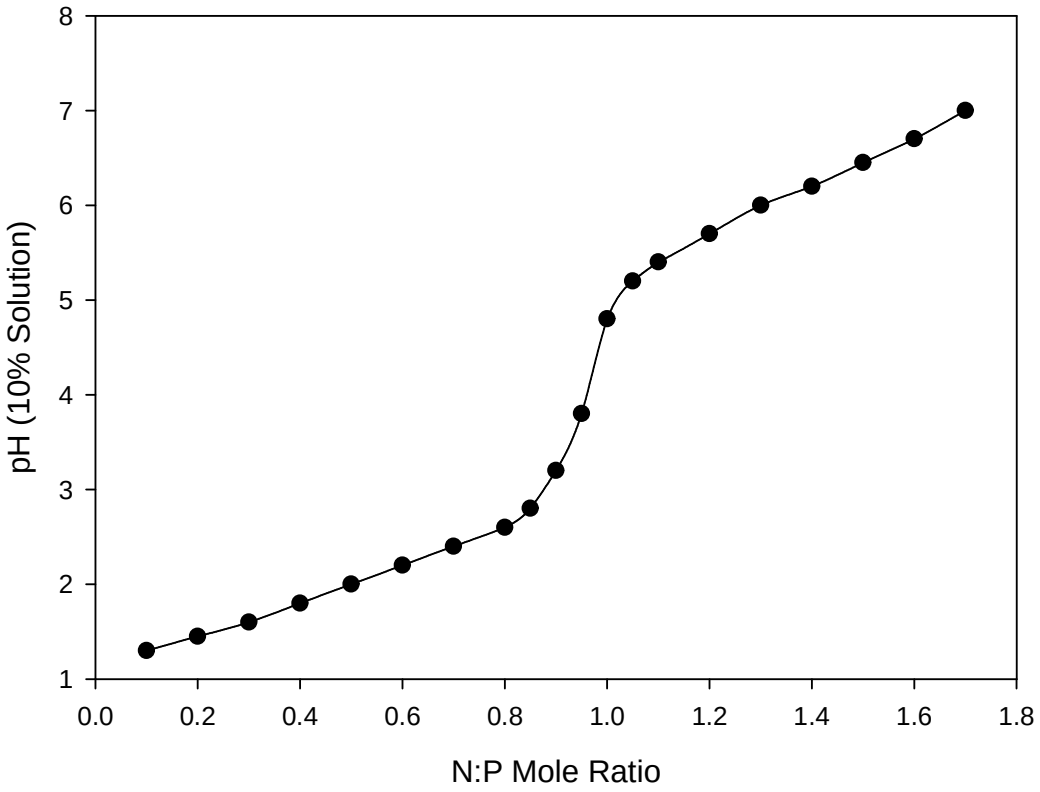

Figure 3: Ph Of 10% Solution Of Slurry In Water Compared With Mole Ratio. Reproduced From (WMC 1999).

2.2 Chemistry

2.2.1 Main Reactions

In the Pre-neutraliser (PN), ammonia is reacted with phosphoric acid to form mono-ammonium phosphate (MAP) and di-ammonium phosphate (DAP) via the following principle reactions (WMC 1999):

$NH_3 + H_3PO_4 \rightarrow (NH_4)H_2PO_4 + \text{Heat}$ (1)

$NH_3 + (NH_4)H_2PO_4 \rightarrow (NH_4)_2HPO_4 + \text{Heat}$ (2)

A significant amount of sulphuric acid is present in the phosphoric acid feed (left over from when the sulphuric acid was added to phosphate rock to produce phosphoric acid). This reacts with ammonia via a secondary reaction:

NH_3 + H_2SO_4 → $(NH_4)_2SO_4$ + Heat (3)

2.2.2 Effect of Impurities

Barbera (1980) stated that NPK type fertilisers are multi-component crystal systems. Many impurities exist within the acid (such as F, Fe, Al, Mg, Si, *etc*). It is not known precisely what compounds these elements will form as they change with varying conditions such as pH, temperature and also chemical composition. Handley (1984) determined that the main components in the fertiliser product were DAP, MAP and ammonium sulphate, with small amounts of other minor constituents. The other minor constituents were not specified with the exception of $MgAl(NH_4)_2H(PO_4)_2F_2$, a newly discovered salt. This salt was claimed to be responsible for higher citrate insoluble P_2O_5 and formed with long (unspecified) retention time in the reactor. Earlier, Achorn et al. (1980) stated that there was disagreement as to the chemical composition of magnesium compounds in the fertiliser product. They then went on to stipulate that recent microscopic examinations determined it to be a different compound, $MgNH_4PO_4.H_2O$. Ando and Akiyama (1972) assessed that the following compounds formed:

- (Fe,Al) $NH_4H_2(PO_4)_2.½H_2O$, or 'Q', first forming after pH 2.5
- (Fe,Al) $NH_4HF_2PO_4$, or 'S', forming from 'Q' with increased ammoniation.
- $Fe_2NH_4OH(PO_4)_2.2H_2O$, or 'U', forming between pH 7 and 8.
- $(NH_4)_3AlF_6$, forming above pH 5 from the dissolving Al type 'Q'.
- $MgNH_4PO_4.H_2O$, $MgHPO_4.3H_2O$, $MgNH_4AlF_6$, all forming from Mg impurities.

Ando and Akiyama (1972) also suggested that gelatinous ferric/aluminium phosphate hydrate and gelatinous silica formed in increasing amounts above pH 6.

Many authors have claimed that fluorine is dominant in altering the compounds that impurities such as iron and aluminium form in the slurry. Achorn et al. (1980) claimed that fluorine has an effect on the formation of iron phosphates. Fluorine acts

to combine with the iron to form Fe-NH_4-PO_4-F-H2O, however at low F:Fe_2O_3 wt. ratios Fe-NH_4-PO_4.nH_2O forms. Handley (1984) expressed surprise at the lack of correlation between the aluminium content of the water insoluble portion of the product compared to the aluminium content of the acid from his data, indicating his expectation of insoluble aluminium-phosphate complexes. His explanation as to this was the high levels of fluorine that were present in each of the tests and the well known ability of fluorine to complex aluminium, presumably tying up the aluminium in an AlF_3 or similar ion. Ando and Akiyama (1972) established a relationship between fluorine and the formation of iron/aluminium based compounds such as Q and S (described earlier). He stated that only 'S', which contains fluorine in an F:(Fe+Al) stoichiometric ratio of 2, formed above pH 3 with F:(Fe+Al) ratios of greater than 1. When the ratio was between 1 and 2, some of the fluorine ions of 'S' were replaced with hydroxyl ions. At a ratio of less than 1, 'Q' and 'S' were both present between pH of 2 and 6, while gelatinous ferric and aluminium hydrate and 'S' were present above pH 6. The aluminium component of 'S' decreased with the formation of $(NH_4)_3AlF_6$. He claimed F ions favour the formation of S and inhibit the formation of Q, while at low pH silica bonds with the F ions, favouring the formation of Q and inhibiting the formation of $(NH_4)_3AlF_6$.

Impurities also have a detrimental effect on the product fertiliser quality indicators, such as the final mole ratio, solubility and nutrient content. Achorn et al. (1980) made the observation that, generally, as the total impurity content increased in the fertiliser product, the amount of key nutrients N and P_2O_5 decreased. They claimed that the total water content (water of hydration + free water) altered the final P_2O_5 and N composition of the product, however he dismissed the perception that the water of hydration in the product impurities was a major cause for this. Frazier (unknown) reports that retention time in the pre-neutraliser is important, as larger retention times lead to the formation of relatively large crystals of $FeNH_4(HPO_4)_2$, which increases the citrus insoluble portion of P_2O_5. Achorn et al. (1980) showed that as the R_2O_3 (Fe_2O_3 + Al_2O_3) content of the product increased, the N content decreased. He commented that the R_2O_3 content of the product did not appear to have a significant effect on the P_2O_5 content, although he admitted his results on this were erratic. Handley (1984) argued that higher aluminium content favoured the production of

MAP rather than DAP, caused by high viscosities, along with a dilution effect. Impurities tended to form compounds with an $N:P_2O_5$ mole ratio of 1, leading to an overall decrease in product mole ratio when producing DAP.

2.3 Rheology

2.3.1 Rheology Theory

Before analysing the viscosity of a slurry, it is important to understand the theory behind viscosity, rheology and its measurement. The viscosity of a Newtonian fluid is a property, but for a non-Newtonian fluid the viscosity will change depending on the rate of shear. Changes in impurity composition, specific gravity, temperature or mole ratio can not only alter the viscosity of the liquid, but its rheological behaviour as well.

Viscosity is a measure of a fluids resistance to shear forces and therefore to flow. It is the property that characterises the fluids flow behaviour. Quantitative assessment of viscosity is based on measuring a fluids resistance to the development of velocity differences as a result of an externally applied force. Rheology is the study of the deformation and flow of matter.

Viscosity is commonly defined by considering two parallel plates of area, A m^2, and distance y metres apart as shown in Figure 4. The upper plate is under a force, F Newtons, resulting in the plate moving at a velocity υ ms^{-1} relative to the lower plate. The shear rate, $\dot{\gamma}$, or velocity gradient, is defined as:

$$\dot{\gamma} = \frac{d\upsilon}{dy} \qquad (1)$$

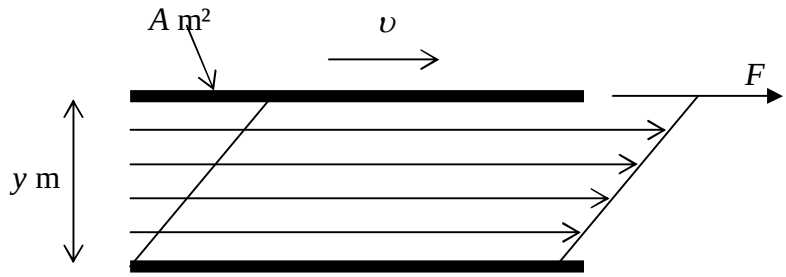

Figure 4: Definition of Viscosity

The shear stress, τ , is defined as:

$$\tau = \frac{F}{A} \qquad (2)$$

where: F is the force required to maintain the constant velocity
A is the area over which the force acts

For a Newtonian fluid, whereby the viscosity does not change with shear rate, the shear rate relates directly to the shear stress as follows:

$$\tau = \eta\dot{\gamma} \qquad (3)$$

where: η is known as the coefficient of viscosity, the dynamic viscosity or simply the viscosity, of the fluid.

Examples of Newtonian fluids include water, simple organic liquids and dilute suspensions.

Other liquids will change their viscosity depending on the shear rate. These liquids are known as Non-Newtonian and can be largely classified into three groups:

- Fluids whereby the shear rate is solely dependant on the shear stress at that point;
- Fluids whereby the shear rate- shear stress relationship is dependant on the period of time the liquid has undergone shear;

- Viscoelastic fluids, which exhibit partial recovery after undergoing deformation.

The first group can be further classified into three sub-groups:

- Pseudo-plastic, or shear thinning, fluids, whereby the viscosity decreases with increasing shear rate
- Dilatant fluids, whereby the viscosity increases with increasing shear rate
- Bingham Plastic fluids with a yield stress, whereby a minimum shear stress must be overcome before the fluid will flow.

Examples of the shear stress- shear rate relationships of time independent Newtonian and non-Newtonian fluids are shown in Figure 5.

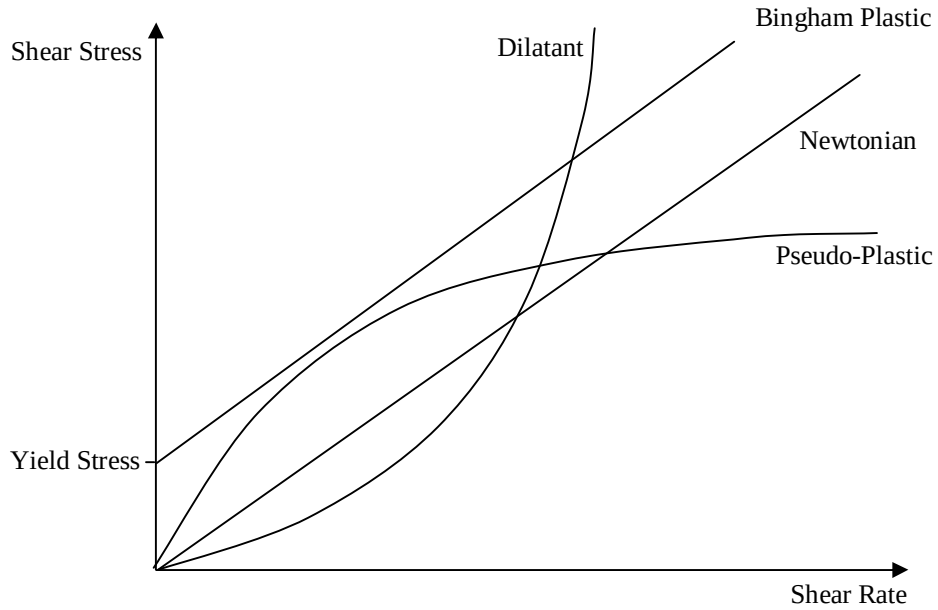

Figure 5: Examples of Time-Independent Rheological Behaviours.

The viscosity of a fluid is always defined as:

$$\eta = \frac{\tau}{\dot{\gamma}} \qquad (4)$$

However in the case of non-Newtonian fluids, where the viscosity changes with shear rate, this is known as the apparent viscosity, which should be specified at the shear rate that it was measured.

Often the rheological behaviour of shear thinning and dilatant fluids can be represented by a power law expression such that:

$$\tau = K\dot{\gamma}^{n} \qquad (5)$$

where: K and n are both empirical constants.

If $n > 1$ the fluid is dilatant, if $n < 1$ the fluid is shear thinning. If $n = 1$ the fluid is Newtonian and the constant, K, becomes the viscosity. As the viscosity changes with shear rate it is important to note that the apparent viscosity at one rate of shear may not be related to the behaviour of the material at different rates of shear. For example, Figure 5 shows that a dilatant material may have lower viscosity than a shear thinning material at low shear rates, but this situation could be reversed at high shear rates.

2.3.2 Ammonium Phosphate Slurries

The rheological behaviour of ammonium phosphate slurries has been found to change as a result of several factors. Barbera (1988) stated "Slurries consist of solid crystalline phases suspended in a liquid phase virtually saturated with salts." This suggests that the amount of precipitated particles will change with solubility and thus affect the rheology. Whilst the author stated the purpose of the paper was not to show particular specific results, he observed the following generalisations:

- As the solid/liquid ratio increases, the viscosity increases exponentially
- As the temperature increases, the viscosity decreases proportionally
- As the water content increases, the viscosity decreases exponentially

He claimed that the suspension viscosity was directly influenced by:

- suspended liquid phase viscosity

- solid/liquid phase weight ratio
- shape, size and nature of solid particles
- electrostatic interactions between solid particles and the liquid phase
- external specific surface of the particles.

The influences identified by Barbera (1988) are difficult to monitor in an industrial setting, because of the complex nature involved in determining them. Factors that influence the viscosity, which are easily determined at plant level, include the specific gravity, mole ratio, temperature and the impurity composition. The extent of the influence of these parameters is described below.

2.3.3 Specific Gravity

Datsun (2002) stated that decreasing the specific gravity has a large impact in reducing the viscosity across all mole ratios. Increasing the water content can reduce the specific gravity. The water content of a slurry is directly related to the specific gravity as shown in Figure 2.

Barbera (1988) examined the change in rheological behaviour with moisture content. Figure 6 shows that slurries with high moisture content will be Newtonian in nature, behaving more non-Newtonian with decreasing water content. Data from a more recent study (Leong 2002) confirms Barbera's (1988) observation. Figure 7 shows that a 0.14 unit change (from 1.49 to 1.63 SG) in the specific gravity can lead to a 10 fold increase in the viscosity.

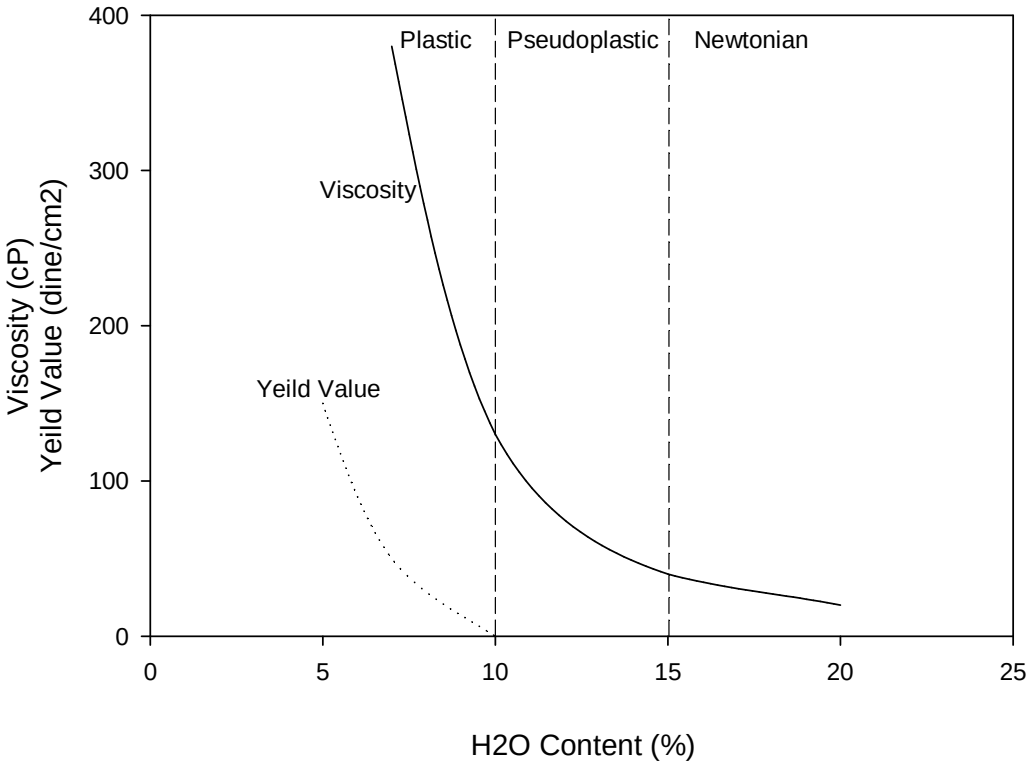

Figure 6: Change in Rheological Behaviour of Slurry with Changing Water Content. Reproduced From Barbera (1988).

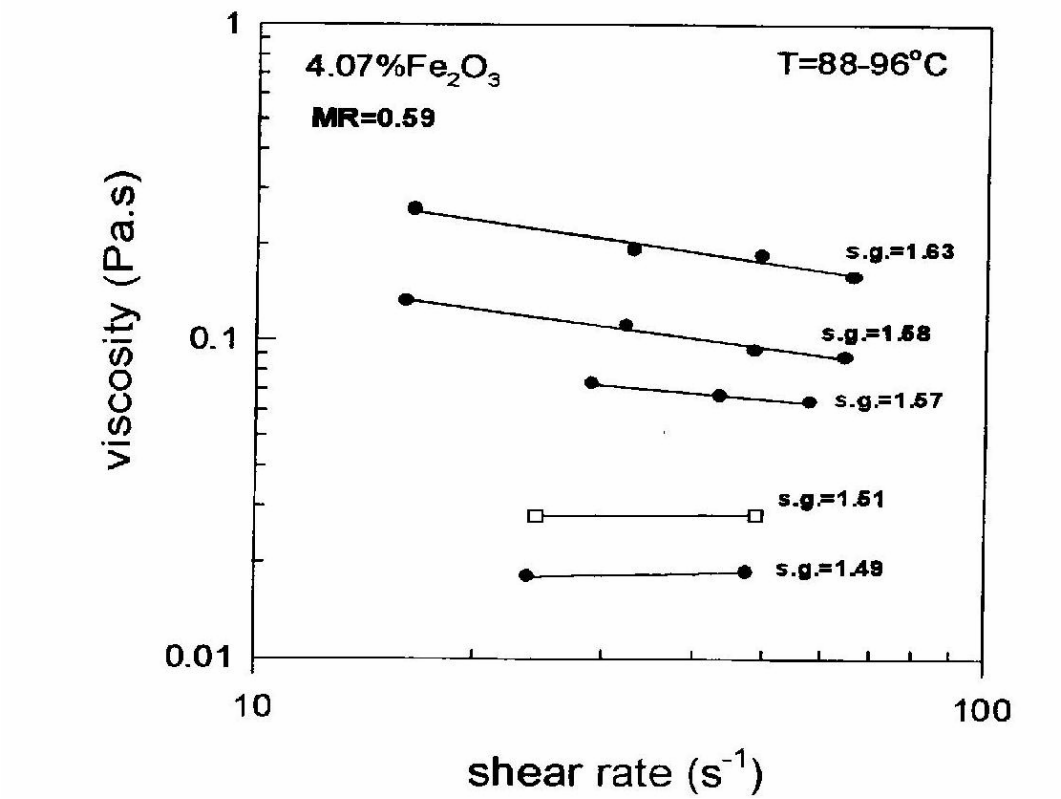

Figure 7: Change In Viscosity With Specific Gravity For Low MR Slurry Spiked With Iron (Leong 2002)

2.3.4 Mole Ratio

Ando and Akiyama (1972) characterised 20% P_2O_5 slurry across a pH range of 2 to 8, first by ammoniating the slurry with ammonia gas and then by acidulating with the original acid back to the starting point, as shown in Figure 8. Ando and Akiyama's (1972) results show a sharp rise in the viscosity, peaking at a pH close to 2.5. This is followed by decrease in the viscosity reaching a low between pH 5 and 6, then a gradual rise up to the end point at pH of 8. During acidulation there appears to be a constant decrease in the viscosity from pH 8 to pH 3.0.

The mole ratio of a typical 40% P_2O_5 slurry (twice the concentration of Ando and Akiyama's (1972) slurry) is related to the pH of the slurry as shown in Figure 3. Figure 3 suggests that the first peak in Ando and Akiyama's (1972) viscosity graph occurs at 0.8-0.9 mole ratio. The viscosity then decreases and reaches a low point at

1.1-1.2 mole ratio. Significantly, the peak does not occur at the least soluble mole ratio of 1.0, which is the mole ratio of pure mono-ammonium phosphate. Ando and Akiyama claimed that this was due to the formation of different iron and aluminium based ammonium phosphate compounds and their particle sizes. Particle size is thought to have an impact on rheology.

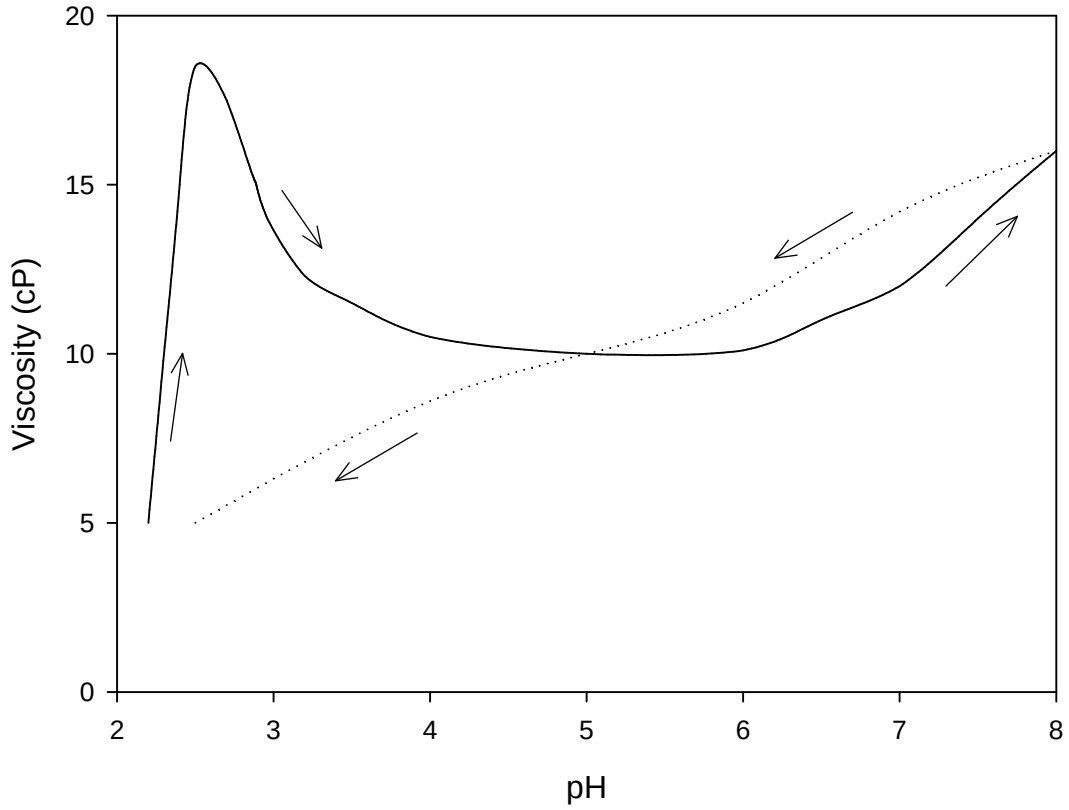

Figure 8: Viscosity Response to the Ammoniation and Acidulation of Ammonium Phosphate Slurry. Reproduced From Ando and Akiyama (1972)

Figure 9 shows the viscosity vs. mole ratio for a more recent study on ammonium phosphate slurries (Tang et al. 2004). The neutralisation degree is the same as mole ratio. The data was taken at a shear rate of 991.6 s^{-1} and water content of 45%. The results are similar to that of Ando and Akiyama with a peak occurring at 0.8-0.9 MR, followed by a decrease in the viscosity until 1.1 MR before rising again with further increase in mole ratio. Below 0.52 MR, the viscosity is relatively consistent.

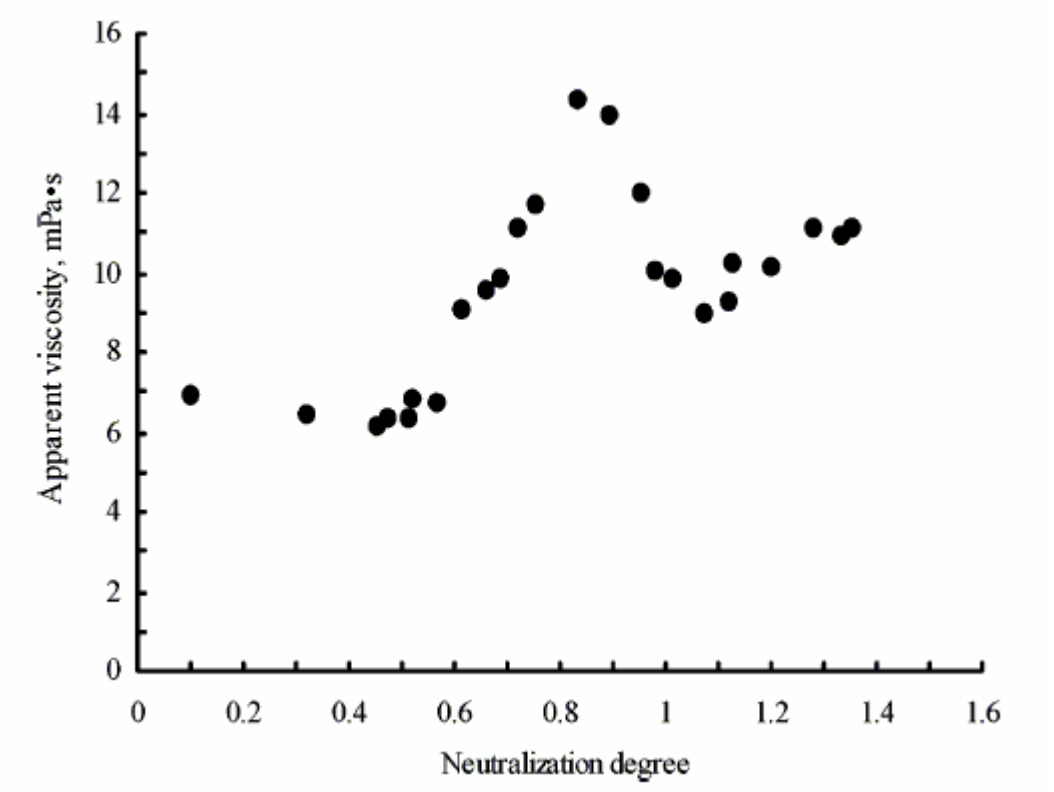

Figure 9: Viscosity Vs Mole Ratio (Neutralization Degree) For Ammonium Phosphate Slurry. (Tang, Guo et al. 2004)

2.3.5 Temperature

The ammonium phosphate slurry in the pre-neutraliser is typically at a temperature of 110-120°C. As the slurry cools, more solids solidify and the viscosity would increase. Figure 10 shows the shear stress shear rate behaviour of a slurry at different temperatures. The results show that a drop of about 10°C (from 105-110 to 98°C) leads to a 10-fold increase in the viscosity at a shear rate of about 0.2 s^{-1}. At a 2 s^{-1} shear rate, the increase is only about 4-fold. This data highlights that temperature control is extremely important when determining the viscosity. It also shows the need to examine the viscosity across a range of shear rates as the proportional difference in the viscosity between tests at high and low shear rates is significant.

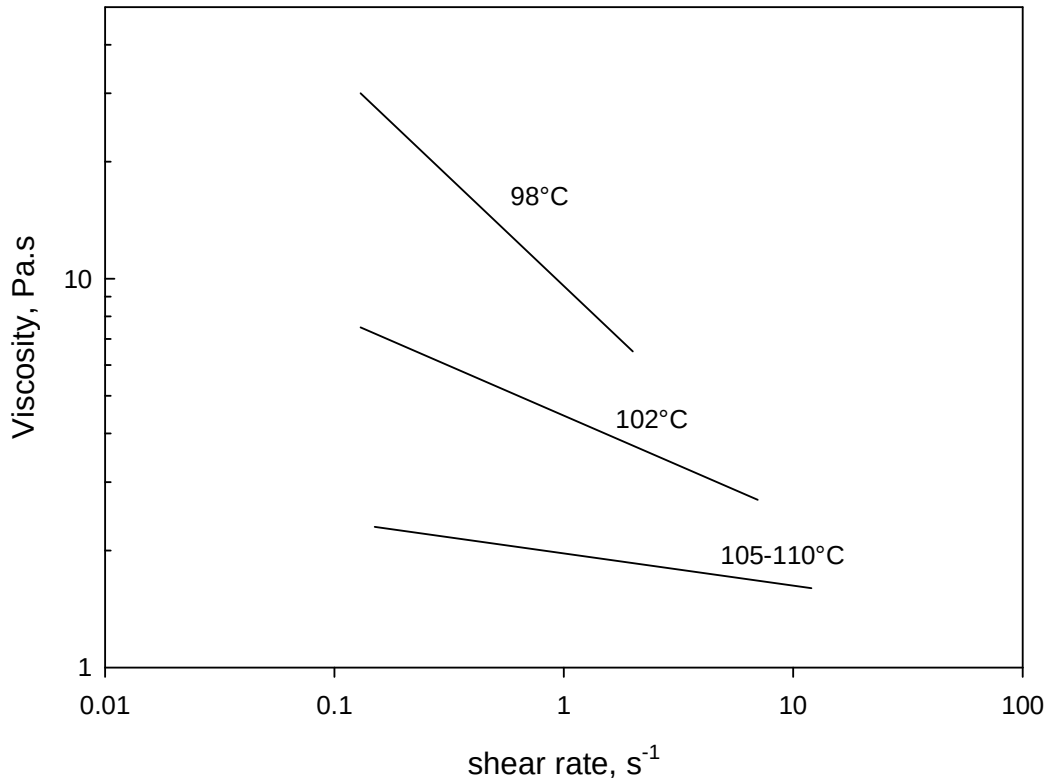

Figure 10: Effect of Cooling On the Viscosity of Ammonium Phosphate Slurry. Reproduced From (Leong 2002). Data Points Omitted.

Figure 11, from Ando and Akiyama (1972), shows the viscosity change due to temperature for 20% P_2O_5 slurry. The temperature specified in these graphs indicates the temperature at which the slurry was ammoniated and tested. The lower temperature slurries have a higher viscosity. The viscosity differences appear to be greater close to pH 3, which would correspond to a mole ratio of a little less than 1.0.

Nyvlt (1972) has shown the dramatic effects that fluctuating temperature can have on crystal size and uniformity, which may lead to changes in the rheology. Ando and Akiyama (1972) also observed that the conditions during the production of the slurry can have an effect on crystal size, making the viscosity not merely a function of the final temperature, but on how the temperature had changed during ammoniation.

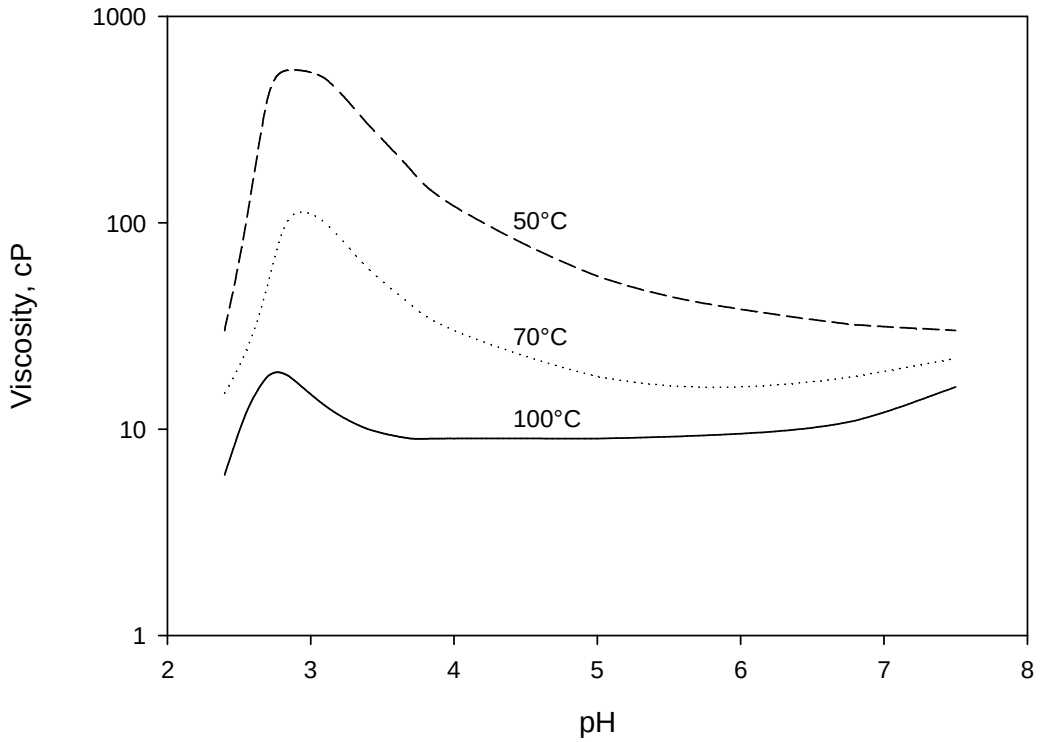

Figure 11: Viscosity Vs Ph For Slurries Ammoniated At Different Temperatures. Reproduced From Ando and Akiyama (1972)

2.3.6 Composition

Changes in the composition of a slurry can also have an effect on the viscosity. The main impurities that are identified as being present in significant quantities in the mined phosphate rock and thus have an affect on the viscosity are magnesium, iron, aluminium and fluorine. Investigations into the effect of these impurities have produced conflicting conclusions.

Handley (1984) established that the ratio of Al_2O_3/P_2O_5 weight showed a logarithmic response to the slurry viscosity. He also concluded that aluminium had the greatest adverse effect on slurry viscosity, iron showed only a slight adverse effect, while magnesium and fluorine were actually beneficial to slurry fluidity. Studies by Ando and Akiyama (1972) and Achorn et al. (1980) claim that the extent of the effect of

iron and aluminium is related to the fluorine content. Achorn et al. claimed that a high iron content formed small colloidal particles with the composition Fe-NH_4-PO_4.nH_2O, increasing the viscosity as shown in Table 2, but the addition of fluorine led to the formation of Fe-NH_4-PO_4-F.H_2O; a coarse crystal resulting in a lower viscosity. In contrast, Ando and Akiyama claimed that high fluorine levels *increased* the viscosity through the formation of small round shaped particles of (Fe, Al)$NH_4HF_2PO_4$. Datsun (2002) claimed that, at high pH, ferric ions form a hydrate matrix with solids, forcing them out of suspension to produce a gel. She later concluded that, at low pH, impurities remain soluble and the slurry does not gel.

Table 2: Change In Viscosity For Two Acids With Different F:Fe2O3 Feed Ratios (Achorn, Dillard et al. 1980).

Test #	H_3PO_4 Feed F:Fe_2O_3 wt. ratio	DAP Product % by weight Fe-NH_4-PO_4-.nH_2O	PN Slurry viscosity, cP
1	1.02:1	4.2	466
2	2.17:1	0.96	166

Ando and Akiyama (1972) produced a viscosity vs pH graph (Figure 8) for ammonium phosphate slurry that had been first ammoniated to pH 8 and then acidulated back to pH 2.5. The viscosity was tested after five minutes curing time at various pH, though these points are not specified. They noted high viscosity readings at pH 2.7 during the ammoniation step, with an insoluble, gelatinous substance forming. Further ammoniation led to a decrease in the viscosity and the amount of gelatinous material present. Ando and Akiyama (1972) determined that the gel like substance formed during ammoniation was (Fe, Al)$NH_4HF_2PO_4$, which he designated as 'S'. He stated that 'S' consisted of small round shaped particles about 20 milli-microns [sic] (probably 20µm) in diameter, although X-ray tested showed that the single crystals were much smaller. The small crystals would have led to a large increase in the slurry viscosity. He commented that the $AlNH_4HF_2PO_4$ component of 'S' belonged to the tetragonal system. Above a pH of 6, Ando and Akiyama believed that the increase in viscosity was due to an increase in gelatinous silica.

Achorn et al. (1980) determined that magnesium had little to no effect on the viscosity of the pre-neutraliser slurry, although this was within a narrow tested range of 0.33 to 0.43 wt% of Mg. As mentioned earlier, Handley (1984) determined that magnesium and fluorine were actually beneficial to slurry viscosity. Ando and Akiyama (1972), on the other hand, demonstrated that magnesium and fluorine increase the viscosity across all mole ratios. Figure 12 shows the affect that magnesium has on two slurries, with varying fluorine content, across a wide pH range. The acid with the higher fluorine content was consistently double the viscosity of the lower fluorine content acid, across the entire pH range. With the addition of magnesium, the graph shows a three order of magnitude increase in the viscosity of the high fluorine slurry close to pH 6, the low fluorine slurry increasing by one order of magnitude. The increase is much less dramatic at low pH, indicating that the effect of magnesium is pH sensitive. Ando and Akiyama observed that magnesium formed a large amount of $MgNH_4AlF_6$ as small crystals, 10 milli-microns [sic] in size (the crystal size is probably 10 μm). He claimed that high levels of fluorine prevented the formation of other magnesium compounds such as $MgNH_4PO_4.H_2O$ or $MgHPO_4.3H_2O$. He stated low F acid contained less fluorine and less silica leading to a lower viscosity on formation of some of these compounds.

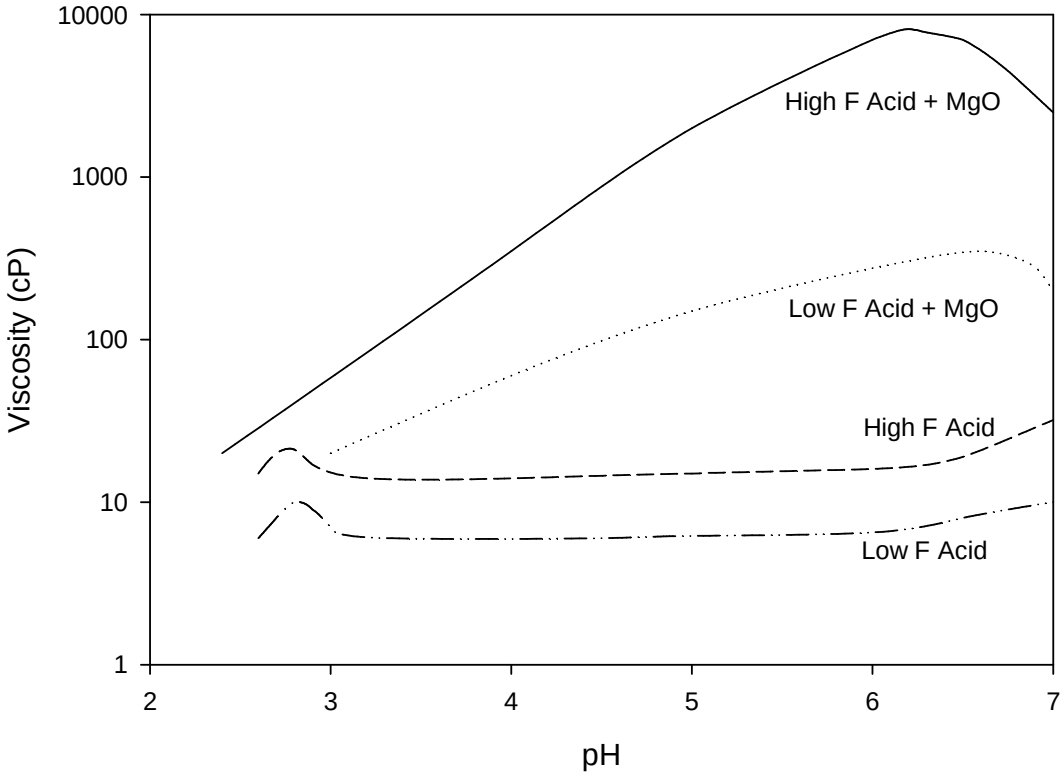

Figure 12: Viscosity Vs Ph for Two Acids with Varying Fluorine Ion Concentration and the Effect of Additional MgO. Reproduced From Ando and Akiyama (1972)

2.3.7 Shear Rate

Early analysis of the viscosity of ammonium phosphate slurries did not determine if the slurry was Newtonian or Non Newtonian. Rheological behaviours of slurries can only be determined through multiple viscosity measurements at different shear rates. If the shear rate has been changed between measurements, the results may be misleading. Results from many early papers appear to be single point measurements, as they do not specify a shear rate. In cases when the viscosity was found to change markedly, by several orders of magnitude, it is possible that the rotational speed and therefore the shear rate used to determine the viscosity was changed between tests. The shear rate can change even if the rotational speed is kept constant. This could

have led to a misrepresentation of the true change in the viscosity. If the shear rate was kept constant, the proportional change in the viscosity at higher or lower shear rates could be different. Dindsdale and Moore (1962) made the comment that "a single point measurement on a non-Newtonian material is completely inadequate for characterising its fluid behaviour."

Data from Leong (2000; 2002) indicate that the slurries used for making MAP and DAP tended to exhibit non-Newtonian behaviour at processing conditions. Figure 7 and Figure 10 both demonstrated changes in the rheological behaviour of a slurry. Newtonian slurries are indicated by a horizontal line, as the viscosity does not change with shear rate. As slurries increase in SG, or decrease in temperature, they become more Non-Newtonian and their viscosity can change markedly with shear rate.

2.4 Related Aspects

2.4.1 Colloids

Colloids consist of small 'particles' of one substance distributed more or less uniformly throughout another (Hunter 1993). The latter phase is referred to as 'continuous' while the 'particle' phase is 'discontinuous', or dispersed.

The ammonium phosphate mixture in the pre-neutraliser is commonly referred to as a 'slurry'. A slurry is commonly thought of as a colloidal dispersion of fine solid particles in a liquid medium (in this case, ammonium phosphate compounds in a diluted phosphoric acid solution). Throughout this thesis the term 'slurry' is used primarily as a generic term referring to the ammonium phosphate mixture, though it may not be technically correct to call all slurry samples by this name.

It has also been noted that, under certain conditions, the 'slurry starts to gel' (Datsun 2002). A gel is a dispersion in which the attractive interactions between the molecules in the disperse phase become strong enough to develop a rigid network structure (Everett 1988). It may consist of solid particles, macromolecules or

surfactant molecules and occurs due to either electrostatic, van der Waals interactions or chemical bonding. In the case of ammonium phosphate slurries, the gels are likely to result from the concentration of the solid particles in the slurry, not from the formation of macromolecules or due to surfactants.

Colloids can affect the rheological properties of the fluid. A fluid which exhibits Newtonian behaviour can behave more non-Newtonian if it contains colloidal particles, due to a complex interplay of interactions. These include hydrodynamic interactions between solid and liquid particles, attractive or repulsive forces between the particles and, in concentrated systems, direct particle-particle contact. In the case of ammonium phosphate slurries, this behaviour is seen with increasing concentration of the solid particles as water is evaporated off during reaction in the PN. Particle concentration also increases around the neutralisation mole ratios of 1 and 2, as more salts crystallise out of solution.

2.4.2 Hydrolysis Products

Figure 13 and Figure 14 show the hydrolysis products for aluminium and iron respectively (Baes and Mesmer 1986). The hydrolysis products can be used to determine the species each metal will form and at which pH range. The pH range that we are concerned with is between 2 (~0.5 MR) and 8 (2.0 MR). Within this range it can be seen that aluminium produced only one dominant hydrolysis product. On the other hand, iron forms several different hydrolysis products over this pH range. We would then expect the chemical interaction of the iron impurity to be more variable across mole ratio, than for aluminium.

In most of the above literature on fertiliser rheology, the slurry is dried and the impurity compounds were determined by X-ray diffraction or optical observation. Drying of solids will bring about crystallization of impurity compounds; whereas the nature of the chemical species of the metal ion impurities formed in the slurry during neutralization have not been examined. These species can be different to those obtained by drying solids. Metal ions are known to form hydrolysis products at

various pH levels (Baes and Mesmer 1986). Hydrolysis products are known to adsorb readily (James and Healy 1972; Leong 2005) and affect slurry rheology (Mpofu, Addai-Mensah et al. 2003; Leong 2005), electrokinetic properties (James and Healy 1972; James and Healy 1972b), coagulation rate (Matijevic, Abramson et al. 1960; Matijevic and Janauer 1966) and flotation recovery (Fuerstenau, Rice et al. 1965). In this study, the role of hydrolysis products on slurry properties will be examined.

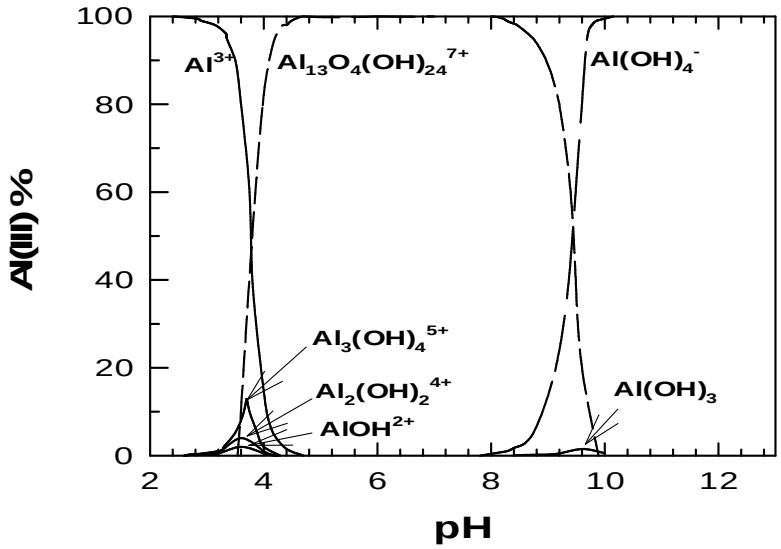

Figure 13: Hydrolysis Products for Aluminium

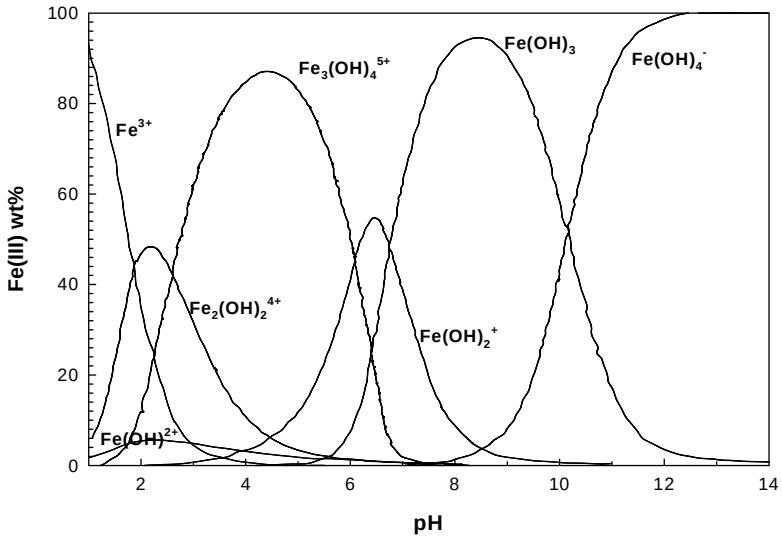

Figure 14: Hydrolysis Products for Iron.

2.5 Summary

It has been shown that it is equally important to ensure that the temperature, specific gravity, the mole ratio and the impurity composition of the slurry is known to a good degree of accuracy before using a viscosity measurement to compare with another. It is also important to examine a range of shear rates and to report the shear rate with the viscosity measurement if the slurry is non-Newtonian. Factory based measurements, or those based on pilot plant data, are inherently flawed as they cannot guarantee a precise slurry specific gravity, temperature and mole ratio at the same time. This puts the viscosity comparisons between various tests into doubt. In order to properly characterise the rheological behaviour of ammonium phosphate slurries, there needs to be tight control on the properties and composition of the slurry. Leong (2002) demonstrated that large changes in the viscosity could occur with small changes in specific gravity. There was also no indication that any non-Newtonian nature of the slurry was taken into account. This puts the validity, or at least the extent, of the results produced by these authors into some doubt.

The literature survey revealed that iron, aluminium and magnesium were primarily thought to be responsible for increases in the pre-neutraliser slurry viscosity. They were also found to be the cause of other problems such as increasing the citrus insoluble content of the fertiliser and lowering the overall mole ratio when producing DAP. Fluorine was found to interact with these impurities, altering the crystal compounds they form. Ando and Akiyama (1972) claimed that high $F:R_2O_3$ (where R is Al or Fe) ratios led to the formation of small colloidal crystals that increased the viscosity for all three elements, however Achorn et al. (1980) claimed that crystals formed in a slurry with high $F:R_2O_3$ ratio were coarser than those with lower levels of fluorine, meaning that fluorine lowered the viscosity of the slurry. Handley (1984) stated that fluorine was beneficial to slurry viscosity, but did not compare his results to the R_2O_3 content. All three had differing opinions in respect to the extent that iron, aluminium and magnesium had in altering the slurry viscosity.

Only Ando and Akiyama (1972) investigated the viscosity through a laboratory measurement across the entire pH range encountered in fertiliser manufacture. This was, however, performed for slurries of lower concentration, typically 26% P_2O_5, than

the concentration used at Phosphate Hill, which is closer to 40% P_2O_5. The specific gravity for this acid was only 1.35, while pre-neutraliser slurry specific gravities are typically closer to 1.60. There is also no indication that any water evaporated off during the process was returned to the slurry, which would have lead to a change in the specific gravity. Whilst the peak on ammoniation at a pH of close to 2.8 is probably due to the formation of MAP, the lack of one at the same point on the acidulation step may be due to the dilution with acid.

There remains the need for a comprehensive examination into the affect of the three main impurities magnesium, iron and aluminium on the rheological behaviour of ammonium phosphate slurries.

3.0 RHEOLOGICAL CHARACTERISATION OF AMMONIUM PHOSPHATE SLURRIES

The principal aim of this project was to characterise the rheology of ammonium phosphate slurries, and determine how the rheology is affected by changes in the impurity composition, mole ratio and specific gravity of the slurry. Since the data is to be used in an industrial mine site, it is not possible to characterise the rheology for every slurry that may be produced. As such, it is more important to focus on the trends in the change in the viscosity, than to precisely define the viscosity of a slurry at a fixed set of values.

The literature survey has identified several factors that are likely to influence the rheology. Whilst trends relating to the change from specific gravity and mole ratio have been established, the effect of varying the impurity content has not been conclusively determined. Therefore, the effect of adding various impurities to a batch of as-received acid that has been collected as a baseline will be examined. This should establish direct changes resulting from the various additions. Furthermore, the effect of these impurities on the rheology of slurry made from laboratory grade ammonia and phosphoric acid will be determined. The results will be compared in an attempt to attribute the cause of any change to a specific impurity, or as a general result of other changes in the slurry, such as reduced water content.

Testing the viscosity of ammonium phosphate slurry appears to be a straight forward process. However, it has been found to be very time consuming and problematic. There is no previously established procedure for conducting such a test. The experimental work is complicated by a multitude of factors, including high temperatures, slow reaction and evaporation times, the precipitation of impurities and the solidification of the slurry, as well as the lag time that results from determining the mole ratio of the slurry.

3.1 Experimental

3.1.1 Materials and Phosphoric Acid Preparation

The materials used were pure ammonia gas, laboratory grade and plant phosphoric acids, analytical grade $FePO_4$ and Al PO_4.

The phosphoric acid used was collected from the 40% acid tanks at the plant and contained some suspended solids. The as-received acid is designated DAP1 and all of these samples were collected at the same time from the same sample location in the plant. $FePO_4$ was dissolved in DAP1 to produce two other phosphoric acids with different Fe(III) content. These acids are denoted as DAP2 and DAP3. The $FePO_4$ was added at room temperature and stirred for 24 hours until it all dissolved. $AlPO_4$ was also dissolved to change the Al(III) content of the as-received phosphoric acid and these are denoted as DAP5 and DAP8. $Mg_3(PO_4)_2$ was added to change the Mg(II) content of the acid and this was denoted as DAP7. Table 3 summarizes the elemental concentrations of the phosphoric acids determined by ICPAES (Inductively-Couple Plasma Atomic Emission Spectroscopy). The elements listed in Table 3 are Al(III), Ca(II), Fe(III), Mg(II), P and S. The difference in Fe(III) concentration between DAP1 and DAP3 is 3-fold while the concentration difference for the other elements is relatively small by comparison. Between DAP 4 and DAP 1, the difference in Al(III) concentration is about 4-fold while the Fe(III) concentration remained essentially constant.

Table 3: Elemental Composition of As-Received and Dosed Acids.

Concentration, mg/kg or ppm						
Element	**DAP 1**	**DAP2**	**DAP 3**	**DAP 5**	**DAP 7**	**DAP 8**
Al	**3140**	**2820**	**2780**	**13000**	**2750**	**5990**
Ca	**217**	**185**	**150**	**155**	**164**	**198**
Fe	**11700**	**22700**	**30300**	**11000**	**12200**	**13400**
Mg	**751**	**819**	**700**	**1070**	**14900**	**1310**
P	**158000**	**166000**	**156000**	**161000**	**151000**	**151000**
S	**7150**	**6520**	**6720**	**4790**	**-**	**-**

Laboratory grade phosphoric acid and pure ammonia gas were also used in this experiment. Analytical grade $FePO_4$, $AlPO_4$ and $Mg_3(PO_4)_2$ were added to the laboratory phosphoric acid to change the respective impurity ion concentrations. The solutions were made up to the specified w/w percentage of the common industrially determined species of each impurity, being Fe_2O_3, Al_2O_3 and MgO (i.e.: the laboratory acid solution with 3% added iron contained 3% w/w of Fe_2O_3, made from the addition of $FePO_4$).

3.1.2 Ammoniation and Sampling

Ammonia gas is bubbled through a continuously stirred solution of phosphoric acid in an 800 ml beaker until the desired mole ratio is reached, as shown in Figure 15. A 30 ml sub-sample is then poured into a test tube, which is weighed to analyse the specific gravity and is also used in determining the viscosity (as described below). The sub-sample is not returned to the beaker. The slurry is heated on a hot plate with stirring to evaporate water over time, thus increasing the specific gravity. A new sub-sample was taken from the beaker periodically in a clean test tube and sampling ends when the slurry becomes too viscous to pour into the test tube, typically after 4-8 sub-samples have been taken.

Figure 15: Experimental Apparatus Used To Ammoniate The Phosphoric Acid.

When performing a test, the acid was poured into a beaker and distilled water added. More distilled water was added for higher mole ratios and for higher impurity content slurries, to ensure the slurry does not solidify and to enable an adequate specific gravity range to be tested.

The reaction is highly exothermic and, therefore, the ammonia addition rate is controlled to ensure that the reaction stays close to the boiling point of the liquid (110-120 ^{o}C). When the slurry is poured into a volume-calibrated cylindrical test tube, it is first weighed to determine the specific gravity before being placed in a hot oil bath for several minutes, until the temperature is consistent, as shown in Figure 16. The hot oil bath is maintained at 110 ^{o}C, thereby ensuring that the viscosity is always measured at the same temperature. Parafilm was placed over the test tube to reduce water evaporation, however in cases where it was not used, no loss of fluid volume was observed. In addition, the slurry was stirred just prior to viscosity measurement to resuspend any settled solids. There was little to no precipitation in most of the experiments.

Figure 16: Experimental Apparatus Used To Test For Viscosity.

3.1.3 Mole Ratio

The ammonia to phosphoric acid mole ratio (MR) is obtained by titration with standard 1M NaOH and 1M HCl solutions. A sample of the slurry was mixed with 90vol% of distilled water. NaOH was added to bring the pH to 8.0 and then followed by HCl to bring the pH to 4.0. The amount of HCl and NaOH added was used to calculate the mole ratio with MR=2-(Volume of NaOH)/(Volume of HCl). The pH of a DAP slurry is 8.0 while that of MAP is 4.0. The (Volume of NaOH)/(Volume of HCl) is the ratio of number of moles of hydroxide ions required to bring the test slurry to DAP to the number of moles of acid required to bring the slurry back to MAP.

3.1.4 Viscometry

The rheology of the slurry was measured with a Brookfield LVDV-II+ viscometer using a concentric cylinder geometry with the cylindrical test-tube being the outer cylinder, as can be seen in Figure 16. In the measurement, the inner cylinder was

immersed in the slurry and the torque exerted on this cylinder, T, was recorded as a function of rotational speed, Ω. The shear rate, $\dot{\gamma}$, of non-Newtonian fluids was calculated using the power law shear rate equation (Dindsdale and Moore, 1962) given by:

$$\dot{\gamma} = \frac{2\Omega n^{-1}}{(1-\varepsilon^{-2/n})} \qquad (6)$$

where Ω is in radian per second, ε is the radius ratio of the outer to the inner cylinder and $n = \frac{d \ln T}{d \ln \Omega}$ is the slope of the log-log plot of T versus Ω. For Newtonian fluid, $n = 1$. For shearthinning power law fluid, n is less than 1.0 and a constant. For a yield stress fluid, n is a function of Ω and is normally obtained by taking the derivative of the polynomial equation that fitted the $\ln T$ versus $\ln \Omega$ data.

3.2 Results

3.2.1 Analysing the Data

The viscosity versus shear rate behaviour at 110 °C of a typical ammonium phosphate slurry produced from impure plant phosphoric acid (DAP1) at MR 1.6 determined as a function specific gravity is shown in Figure 17. At low specific gravity, the flow behaviour is Newtonian in the range of shear rate characterised. The slurry displayed non-Newtonian shear thinning behaviour at higher specific gravity. This is reflected by a decreasing viscosity with increasing shear rate. The viscosity versus shear rate curve is a log-log plot and the decrease in viscosity with shear rate is linear. So the flow behaviour can be represented by a power law model:

$$\eta = K\dot{\gamma}^{n-1} \qquad (7)$$

where $\eta = \frac{\tau}{\dot{\gamma}}$ is the viscosity defined as the ratio of shear stress to shear rate, *K* the consistency index and *n* the power law index which should be less than 1.0 for a shear thinning slurry. Figure 18 shows the viscosity versus shear rate behaviour of

ammonium phosphate slurries produced from DAP 3 acid at MR 0.9. The flow behaviour is more shear thinning compared to the DAP 1 acid at MR 1.6. The shear rate range analysed reflects the limitations of the testing equipment. The agitator in the PN vessel rotates at 60 rpm.

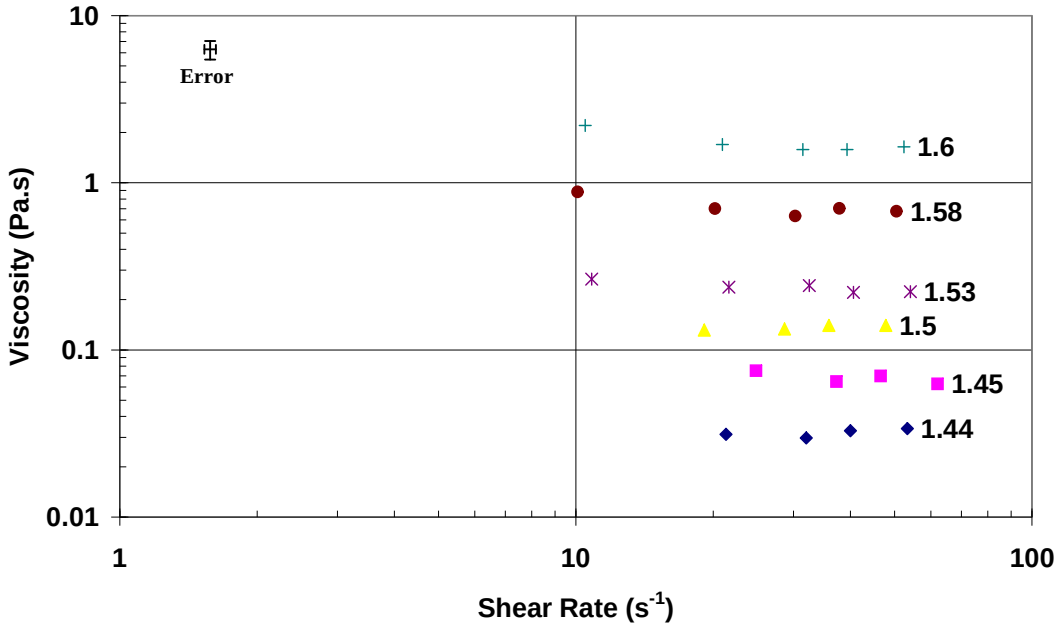

Figure 17: Viscosity Vs Shear Rate Behaviour for DAP1 Slurry at 1.6 MR. The Values Indicate The Specific Gravity Of The Slurry.

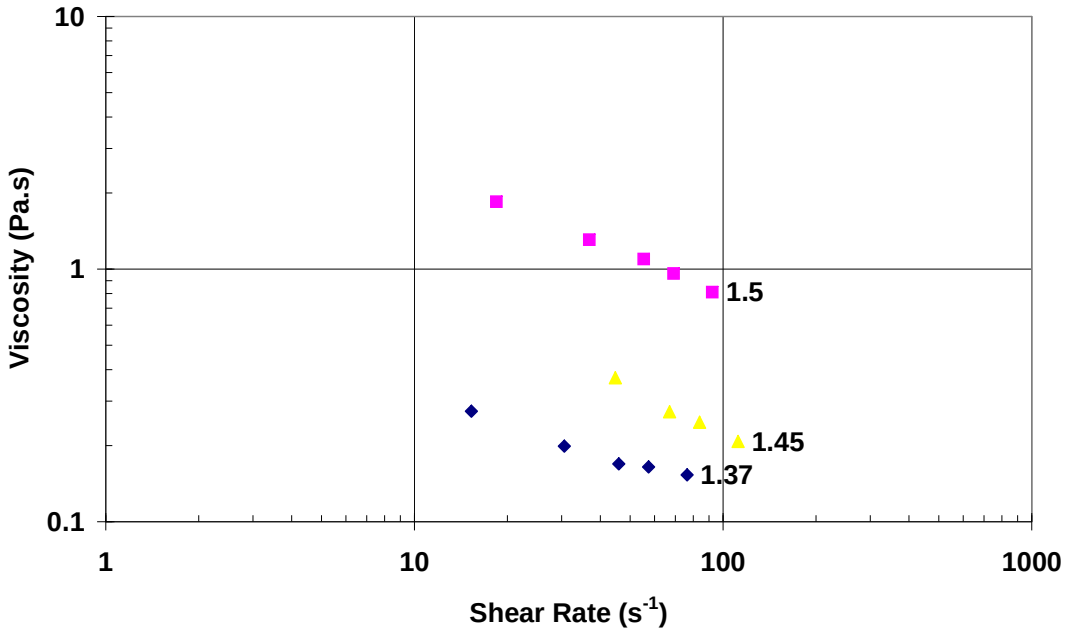

Figure 18: Viscosity Vs Shear Rate Behaviour for DAP3 Slurry at 0.9 MR. Values Indicate The Specific Gravity Of The Slurry.

The viscosity data of Figure 17 was extracted at $40s^{-1}$ shear rate and plotted as a function of specific gravity. The plot of log viscosity vs specific gravity for the 1.6 MR slurry is shown in Figure 19. A linear relationship is clearly seen ($R^2 = 0.97$). The relationship for an SG from 1.44 to 1.60 can be represented by:

$$\eta = 2.620 \times 10^{-7} SG^{32.61} \qquad (8)$$

Where SG is the specific gravity of the slurry.

To provide consistency when analysing the data, all viscosity values are interpolated at 40 s^{-1} shear rate and an SG of 1.55. The shear rate was chosen as it is central in the range of shear rates analysed, whilst an SG of 1.55 is reflective of conditions inside the PN vessel.

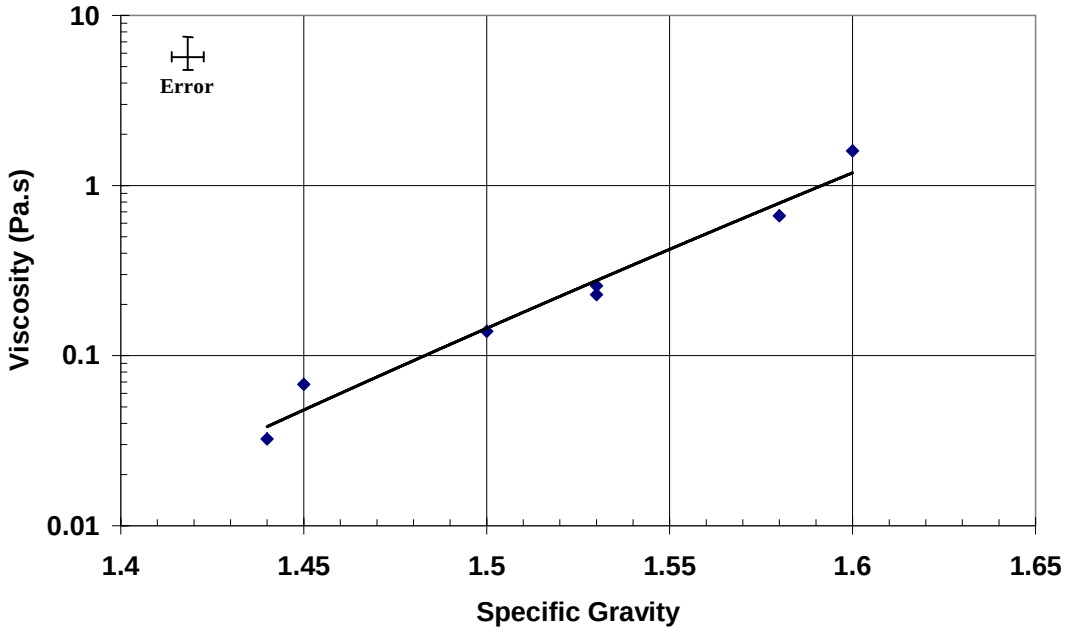

Figure 19: Viscosity of DAP1 Slurry at 40/s Shear Rate And 1.6 MR Vs Specific Gravity.

The viscosity increases exponentially with increasing slurry specific gravity (or decreasing water content of the slurry). The specific gravity of slurry is directly related to the free moisture content in the slurry at given mole ratio, MR. In general, the moisture content increases linearly with decreasing specific gravity and also with decreasing MR. So specific gravity provides a measure of the solid concentration in the slurry. Slurry viscosity increases with specific gravity at any given mole ratio. The viscosity vs. shear rate data for each experiment is shown in APPENDIX II – VISCOSITY GRAPHS.

3.2.2 Error and Reproducibility

Slurry rheology is dependent upon a number of factors; i) surface chemistry, ii) nature and concentration of metal ions impurities, iii) particle size, iv) particle volume fractions and v) particle morphology. Surface chemistry is dependent upon the pH or MR ratio of the slurry. The nature and concentration of the metal ions in solution are

dependent upon the phosphoric acid used. However, the particle size distribution, volume fraction and morphology are dependent upon the slurry preparation conditions. These include the temperature, rate of ammoniation and the flow field or pattern in the reactor. The flow pattern is dependent upon the geometry of the slurry reactor, the starting volume of phosphoric acid used and the stirrer speed. It is not possible to reproduce exactly all the slurry preparation conditions and hence there is a degree of variability in the experimental viscosity.

Furthermore, it was observed that thick slurries, diluted with water to decrease their SG, generally do not return to the same viscosity once the water has been evaporated. Moreover, the temperature history experienced by slurry during the transfer from the reactor to the cylindrical tube and the transport of the tube to the temperature bath and exposure to a relatively cool inner measuring cylinder during the viscosity characterization, affects the slurry in terms of more solids formation due to crystallization at cooler temperature. It is therefore important that all the slurries are prepared in the same manner including the procedure for the transfer and rheological characterization of the slurry

Several experiments were repeated to test the reproducibility of the data and refine the experimental procedure. Figure 20 shows the viscosity vs. specific gravity correlations for DAP1 acid ammoniated to 0.9 MR. The viscosity of the repeated test (b) is 25% less than the original at 40 s^{-1} shear rate and 1.55 SG. Figure 21 shows the viscosity vs specific gravity correlations for DAP1 acid ammoniated to 1.3 MR. In this case the repeated test has a 25% higher viscosity than the original. Given the sensitive nature of the reaction and testing procedure, the repeats were considered to be in good agreement, as both are within experimental error. Furthermore, the changes in viscosity that we anticipate are at least an order of magnitude greater than this error. Slurries produced at higher mole ratios are expected to be the hardest to reproduce and hence have the largest error.

An estimate of the error resulting from the measurement equipment for each type of graph is shown in Figure 17, Figure 19 and Figure 22. Table 4 shows an estimate of

the experimental error for the individual parameters that were used to create the error bars. These errors should be similar for all experiments.

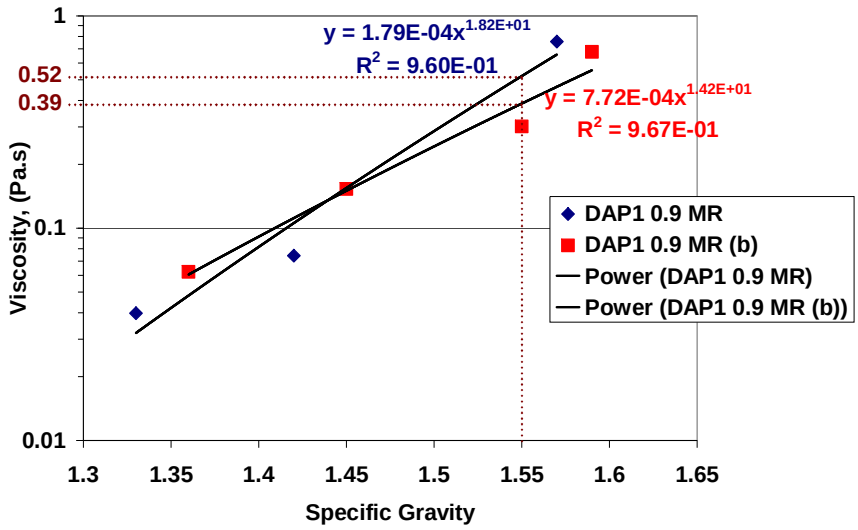

Figure 20: Viscosity Vs. Specific Gravity For DAP1 Slurry Ammoniated To 0.9 MR.

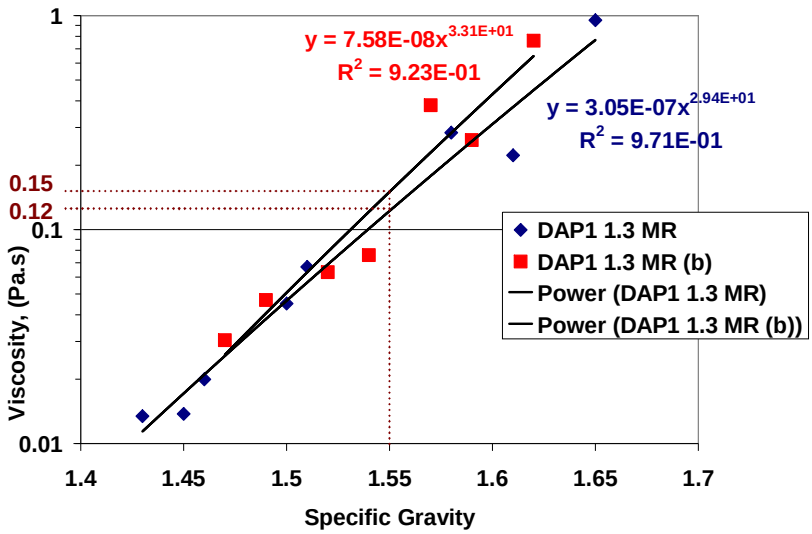

Figure 21: Viscosity Vs. Specific Gravity For DAP1 Slurry Ammoniated To 1.3 MR.

Table 4: Estimate of Experimental Error

Measurement	Estimate of Error
Shear Stress	± 10 %
Cylinder diameter	± 0.5 mm
Specific Gravity	± 0.05
Mole Ratio	± 0.03

3.2.3 Qualitative Observations

Pure acid slurries containing iron are yellow in colour above 1.5 MR, whilst slurries below 1.3 MR are white in colour. There is a progressive change in the colour between 1.3-1.5 MR and this is further discussed in the next chapter. Occasionally low mole ratio slurries (<1.3 MR) turn yellow during ammoniation. After ammoniation has ceased and the slurry has been maintained at temperature for several minutes, they turned back to white. This observation occurred sporadically during testing. Each time the colour change reversal occurred, the viscosity of the sample was much higher than expected. Repeat tests that did not go through this process had lower viscosities. The observation occurred more frequently in laboratory based slurries than in plant-acid slurries, and also more frequently in 2% Fe_2O_3 slurries than 3% Fe_2O_3 slurries. It is possible that a similar event was occurring in aluminium based slurries, but high mole ratio Al_2O_3 slurries are white or translucent and therefore no visual change would have been easily observed. The observation highlights the difficulty involved in replicating slurry characteristics and viscosity.

3.2.4 Plant Acid Results

3.2.4.1 DAP 1 Acid

The acid designated DAP1 was the unaltered, as-received acid from Phosphate Hill. It was especially important that the viscosity of this acid was accurately determined, as it would form the basis of comparison for the subsequent tests involving the addition of metal ions.

The viscosity was determined between 0.80 MR and 1.70 MR at 0.10 MR increments, with 0.90 and 1.30 mole ratio being duplicated. The results are shown in Figure 22. Each set of viscosity vs specific gravity data used to produce this graph exhibited good correlation with a power law formula, with the average R^2 value being 0.958. The lowest R^2 value was for 0.80 MR, at 0.820, and the highest was for 1.4 MR at 0.999, both shown in Figure 23. Figure 22 shows that DAP 1 follows a trend of rising

viscosity until 0.9 MR followed by a drop to 1.1 MR. The viscosity then rises steadily after 1.2 MR and dips slightly at 1.7 MR.

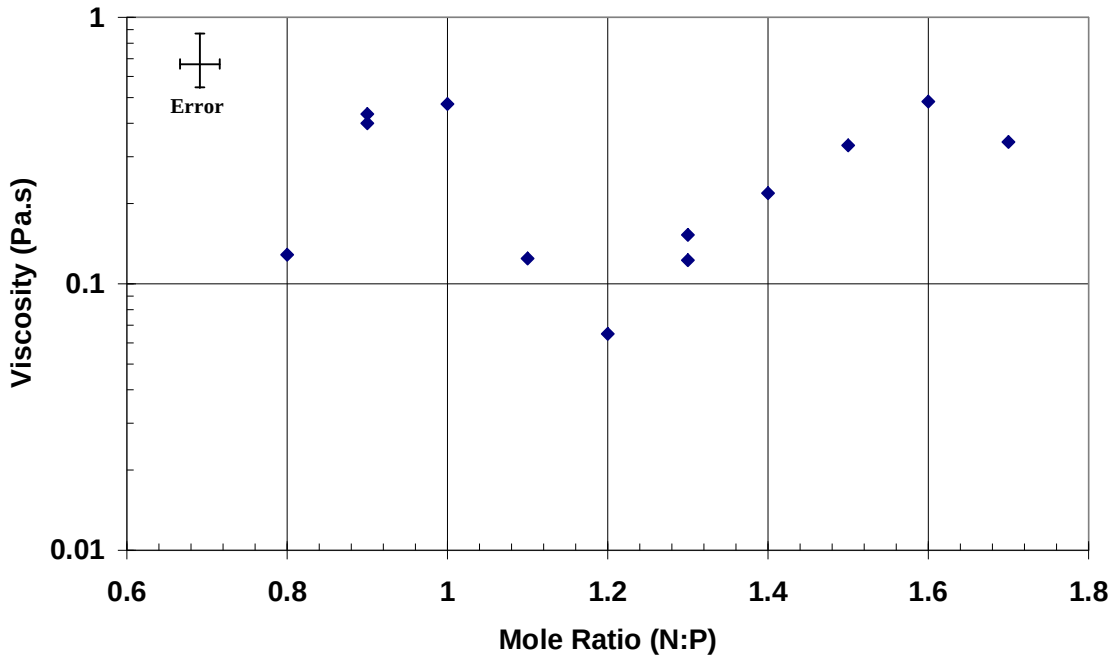

Figure 22: Viscosity Vs Mole Ratio Plot For Slurries Made From DAP1 Acid.

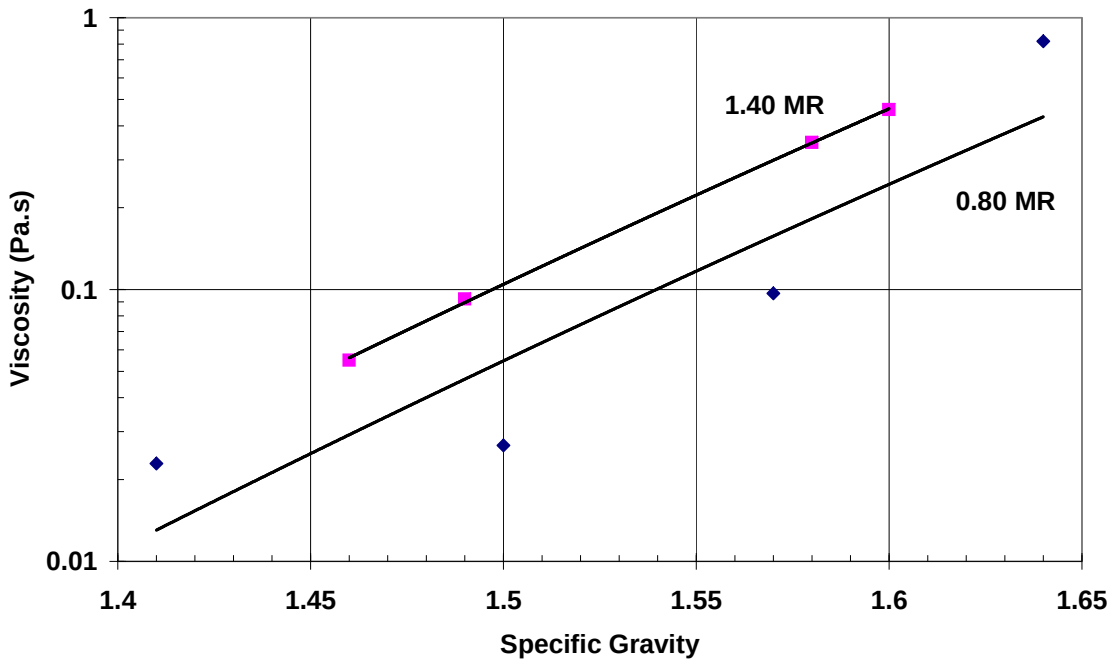

Figure 23: Viscosity Vs Specific Gravity For Slurries Made From DAP1 Acid.

3.2.4.2 DAP 2 Acid

DAP 2 acid was prepared by dissolving a known amount of iron phosphate in the as-received DAP 1 acid. The iron concentration is essentially double. The viscosity follows a similar trend to that in DAP 1 acid. Figure 24 shows that the viscosity rises up to 0.9 MR, before falling again from 0.9 to 1.1 MR. The viscosity then increases, up to 1.4 MR, after which there is some fluctuation. The best correlation between the specific gravity and the viscosity was for 1.50 MR with an R^2 value of 0.997. The worst R^2 value was 0.764, for 1.60 MR although this sharpens to 0.998 when the first data point is removed. Despite removing this data point the interpolated viscosity at 1.55 SG and 40 s^{-1} shear rate does not change significantly.

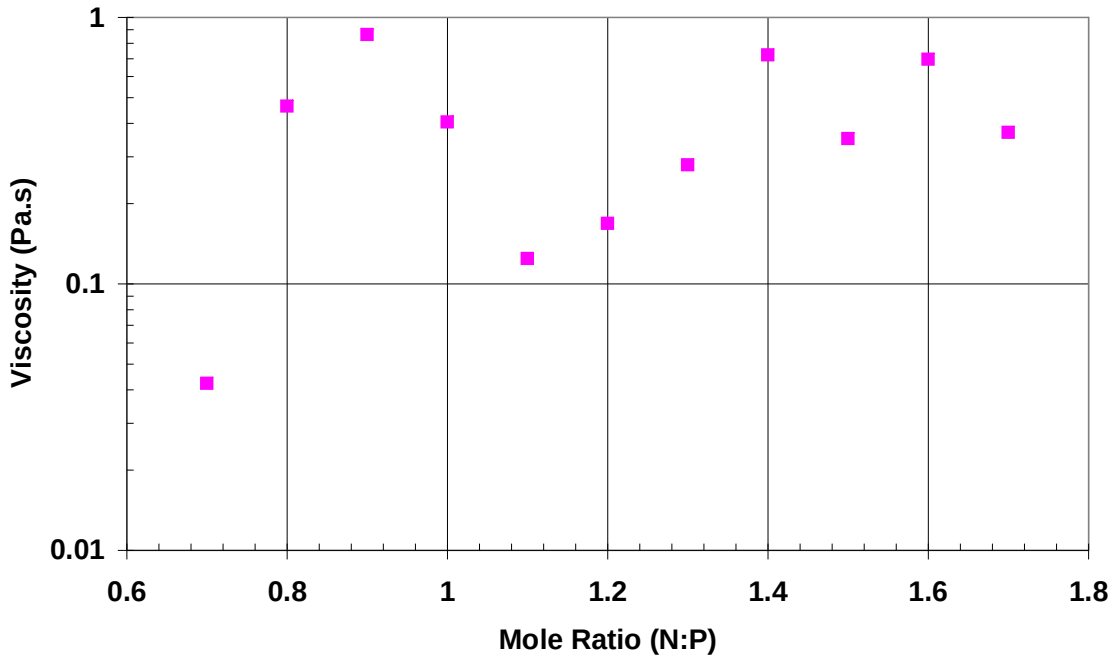

Figure 24: Viscosity Vs Mole Ratio For Slurries Made From DAP2 Acid.

Two tests were performed at 0.9 MR. There is a greater than 10-fold difference between these tests, as shown in Figure 25. The higher viscosity test is considered to be more accurate as it is in line with trends seen in other acids, of increasing viscosity to 0.9 MR. Both sets of data for 0.90 MR had good R^2 values of 0.96 and 0.98 for the higher and lower viscosity correlations respectively. The lower viscosity was

considered an anomaly, hence why it was repeated. This result highlights the large fluctuations in viscosity that are possible when trying to replicate a slurry.

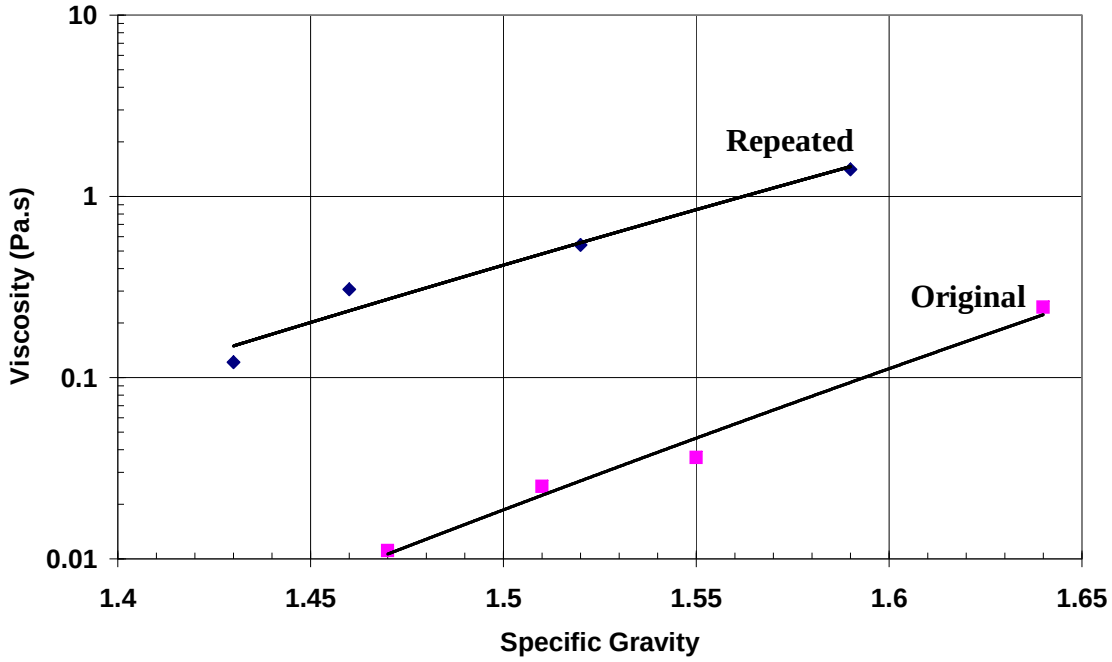

Figure 25: Original and Repeated Viscosity Vs Specific Gravity for Slurry at 0.90 MR Made From DAP2 Acid.

3.2.4.3 DAP 3 Acid

DAP 3 acid was made from the addition of iron phosphate to the as-received DAP 1 acid, as with DAP 2. In this case, the iron content is triple that of DAP 1. The viscosity also follows a similar trend to that in DAP 1 and DAP 2 acid, as shown in Figure 26. There is an increase in the viscosity up to 0.9 MR followed by a decrease down to 1.1 MR. The viscosity continues to increase above 1.1 MR, with some fluctuation at higher mole ratio. The R^2 value for the viscosity vs specific gravity correlation was between 0.908 and 0.995, with 0.9 MR and 1.1 MR being the respective extremes.

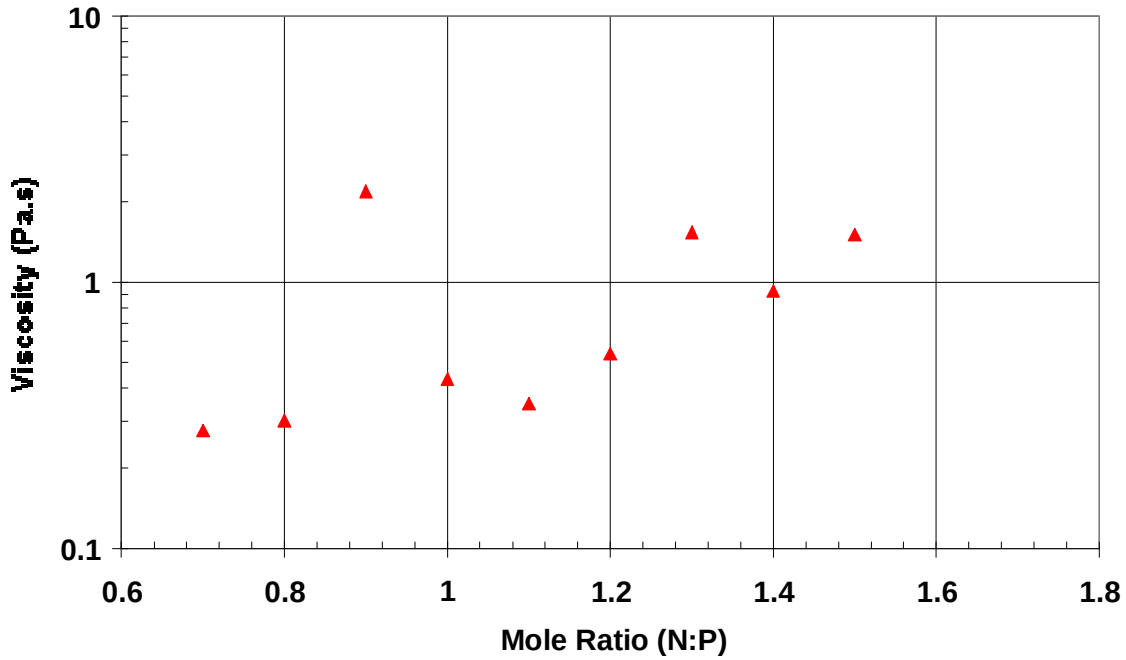

Figure 26: Viscosity Vs Specific Gravity for Slurries Made From DAP3 Acid

3.2.4.4 DAP 5 Acid

DAP 5 acid was made from the addition of aluminium phosphate to the as-received DAP 1 acid. The aluminium content is four times that in DAP 1. In terms of mass of impurity added, which will be discussed in a later section, the weight of aluminium ion is slightly higher (15%) than the weight of Fe ion in this acid (or in DAP 1 acid, as the iron level is unchanged) and the number of moles of aluminium in this acid is slightly higher (20%) than the number of moles of Fe in DAP 2 Acid.

The viscosity trend for DAP5 was very different to that of DAP1, DAP2 and DAP3. Figure 27 shows that there is an increase in the viscosity up to 1.04 MR followed by a decrease down to 1.40 MR. After this point the viscosity remains fairly steady, with a drop at 1.7 MR. The R^2 values for the correlation between viscosity and specific gravity were between 0.915 and 0.996. These values were for 1.04 and 1.60 MR respectively.

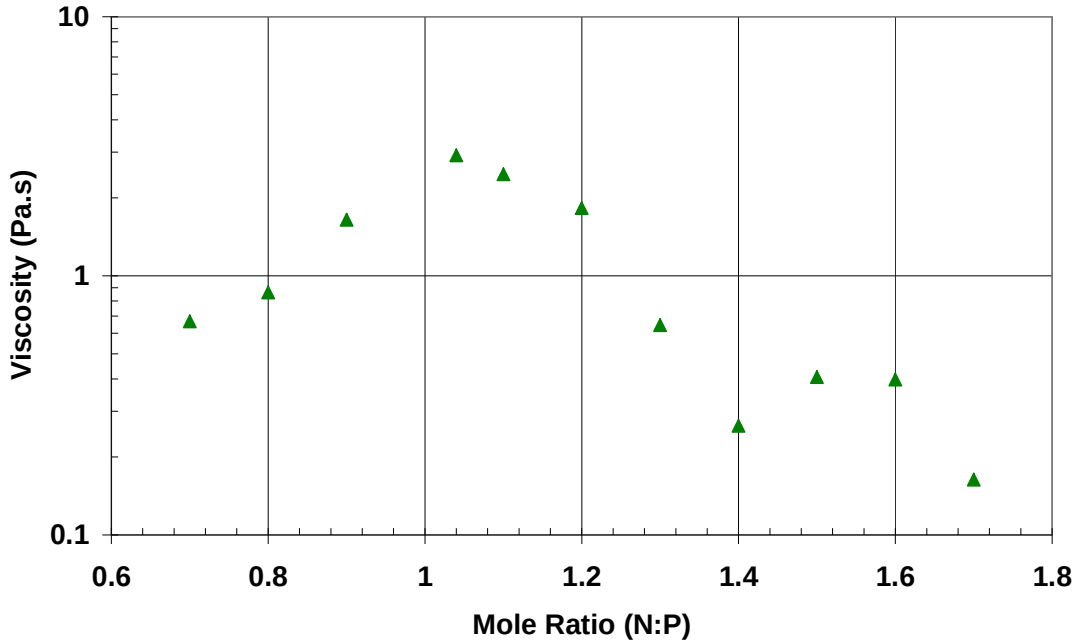

Figure 27: Viscosity Vs Specific Gravity For Slurries Made From DAP5 Acid.

3.2.4.5 DAP 7 Acid

DAP 7 acid is the as received DAP 1 acid with magnesium phosphate added to it. The amount of magnesium is roughly 20 times that in DAP 1. The weight of magnesium ions added to the acid is roughly 50% greater than the weight of iron and aluminium added to DAP 2 and DAP 5, respectively. Almost twice the number of moles of Mg(III) were added to form DAP 7 acid than moles of aluminium and iron that were added to DAP 5 and DAP 3, respectively.

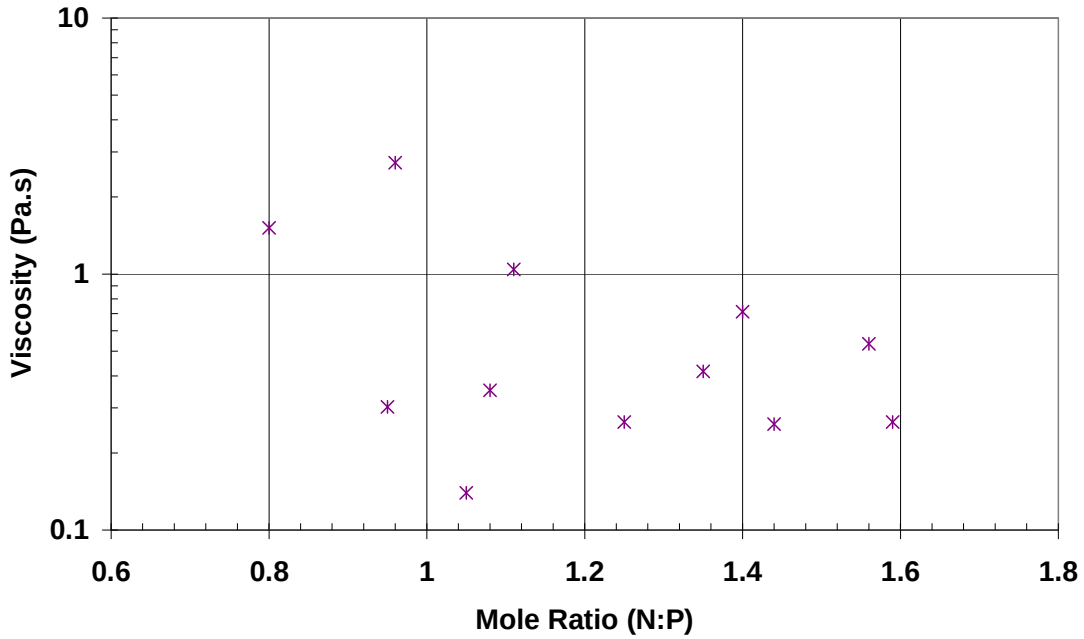

Figure 28: Viscosity Vs Specific Gravity For Slurries Made From DAP7 Acid.

Unlike previous DAP acid tests, this acid was not tested at 0.1 MR increments. The results in Figure 28 show no distinguishing trend in the viscosity. As with previous acids, repeats were performed on points that did not appear consistent with expected trends. Unfortunately in this case, the repeated and original tests together are erratic and no conclusion could be drawn from them.

The correlation between specific gravity and viscosity for DAP 7 acid is quite poor, with average R^2 values of 0.742. The greatest correlation was for 1.25MR, with a value of 0.995. The worst was for 1.40 MR with a value of 0.263. The poor correlation is due to the data being flat (small change in viscosity with changing SG), which reduces the effectiveness the fitting a power law formula, as the error in the viscosity reading becomes significant when compared to the slope of the graph.

Most of the viscosity vs specific gravity correlations for this acid have been observed to be quite flat. The average power law exponent for DAP 1, DAP 2 and DAP 3 was 25. For the two acids with additional aluminium (DAP 5 and DAP 8), the average value is 20. For slurries made from DAP 7, the average is just 7.5. It would not be

regarded as unusual for some exponents to fall to low values due to the many factors that influence the viscosity. However, the DAP 7 acid has shown consistently low power law exponents. These low values contribute to the scattered nature of the viscosity vs mole ratio graphs and make interpretation of the effect of magnesium on the viscosity of ammonium phosphate slurries difficult.

3.2.4.6 DAP 8 Acid

DAP 8 acid is the as-received acid with additional aluminium. The amount of aluminium added is much less than in DAP 5 acid, with the total aluminium content being equivalent to about twice that of DAP 1 acid. Although DAP 8 acid did not have any magnesium or iron added to it, both of these elements were analysed to have increased in concentration, presumably due to water evaporation.

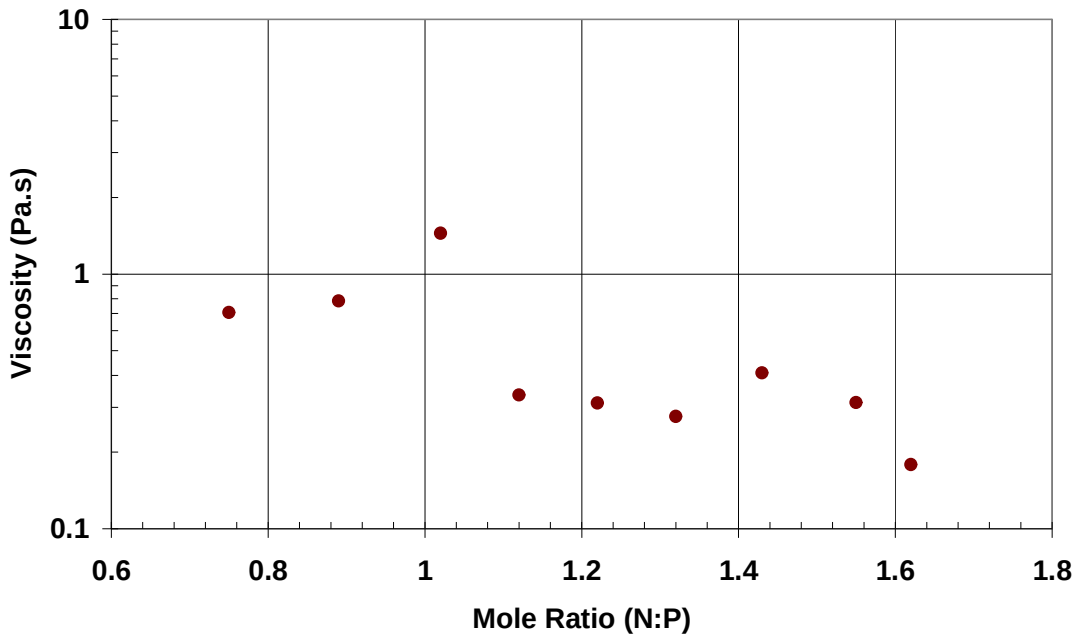

Figure 29: Viscosity Vs Specific Gravity For Slurries Made From DAP8 Acid.

Similar to DAP 7 acid, DAP 8 acid was not analysed at 0.1 mole ratio increments. Figure 29 shows that the viscosity appears to remain fairly consistent between 0.75 and 0.89 mole ratio, before rising to a peak at 1.02 MR and falling to 1.22 MR. After

this the viscosity is fairly flat, with a drop occurring at 1.64 MR. The lowest R^2 value for the viscosity vs specific gravity correlation was 0.809 for 1.64 MR.

3.2.5 Comparison of Plant Acid Results

3.2.5.1 Changes with Iron Content

Figure 30 shows the change in viscosity (at $40s^{-1}$ shear rate, 1.55 specific gravity) vs mole ratio (MR) for the as-received acid (DAP1) and the acids containing additional iron content (DAP2 and DAP3). The as-received acid increases in viscosity up to 0.90 MR, before decreasing to 1.2 MR and rising again. This trend is consistent with Tang et al. (2004) and Ando and Akiyama (1972). With increasing iron content, the viscosity increases for each mole ratio, except between 1.0 MR to 1.1 MR. At these mole ratios the viscosity of each acid appears to converge. The influencing factor that results in the increase in the viscosity with iron content at other mole ratios is nullified. At higher mole ratios, some fluctuation in the viscosity data is apparent. This is caused by the precipitation of ammonium phosphate salts and resultant changes in particle size, solids concentration and the nature of the impurities. Whilst effort has been made to ensure consistent experimental procedure, the difficulties involved in replicating slurry conditions inevitably lead to some error in the reported viscosity.

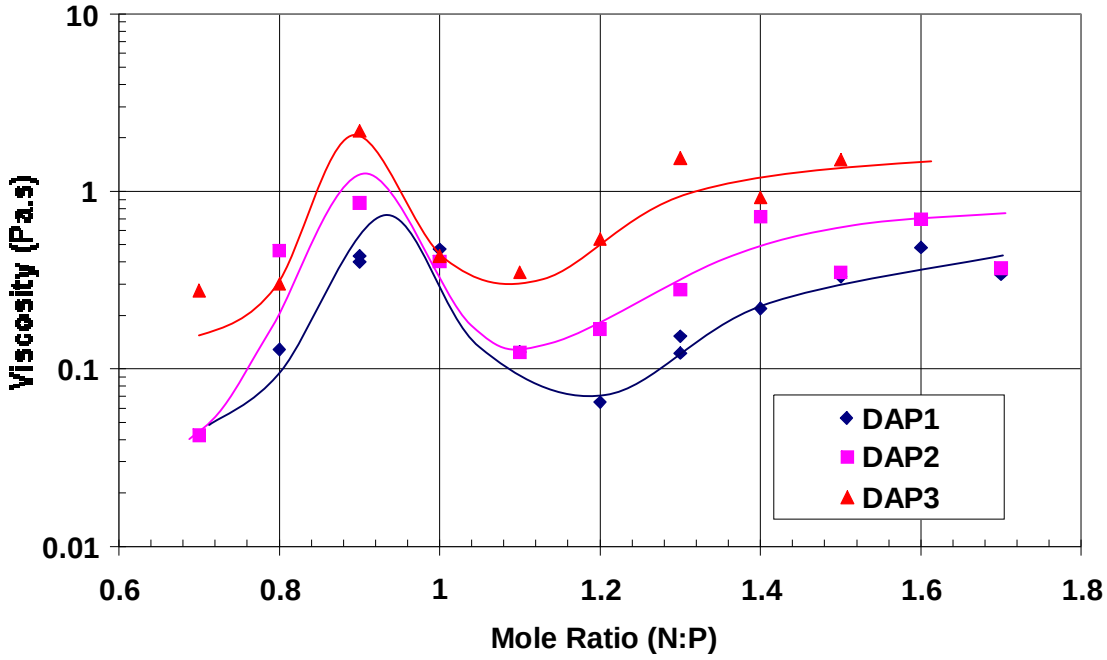

Figure 30: Change in Viscosity for Slurries with Varying Iron Content

3.2.5.2 Changes with Aluminium Content

Figure 31 shows the change in viscosity (at 40 s^{-1} shear rate, 1.55 specific gravity) vs mole ratio (MR) for the as-received acid and the acids containing additional aluminium content (DAP5 and DAP8). Aluminium increases the viscosity across all mole ratios tested below 1.4 MR. Unlike the additional iron based slurries, the aluminium alters the trend in the change in viscosity vs mole ratio from that of the as-received acid (DAP1). Increased aluminium does not reproduce the same sharp decrease in viscosity seen between 0.9 to 1.2 MR for iron based slurries. The peak in the viscosity occurs between 1.0 and 1.1 MR. Above 1.4 MR, the increased aluminium appears to result in a lower viscosity than the unaltered as-received acid (DAP1).

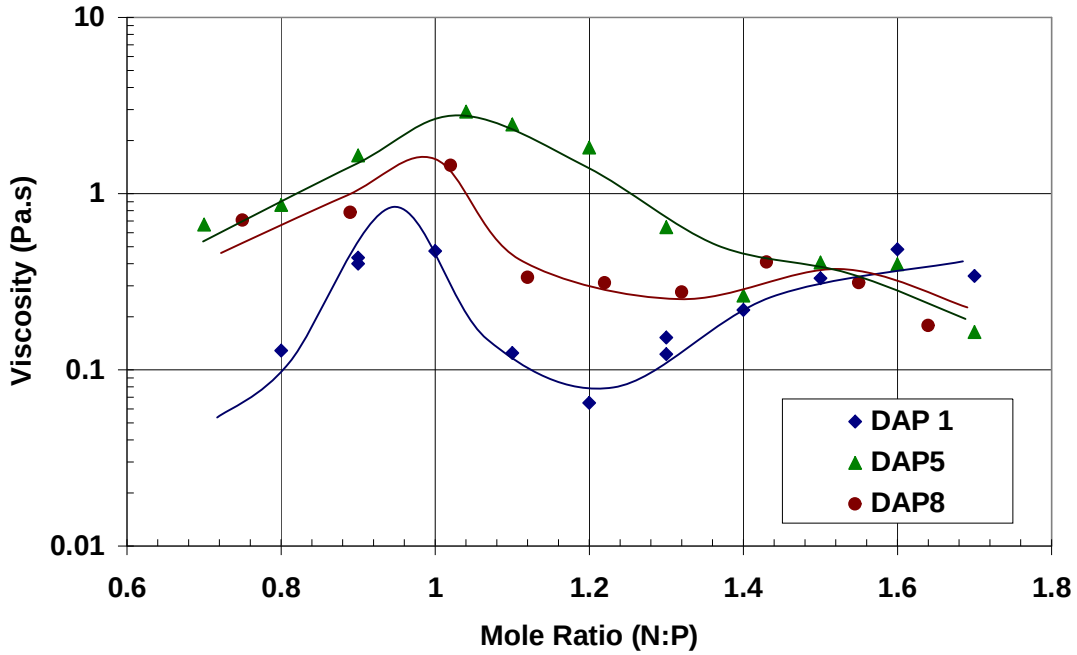

Figure 31: Change in Viscosity for Slurries with Varying Aluminium Content

3.2.5.3 Changes with Magnesium Content

Figure 32 shows the change in viscosity (at 40 s^{-1} shear rate, 1.55 specific gravity) vs mole ratio (MR) for the as-received acid and the acid containing additional magnesium content (DAP7). There is no clear consistent trend in the change in viscosity with this data. The mole ratio vs specific gravity correlations used to gather this data tended to be quite poor. There was insufficient remaining as-received acid to perform additional testing with magnesium. It is possible that additional magnesium increases the sensitivity of the viscosity to inconsistencies between experiments.

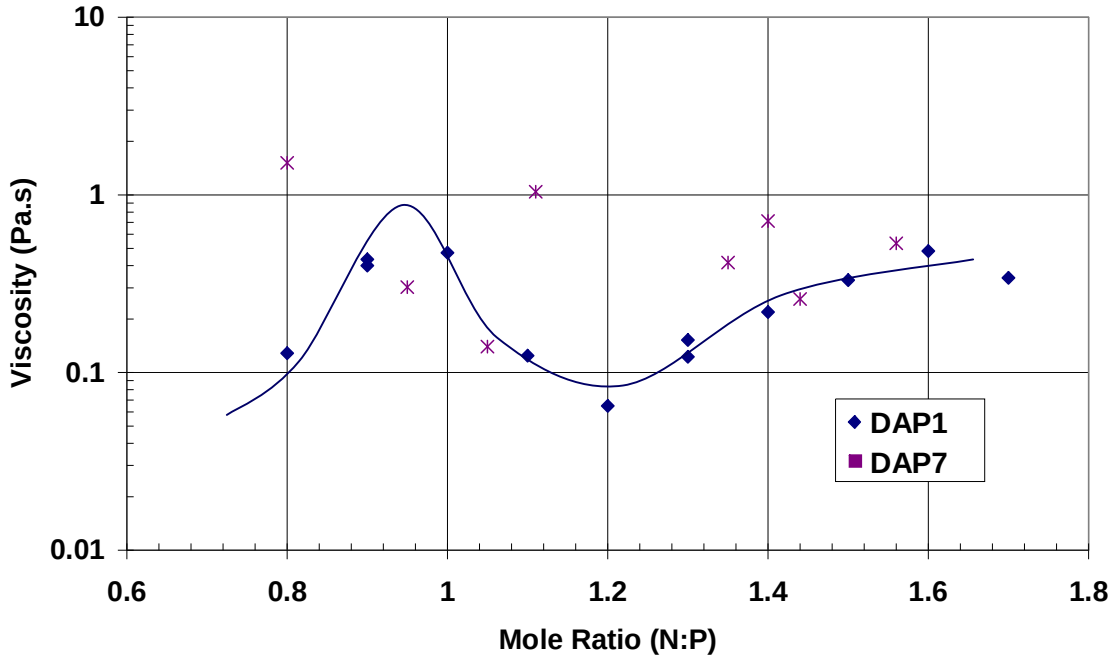

Figure 32: Change in Viscosity for Slurries with Varying Magnesium Content

3.2.5.4 Changes with Similar Mass of Impurity Added

Whilst some viscosity changes may be the result of interactions of the specific metal impurities, such as through a change in surface chemistry, or chemical composition, it is also possible that the addition of the impurity by itself, regardless of the type, could result in the viscosity change. Such a change could occur due to an increase in solids loading, for instance. To isolate such changes, the results for different impurities with similar weight content are examined together.

Figure 33 shows the change in viscosity with mole ratio for DAP 1, DAP 2, DAP 5 and DAP 7. In terms of the weight of metal impurity added to the as received DAP 1 acid, DAP 2 and DAP 5 are very similar. The weight of magnesium added to produce DAP 7 was about 50% greater than the weight of iron and aluminium added to form DAP 2 and DAP 5 respectively. There does not appear to be any correlation between the viscosity of a slurry and the weight of metal ion impurity added to it.

Furthermore, the graph shows that each element acts independently in the way it alters the viscosity.

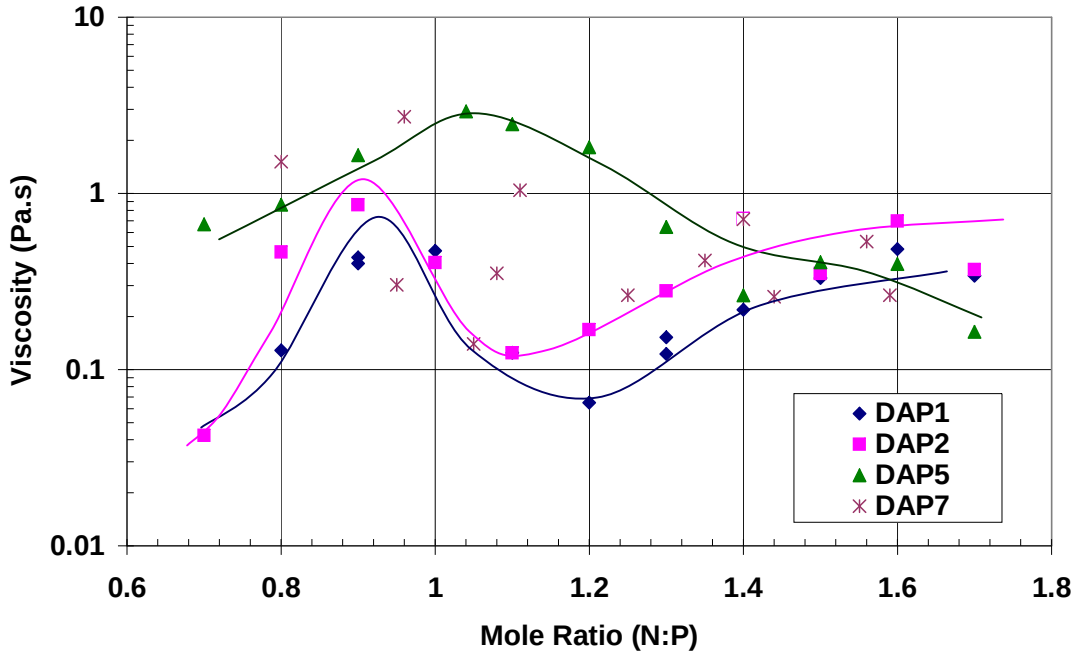

Figure 33: Viscosity Vs Mole Ratio For Slurries With Similar Mass Of Impurity Added.

3.2.5.5 Viscosity Response to the Specific Gravity

An increase in specific gravity correlates to a decrease in the water content for a given slurry, resulting in a higher viscosity. A power law correlation was (generally) fitted to the viscosity vs specific gravity data, in the form of $\mu = K(SG)^n$, where μ is the viscosity, *SG* the specific gravity and *K* and *n* are empirical constants. A higher exponent value, n, for these correlations should indicate the sensitivity of the viscosity to changes in specific gravity. Whilst no consistency was found for changes in the exponent value with changing mole ratio, the average value for the exponent value across all mole ratios did change, for each acid tested. The average value for the as-received acid and the acids with additional iron was 25. With the aluminium acids this decreased slightly to 20, whilst the magnesium acid's average exponent value was

just 7.5. This means that the additional magnesium in effect reduces the comparative viscosity increase resulting from an increasing specific gravity, as shown in Figure 34.

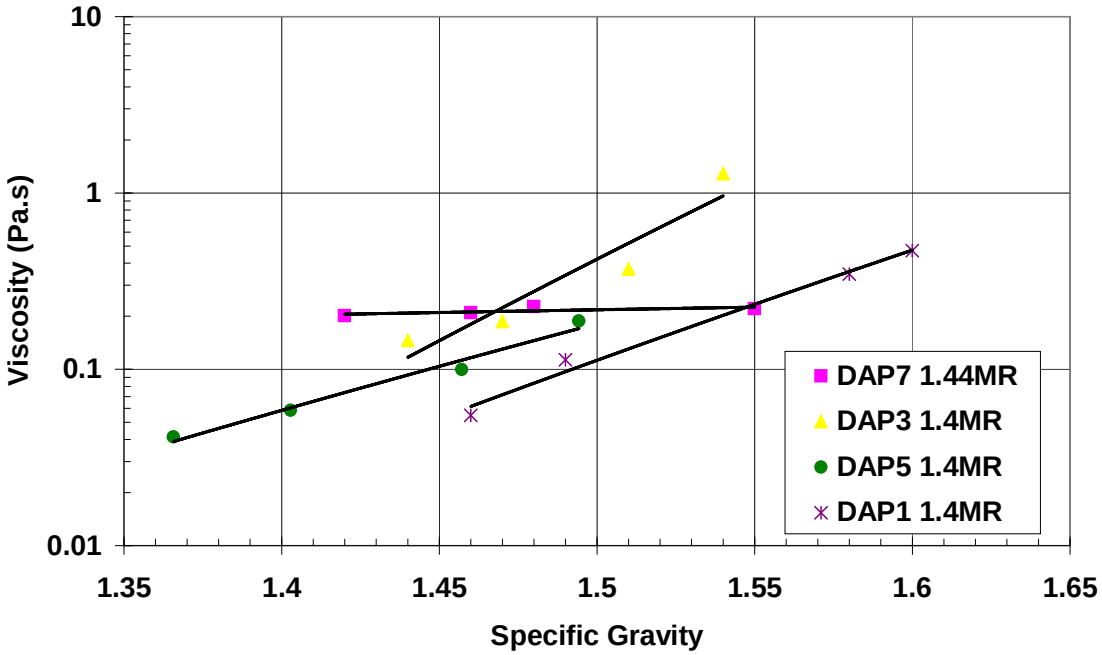

Figure 34: The Effect of Specific Gravity on the Viscosity for Acids Containing Additional Iron (DAP3), Aluminium (DAP5) And Magnesium (DAP7) at ~1.4 MR Compared to the As-Received Acid (DAP1). A Power Law Regression Has Been Fitted To Each Set Of Data.

3.2.6 Laboratory Based Slurries

Slurries made from pure phosphoric acid with fixed impurity concentrations were produced to attempt to isolate any changes in the viscosity to the specific metal ion impurities that caused them. As a baseline, pure phosphoric acid with zero impurity was produced. However, the solution formed large crystals. These crystals settled to the bottom of the solution. The top portion of the slurry subsequently lowered in viscosity, whilst the lower portion increased in viscosity as the crystals settled and compacted, making the rheology unmeasurable.

3.2.6.1 Pure Phosphoric Acid Based Slurries With 3% Impurity

The change in viscosity of slurries made with 40% P_2O_5 and 3% impurity are shown in Figure 35. The impurity level is in terms of weight percent of MgO, Al_2O_3 and Fe_2O_3 for the magnesium, aluminium and iron respectively. In terms of moles of each metal present, the aluminium doped acid had 57% more moles of aluminium than the iron doped acid had moles of iron. The magnesium doped acid had the highest number of moles of impurity added, with twice the number of moles of metal impurity than in the iron doped acid. The mole ratio is important as the number of compounds or hydrolysis products formed from the impurities are likely to have a greater effect on viscosity than the mass of the impurities. Viscosity values are for a specific gravity of 1.55 and a shear rate of 40 s^{-1}. These values were interpolated from viscosity trends over several specific gravity determinations, as with the plant acid samples.

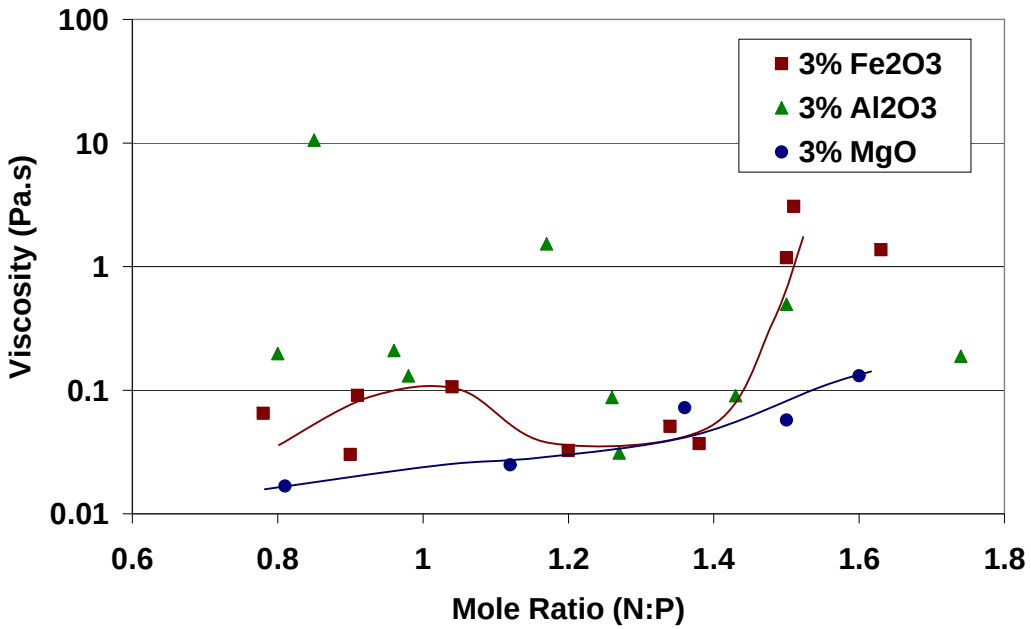

Figure 35: Viscosity Vs Mole Ratio for Pure Ammonium Phosphate Slurries Containing Metal Impurity.

Magnesium has the lowest viscosity across almost all mole ratios. In general, the viscosity gradually increased with increasing mole ratio, from 0.017 Pa.s at 0.81 MR to 0.13 Pa.s at 1.6 MR.

Iron displayed higher viscosity levels than magnesium across the majority of mole ratios. There appeared to be a wide hump in the viscosity close to 1.0 MR, probably due to the crystallisation and dissolution of mono-ammonium phosphate. The viscosity was at a low of between 0.3 and 0.5 Pa.s for mole ratios between 1.2 and 1.4. After 1.4 MR the viscosity increased markedly and appeared to remain consistent at above 1.0 Pa.s for mole ratios above 1.5.

Aluminium was more erratic than the other two elements and had a generally higher viscosity in the lower mole ratio range.

3.2.6.2 Pure Phosphoric Acid Based Slurries Containing Fluorine

Spot tests were performed on solutions containing metal impurities with fluorine. The tests were only performed at one or two specific gravities, therefore the results need to be compared to the viscosity versus specific gravity data of the solutions prepared without fluorine. It was intended that one high and one low mole ratio sample be gathered for each metal impurity with fluorine, however a low mole ratio magnesium sample was not performed as crystals were not observed to have formed.

Figure 36 shows a single point viscosity measurement for slurry containing 3% MgO and 2% F plotted against the trends in viscosity found for different mole ratios for a 3% MgO slurry. The fluorine-containing sample showed approximately a 3-fold increase in the viscosity compared to the sample without fluorine, for the same specific gravity and mole ratio.

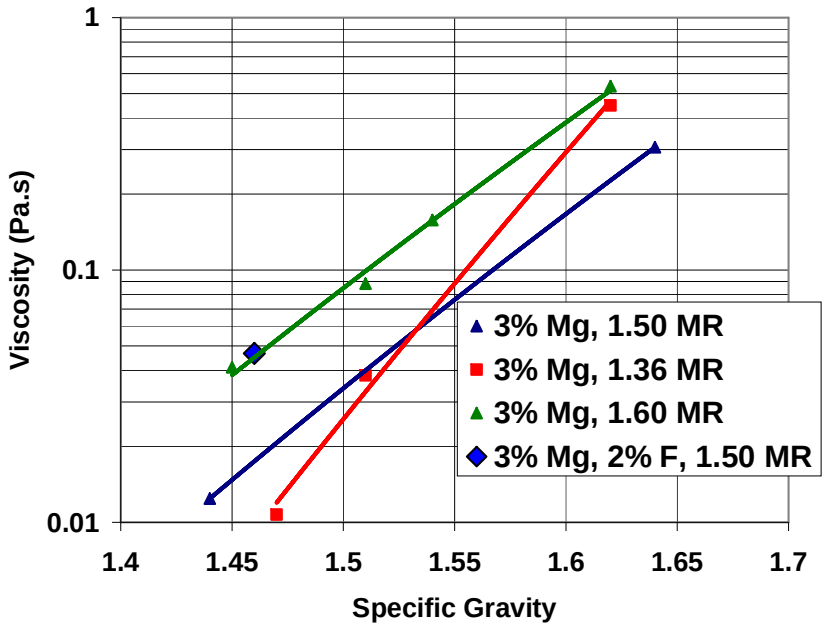

Figure 36: Change in Viscosity on Addition of Fluorine for Pure Ammonium Phosphate Slurries Containing Magnesium.

Fluorine appears to have reduced impact on the viscosity at low mole ratio in high aluminium slurries. Figure 37 shows that a 0.86 MR slurry containing fluorine has a viscosity that is about 30% less than a 0.85 MR slurry without fluorine. This difference can be considered to be within experimental error and it would not be unusual to see this level of fluctuation between repeat measurements. Figure 38 on the other hand, shows a 20-fold increase in the viscosity of a 1.46 MR slurry with fluorine compared to a 1.43 MR slurry without fluorine. Whilst only a single point is shown, it is clear that the addition of fluorine has had a substantial affect on the viscosity at high mole ratio.

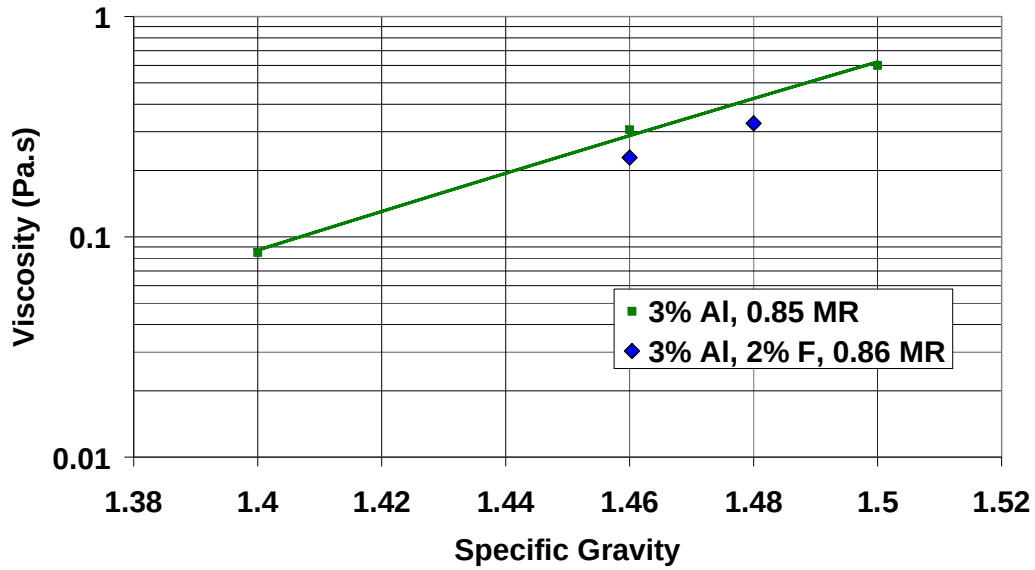

Figure 37: Change in Viscosity on Addition of Fluorine for Pure Ammonium Phosphate Slurries Containing Aluminium at Low MR.

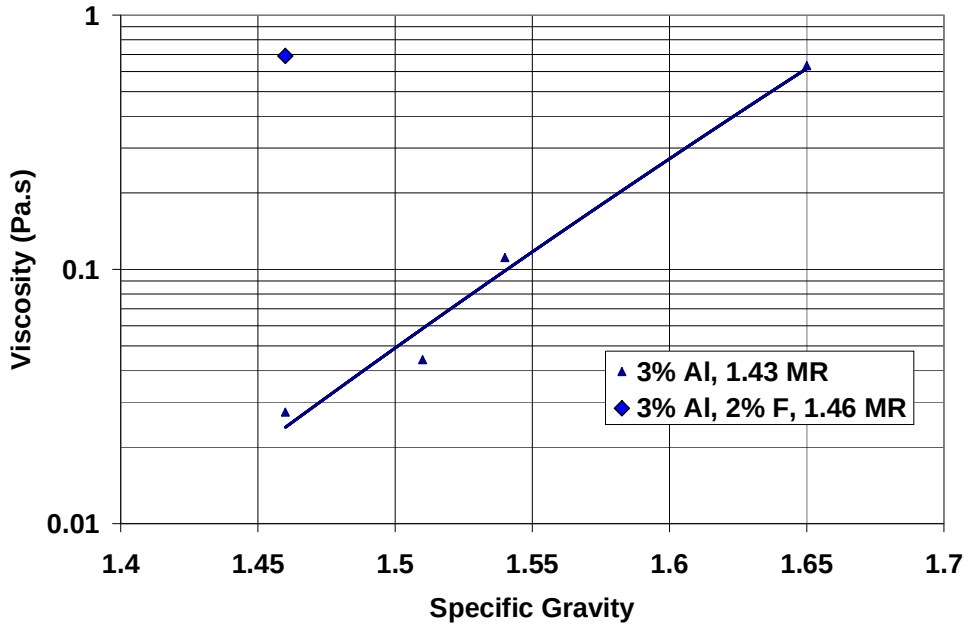

Figure 38: Change in Viscosity on Addition of Fluorine for Pure Ammonium Phosphate Slurries Containing Aluminium at High MR.

Similar to aluminium, low mole ratio slurries containing iron did not appear to be significantly affected by the addition of fluorine, whereas high mole ratio slurries were. Figure 39 shows that the viscosity for a 0.85 MR slurry containing fluorine lies intermediate of a 0.78 MR and a 0.91 MR slurry without fluorine. Figure 40 appears to show that fluorine leads to an increase in viscosity at high ME and Fe content. Unfortunately, the data for the 1.63 MR slurry without fluorine does not follow the expected trend of increasing viscosity with increased specific gravity and therefore should be examined with caution. Nevertheless, the sample with fluorine has a high enough viscosity to conclude that the addition of fluorine leads to a viscosity increase.

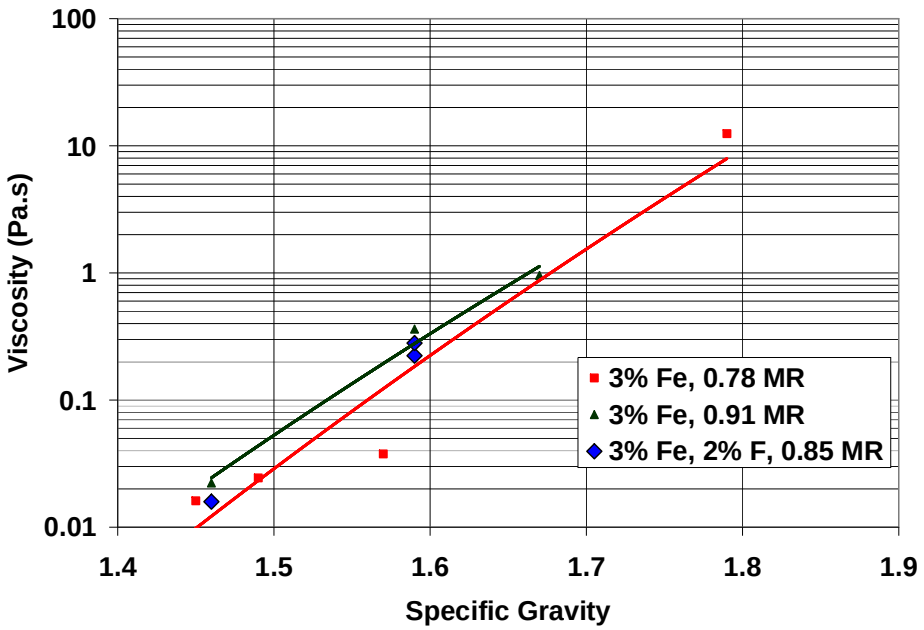

Figure 39: Change in Viscosity on Addition of Fluorine for Pure Ammonium Phosphate Slurries Containing Iron at Low MR.

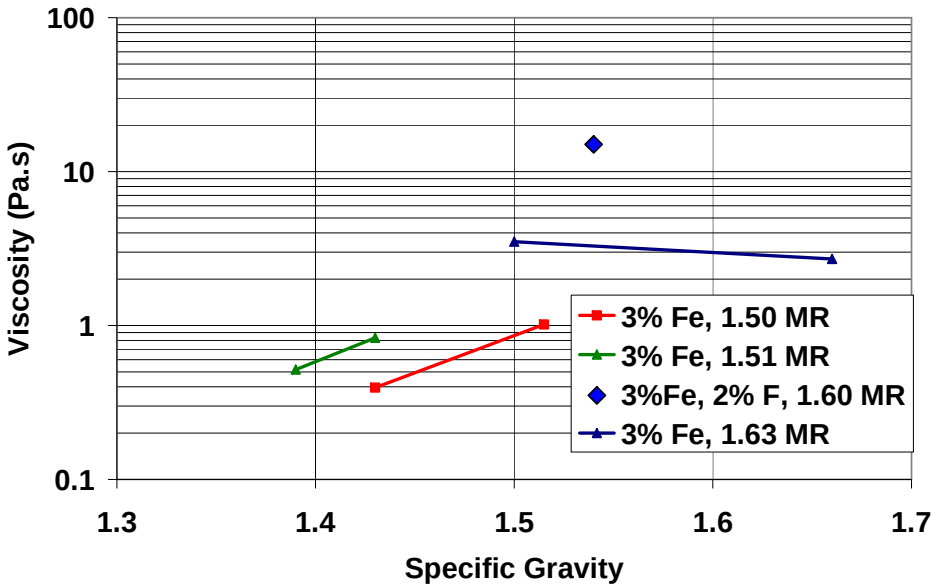

Figure 40: Change in Viscosity on Addition of Fluorine for Pure Ammonium Phosphate Slurries Containing Iron at High MR.

3.3 Discussion

The DAP1 plant acid slurry viscosity vs. mole ratio trend compares favourably to the literature. Both Ando and Akiyama (1972) and Tang et al. (2004) showed trends with a peak in the viscosity occurring at 0.8-0.9 MR as with the DAP1 data. This is unexpected because the minimum solubility point of MAP occurs at 1.0 MR. Maximum solids content should coincide with the maximum viscosity. The similarity to the literature means that the trends in the results can be considered reflective of typical slurry characteristics.

The slurries containing additional iron (DAP2 and DAP3) showed increases in the maximum viscosity of the peak occurring at 0.9 MR and also increased viscosity above 1.2 MR for increased iron content. It can therefore be concluded that iron will have a significant effect on the viscosity during the production of di-ammonium phosphate, where the mole ratio in the pre-neutraliser is typically 1.55-1.60. During

production of mono-ammonium phosphate, where the slurry mole ratio is typically 0.65-0.7, the iron content does appear to have an influence on the viscosity; however the viscosity is around an order of magnitude lower for the same specific gravity and shear rate, compared to that during di-ammonium phosphate production. This means that ore with high iron content can be more effectively processed under MAP conditions than under DAP conditions.

The slurries containing additional aluminium (DAP5 and DAP8) showed an increase in the viscosity across all mole ratios below 1.3 MR. Above 1.4 MR the viscosity shows no significant change and may in fact decrease with increased aluminium content. This observation would lead us to believe that slurries containing high aluminium content should not be processed under MAP conditions. Under DAP conditions the aluminium content appears to have no effect.

The slurries containing the additional magnesium (DAP7) showed irregular and inconclusive changes in the viscosity with changing mole ratio. The change in the viscosity was not considered significant, since the magnesium content of the slurry was increased approximately 15-fold. When also considering that magnesium has a lower molecular weight than aluminium and iron (the relative molar masses being 24.3, 27 and 58.7 respectively), and therefore should have a greater number of moles of metal ion in solution, the changes in the viscosity of the slurry are not noteworthy. It can be concluded that production under DAP conditions would not be affected by increased magnesium. The amount of data for below 1.0 MR is small however, so there may be an affect during production under MAP conditions.

Interestingly, the shape of the viscosity vs mole ratio curves was different for aluminium and iron. In the literature, the aluminium and iron are commonly referred to together, as R_2O_3, where R can be either Fe or Al. Therefore, it was assumed that the effect of altering the concentration of either would be similar, although not identical. Instead, the effect is completely opposite. Iron increases the peak of the viscosity at 0.9 MR. Aluminium has a significant affect on broadening the peak, particularly on the side above 0.9 MR. Iron increased the viscosity in the higher mole

ratio range, whilst aluminium had no real effect. This suggests that high iron and high aluminium ores will be problematic to process at any mole ratio.

The graphs based on pure ammonium phosphate with added impurity reflect some of the observations of the plant acid slurries. Slurries containing iron showed sharp increases in the viscosity above 1.5 MR. In the plant acid slurries, this increase in the viscosity at higher mole ratios manifested itself at a lower mole ratio for each increase in iron content. A small hump in the viscosity can be observed around 1.0 MR for the 3% Fe_2O_3 slurry. This hump was not as large as that seen in DAP1, DAP2 and DAP3 and also occurred as originally expected at 1.0 MR, rather than at 0.9 MR for the plant acid slurries and in the literature. The pure acid slurries containing aluminium were generally higher in viscosity than the iron containing slurries for low mole ratios and lower in viscosity for high mole ratios. The pure slurry containing magnesium was low in viscosity across all mole ratios.

It is clear that, due to the three impurities having different effects on the viscosity of the slurries, changes in the viscosity can not be put down to simple physical changes such as increased solids content. Possible reasons for the varying effects include changes in particle size, formation of varying chemical complexes and the interparticle effects and pH range of formation for such compounds. It is the intention of the subsequent chapter to further investigate these areas. Furthermore, the effect of viscosity on the operation of the industrial PN reactor is examined in appendix I using computational fluid dynamics.

4.0 PROPERTIES OF AMMONIUM PHOSPHATE SLURRIES

4.1 Introduction

In addition to the viscosity characterisation work performed on the ammonium phosphate slurries, auxiliary work on the properties of ammonium phosphate slurries was conducted in order to better understand the mechanisms involved in viscosity change. This chapter presents:

- Crystal composition of slurries determined by XRD/XRF
- Particle size of slurries determined by Malvern Particle Size Analyser
- Visual observations on crystal size and colour
- Solubility of metal ion impurities with mole ratio
- The effect of impurities on the titration used to determine the mole ratio
- A discussion on the mechanisms for viscosity change, based on the above experiments and the viscosity work.

4.2 Composition of Plant Acid Slurries

For each mole ratio tested for the acids DAP 1, DAP 2 and DAP 3, a cooled sample of the slurry was sent away for XRD and XRF Analysis to determine their chemical composition. The results from these tests are summarised in Table 5,
Table 6 and Table 7 for DAP 1, DAP 2 and DAP 3, respectively. The highlighted sections indicate the mole ratios where the respective impurity was detected. The crystal structure results showed that the predominant compounds present were mono-ammonium phosphate and di-ammonium phosphate. Mono-ammonium phosphate was found in each slurry examined. In general, di-ammonium phosphate was also found above a mole ratio of 1.2. Di-ammonium Sulphate was also found at 1.1 MR for all three acids and was also found at several other mole ratios in DAP 1 and DAP 2.

The majority of the compounds detected that were not made purely of ammonia, phosphate or sulphate compounds (or closely related compounds) contained iron. Iron was present in DAP 1 acid at 12000 ppm, aluminium at 3200 ppm, and magnesium at 750 ppm. In DAP 2 and DAP 3, the concentration of iron was significantly increased. No aluminium or magnesium compounds were detected during testing. Most of the iron based compounds detected were found in the lower mole ratio range. It is possible that further precipitation of ammonium phosphates at higher mole ratios effectively diluted these compounds to an extent that they are barely detectable.

The high concentration of ammonium phosphate crystals dwarfed the amount other crystalline compounds formed by metal ions. As a result it is not possible to determine the concentration of these impurities crystalline compound accurately. Many of these compounds were tagged with 'minor' (M), 'possible' (P) or 'trace' (T), reflecting the high degree of inaccuracy of the determination at very low concentrations. As a result there was no consistency with the compounds found over varying mole ratio or changing iron content. Several laboratory ammonium phosphate samples (with various levels of metal ions impurities and at different mole ratios) were also sent for XRF/XRD analysis. Interestingly some of the samples are predominantly amorphous or had very low crystalline content. The reason for this result is yet unclear and this may have something to do with the procedure of collecting and drying the slurry for the test. XRF/XRD is useful as it can be used to determine the compounds formed by metal ions impurities provided the compounds are crystalline in nature.

Table 5: Impurity Composition in DAP1 Slurries Determined By XRD/XRF. A Highlighted Cell Indicates The Mole Ratio Where The Compound Was Detected.

DAP 1	Mole Ratio											
					1	1.1	1.2	1.3	1.4	1.5		1.7
AmmPhosphates/Sulphates												
$NH_4H_2PO_4$												
$(NH_4)_2HPO_4$												
$(NH_4)_2SO_4$												
Iron sulphates												
$Fe_2(SO_4)_2(OH)_5(H_2O)$					TP							
Iron Phosphates												
$Fe_2P_2O_7.2H_2O$										M		
Iron-Amm-Sulphates												
$NH_4Fe(SO_4)_2$										M		
Iron Oxides												
Fe_3O_4									MP			

Table 6: Impurity Composition in DAP2 Slurries Determined By XRD/XRF.

DAP 2	Mole Ratio											
		0.7	0.8	0.9	1	1.1	1.2	1.3	1.4	1.5	1.6	1.7
AmmPhosphates/Sulphates												
$NH_4H_2PO_4$												
$(NH_4)_2HPO_4$												
$(NH_4)_2SO_4$												
NH_4HSO_4		MP										
$(NH_4)_5P_3O_{10}.2H_2O$										M		
Iron Sulphates												
$FeSO_4.4H_2O$				MP								
$Fe_3(SO_4)_4.14H_2O$												
$Fe(OH)SO_4$			M	MP								
Iron Phosphates												
$Fe_5P_4O_{20}H_{10}$		MP		M								
$Fe_7(PO_4)_6$			MP	MP	MP		MP		MP			
$FeH_2P_3O_{10}.H_20$		MP										
$FePO_4.2H_2O$				MP								
$Fe_2PO_4(OH)$										P		
$Fe_2P_2O_7.2H_2O$												
Iron Oxides												
$Fe_2O_3.1½H_2O$										P		
$Fe(OH)_3$			M									
$FeO(OH)$												
Iron-Amm-Phosphates												
$(NH_4)_2FeOHP_2O_7.2H_2O$										M		
Others												
$Ca_{10}(OH)_2(PO_4)_6$										M		
SiO_2												

Table 7: Impurity Composition in DAP3 Slurries Determined By XRD/XRF.

DAP 3	Mole Ratio											
		0.7	0.8	0.9	1	1.1	1.2	1.3	1.4	1.5	1.6	
AmmPhosphates/Sulphates												
$NH_4H_2PO_4$												
$(NH_4)_2HPO_4$												
$(NH_4)H_5(PO_4)_2$				MP	MP	MP						
$(NH_4)_2S_2O_5$				MP	MP							
$(NH_4)_2SO_4$							MP					
Iron Sulphates												
$Fe(OH)SO_4$			MP									
$FeH(SO_4)_2.4H_2O$				MP	MP							
$Fe_4(OH)_{10}SO_4$		T										
Iron Phosphates												
$Fe(PO_3)_2$		T										
$Fe_7(PO_4)_6$		MP						MP	MP	MP		
$Fe_3(PO_4)_2(OH)_3$		T	MP									
Iron-Amm-Sulphates												
$(NH_4)Fe_3(SO_4)_2(OH)_6$												
Iron Oxides												
FeO(OH)							MP					
$Fe(OH)_3$												
Iron-Amm-Phosphates												
$NH_4Fe(HPO_4)_2$			MP									
Others												
SiO_2		T	MP									

4.3 Particle Size

Observations made on the slurries produced for the viscosity tests demonstrated that pure phosphoric acid formed large crystals that settled very rapidly to the base of the solution, as shown in Figure 41. The settled layer is very compact and becomes difficult to redisperse by mixing. However, the ammoniation of pure phosphoric acid doped with soluble aluminium or iron did not produce the same large crystals that settled rapidly. See Figure 41 (ii) and (iii). The slurries are flocculated and the particle size must be very small; in the colloidal size range. They settled with a thin layer of supernatant liquid, a characteristic typical of flocculated dispersions. In engineering terms, these slurries are considered stable as they will not settle to form a hard compact layer. It is possible to measure the rheological properties of these

slurries. The significant reduction in the crystal size is due to the metal ion impurities. The mechanisms for the particle size reduction will be discussed in a later section.

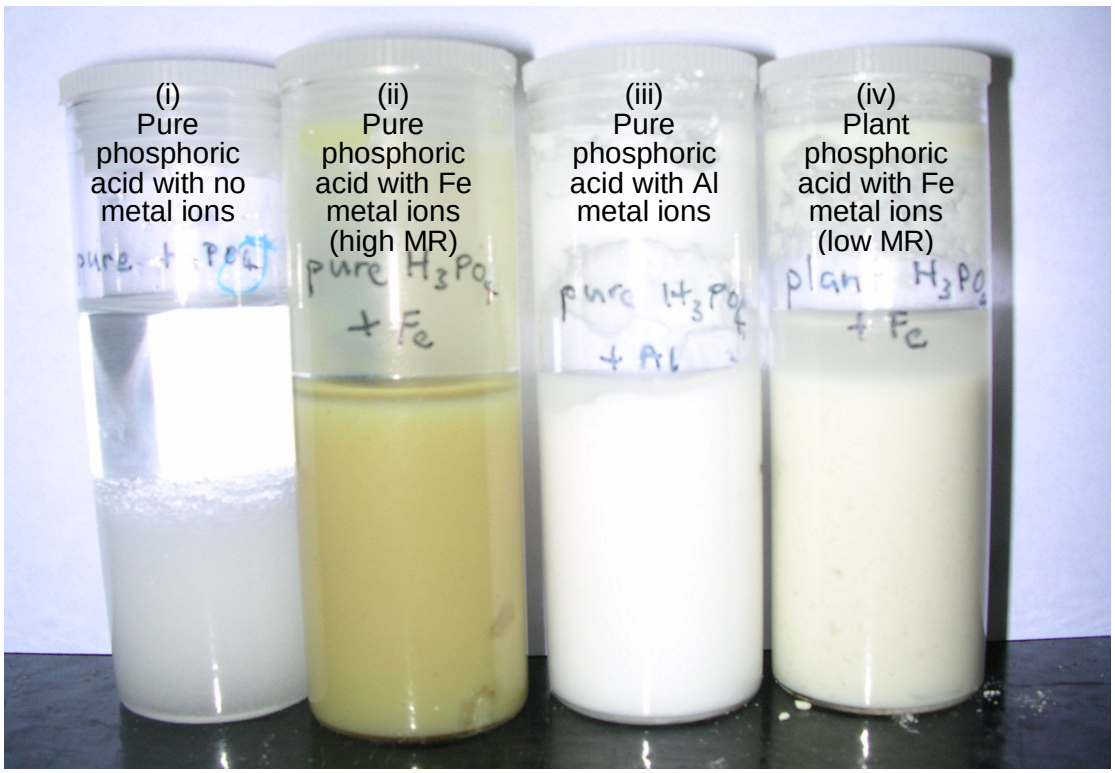

Figure 41: Images Of Slurries Prepared From Pure Phosphoric Acid With (I) No Metal Ions Impurities, (Ii) Fe Added (High Mole Ratio), (Iii) Al Added And (Iv) From Plant Phosphoric Acid (Low Mole Ratio).

4.3.1 Plant Acid Slurries

Tests were performed to determine the particle size distribution of the slurries formed from plant phosphoric acid at various mole ratios. Each acid was continuously ammoniated as per section 3.1 and samples were removed periodically at different mole ratios. Each sample was sized with the Malvern Particle Size Analyser. The Malvern Particle Size Analyser uses a laser diffraction light scattering technique. The samples were also sonicated to ensure particles did not coagulate, however this had no effect on the result.

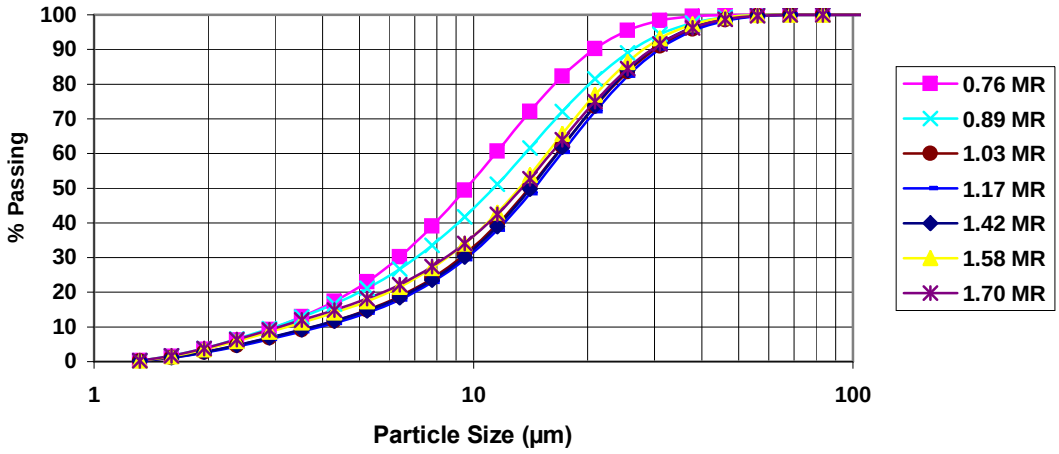

Figure 42: Particle Size Distribution For Various Mole Ratios Of Slurry Made From DAP 1 Acid.

Figure 42 shows the particle size distribution at various mole ratios of slurries made from DAP 1 acid. The smallest particle average particle size is at the lowest mole ratio of 0.76. The average particle size or d50 increases with increasing mole ratio, up to 1.17 MR. Between 1.17 and 1.42 MR, the particle size distributions overlay. However, at 1.58 and 1.7 MR, the particle size distribution becomes coarser, as reflected by the small decrease in the d50. The difference between the 50% passing sieve size for slurry with a mole ratio of 0.89, compared to that with a mole ratio of 1.17 is only about 30%. However, the viscosity difference for the same mole ratios was found to be about 600%. It is unlikely that the observed change in the particle size distribution can account for a viscosity difference of this magnitude.

Particle size analysis was repeated for slurries made with DAP2 and DAP3 acid, as shown in Figure 43 and Figure 44, respectively. Both show little variation in the particle size distribution with changing mole ratio. The trend for the particle size change was dissimilar to the particle size trend for DAP1 slurries, above. Instead, it appears that as the mole ratio increased the proportion of smaller particles also increased. Overall, there is not a significant change in the particle size distribution of DAP1, DAP2 and DAP3, as they change with mole ratio or as they relate to each other, that would adequately explain the observed viscosity differences.

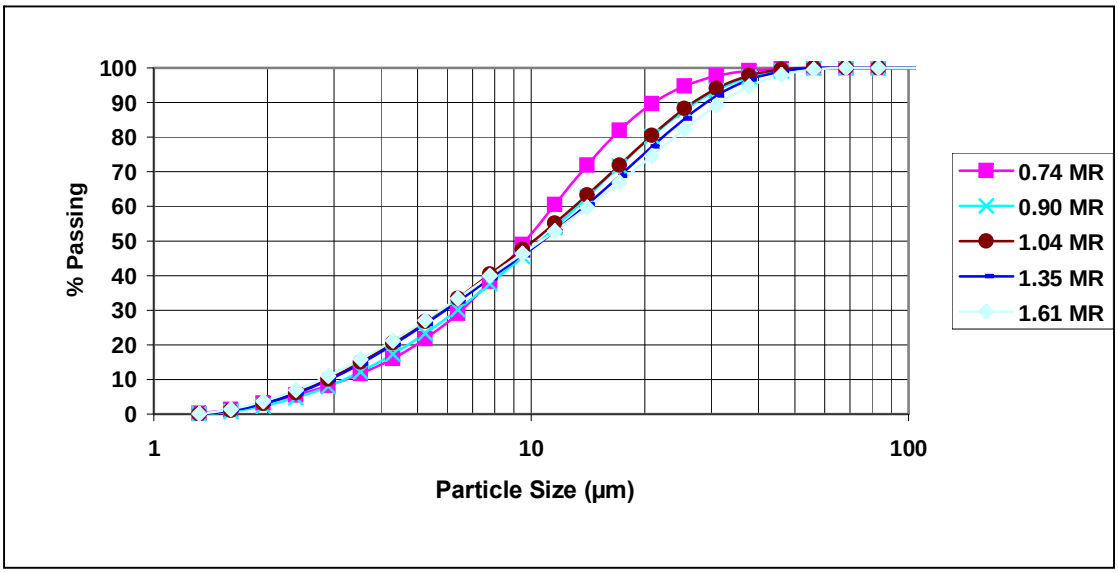

Figure 43: Particle Size Distribution For Various Mole Ratios Of Slurry Made From DAP 2 Acid.

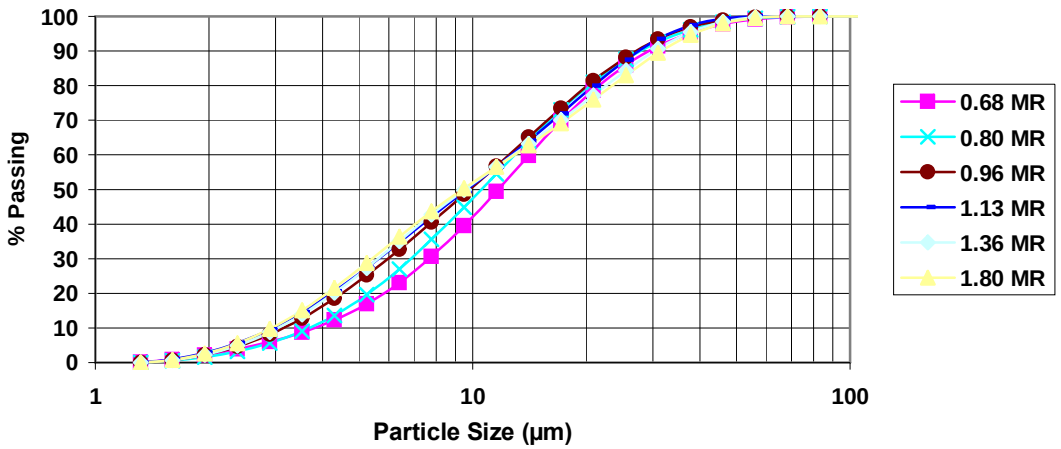

Figure 44: Particle Size Distribution For Various Mole Ratios Of Slurry Made From DAP 3 Acid.

In attempting to find the particle size distribution of pure ammonium phosphate, it was found that the pure crystals dissolve rapidly in water. As the particle sizing machine requires the sample to be dispersed in a large volume of water, it can then be assumed that the particle size distributions determined for DAP1, DAP2 and DAP3 resulted from insoluble compounds that contained the metal ion impurities and any pure ammonium phosphate compounds were likely to have dissolved.

4.3.2 Laboratory Slurries

Samples were taken at various mole ratios and analysed using a Malvern Sizer Machine for slurries made from laboratory acids. It is clear to the naked eye that the impurities in the slurries led to smaller crystal sizes, as seen in Figure 45. Pure ammonium phosphate crystals are coarse, close to 1mm in size. With the addition of aluminium or iron, a fine talc-like powder results from the dried solution. Magnesium does lead to smaller crystals but not to the same extent, as the crystals seen are still relatively large. To give a real life example, the grain size of crystals resulting from pure slurries, slurries containing magnesium and slurries containing iron or aluminium could be compared to white sugar, castor sugar and icing sugar, respectively.

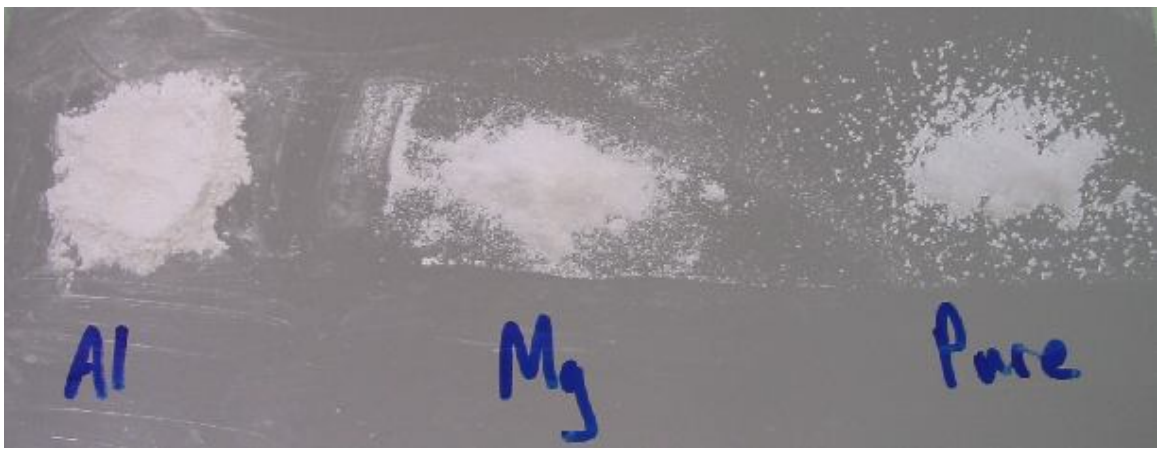

Figure 45: Dried Slurry Made From Pure Phosphoric Acid With 3% Impurity.

4.3.2.1 Pure Ammonium Phosphate Solutions

In the Malvern sizer machine, a portion of the sample is added to a large volume of water. When producing pure ammonium phosphate slurries without impurities, large crystals form. None of these crystals remain in solution when placed into the particle size machine; therefore their size could not be determined. Therefore, in the subsequent tests on slurries that contain impurities, it is highly likely that only the water insoluble content of the slurry is sized.

4.3.2.2 Iron

The mean and 10% passing size for various pure ammonium phosphate samples containing iron are shown in Figure 46. The low mole ratio 3% Fe_2O_3 sample has a relatively low mean particle size as it was collected when precipitates were first observed to be forming in the reactor beaker. The low mole ratio 6% Fe_2O_3 sample displayed a relatively high 50% passing particle size. However this was also collected at a very low mole ratio when only a small amount of precipitates would have formed and may be subject to error. Subsequent samples show a steady decline in the particle size with increasing mole ratio. These samples were repeated to confirm the trend as shown in Figure 46. This steady decline was reproduced. Mole ratios for the repeated data were not determined at the time. However, the data is presented in order of increasing mole ratio.

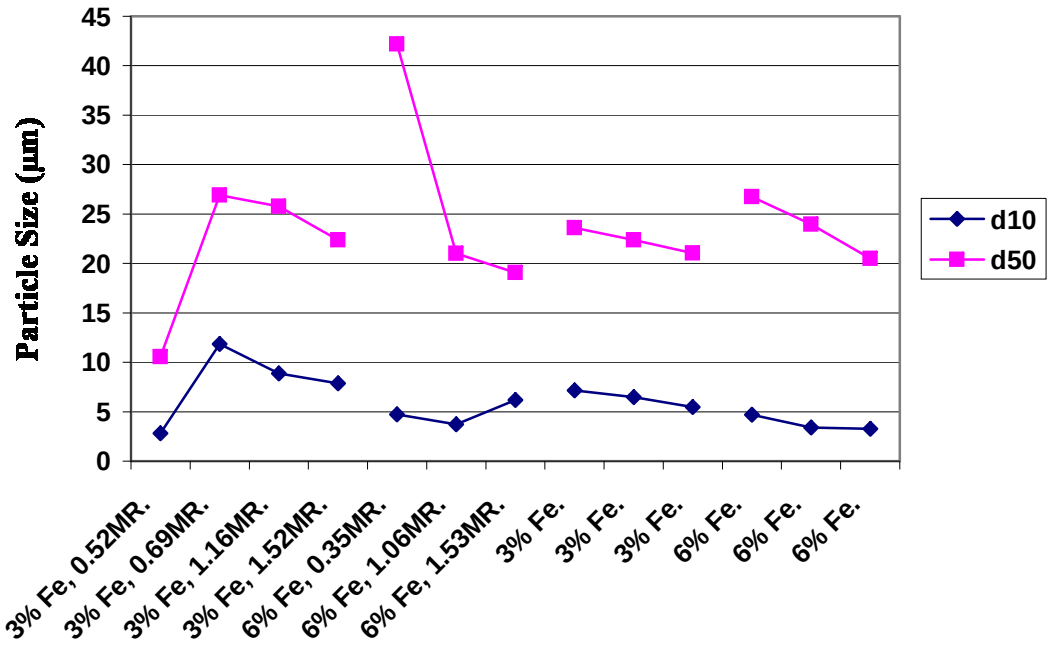

Figure 46: Mean (D50) And 10% Passing (D10) Particle Size Data For Pure Ammonium Phosphate Slurries Containing Iron.

4.3.2.3 Aluminium

Aluminium showed no apparent trend in the mean and 10% passing particle size data for 3% Al_2O_3 concentration, as seen in Figure 47. The average particle size was the lowest for the three metal ion impurities tested. The 1% Al_2O_3 slurry showed a sharp peak in the mean and 10% passing particle size at 1.47 MR.

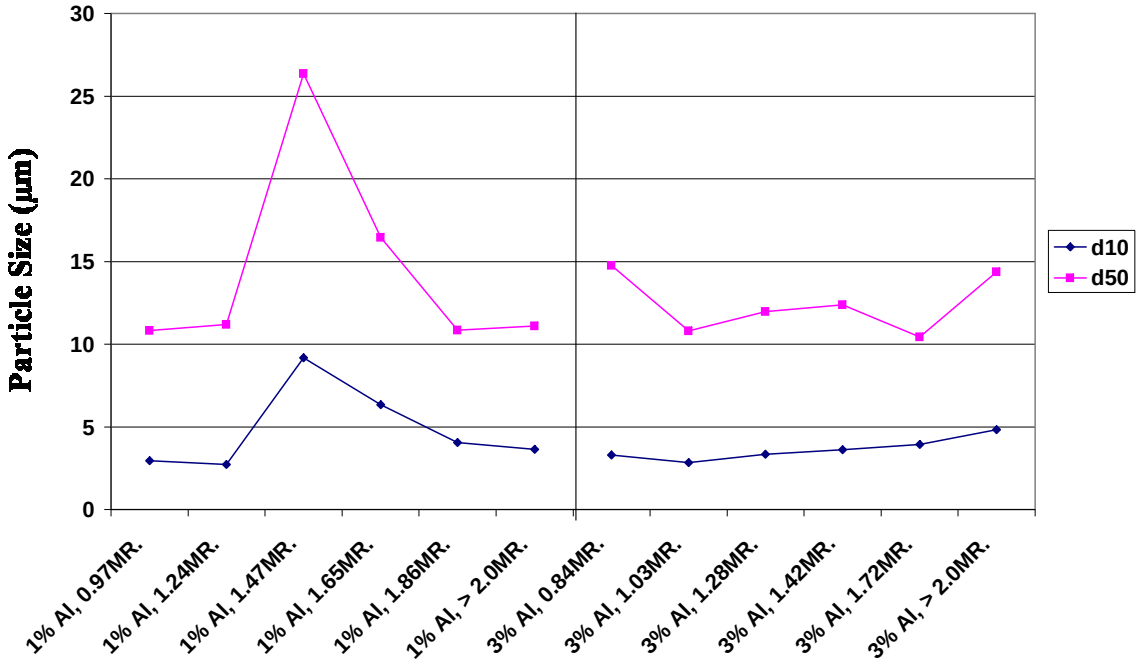

Figure 47: Mean (D50) And 10% Passing (D10) Particle Size Data For Pure Ammonium Phosphate Slurries Containing Aluminium.

4.3.2.4 Magnesium

Figure 48 shows that the particle size for slurry with 1% and 3% MgO does not change significantly with mole ratio, for both mean and 10% passing particle size, except at 1.28 MR for the 3% MgO sample. However, this spike occurs at the mole ratio that particles first form, possibly introducing some error into the determination. Magnesium had the largest insoluble particle size of the three metal impurities.

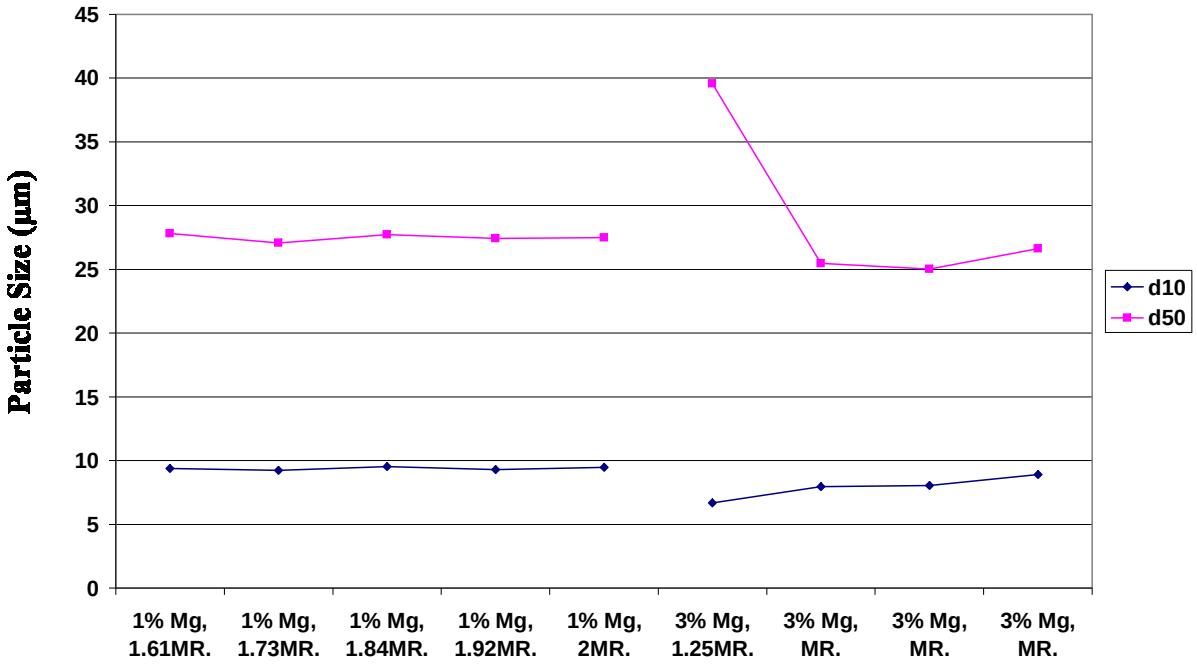

Figure 48: Mean (D50) And 10% Passing (D10) Particle Size Data For Pure Ammonium Phosphate Slurries Containing Magnesium.

4.3.2.5 Addition of Fluorine

Figure 49, Figure 50 and Figure 51 show that the addition of fluorine leads to a decrease in particle size. In Figure 49, the 10% passing and the mean particle size for the 3% Fe_2O_3 with 2% F acid, are just over half the values for the 3% Fe_2O_3 solution without fluorine. The most dramatic decrease is in the case of magnesium, where the 50% passing particle size has decreased from around 25um to 8um and the 10% passing particle size decreases from around 8um to less than 3um. The particle size data for aluminium with fluorine is erratic. However, there does appear to be a slight decrease in the 10% passing size. The particle size of aluminium with and without fluorine is as low as those of iron with fluorine and magnesium with fluorine, indicating that a minimal particle size may have already been reached.

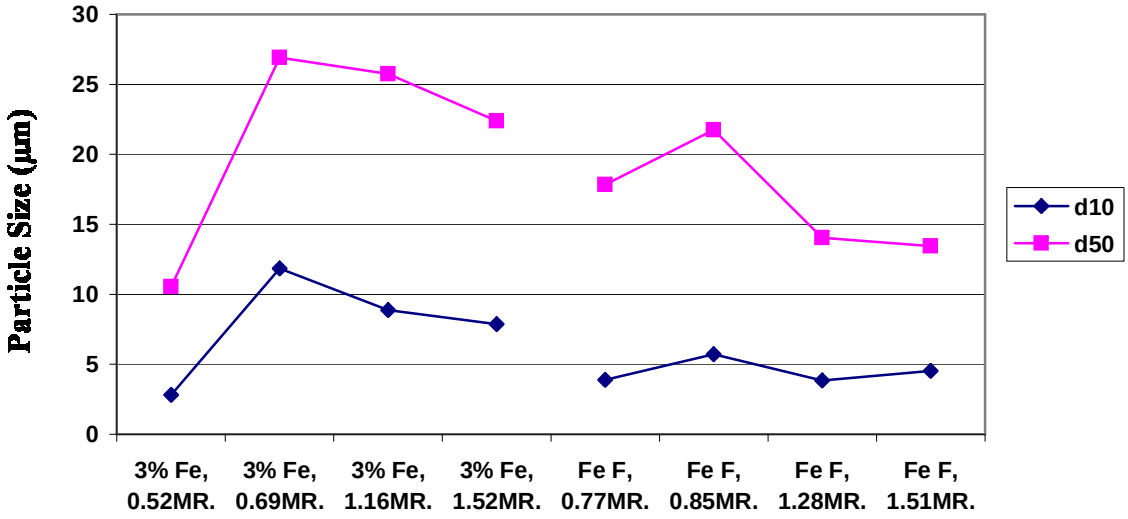

Figure 49: Particle Size Data for Slurry Containing 3% Fe_2O_3, With and Without Fluorine.

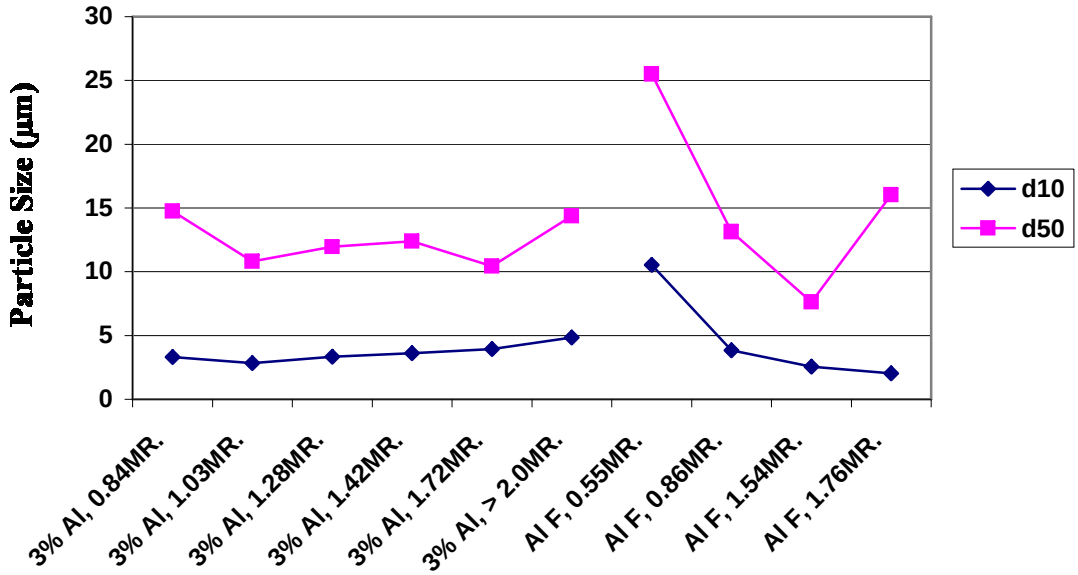

Figure 50: Particle Size Data for Slurry Containing 3% Al_2O_3, With and Without Fluorine.

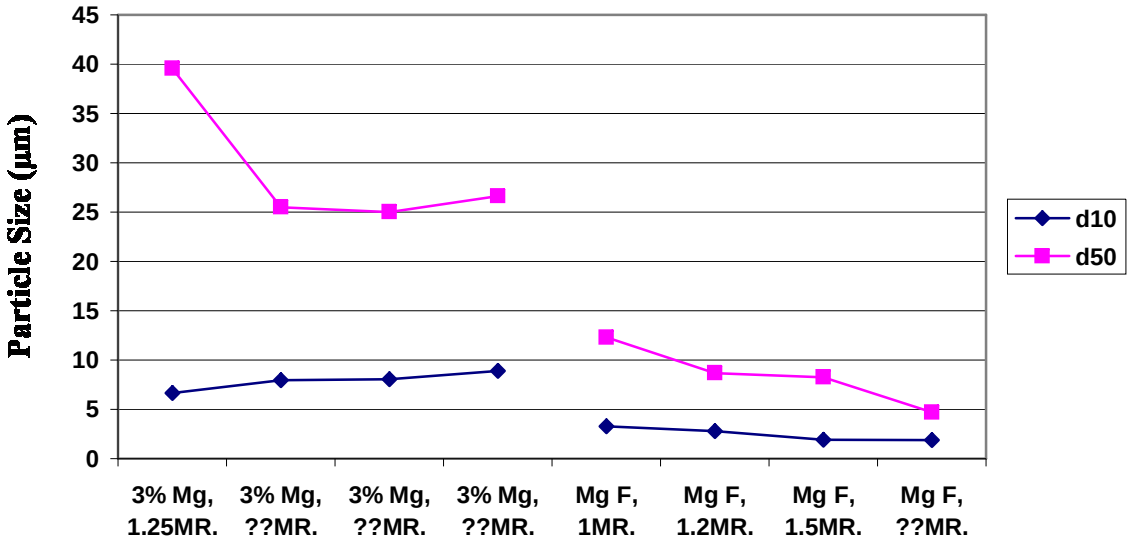

Figure 51: Particle Size Data for Slurry Containing 3% MgO, With and Without Fluorine.

4.3.2.6 Images under a Microscope

Figure 52 shows the pure phosphoric acid slurries with impurities viewed under a microscope. The affect of the addition of impurities on the crystal size of the slurry can be clearly seen. Furthermore, the microscope images allow us to view the soluble crystals that would have dissolved in the Malvern Sizer machine during the particle size analysis.

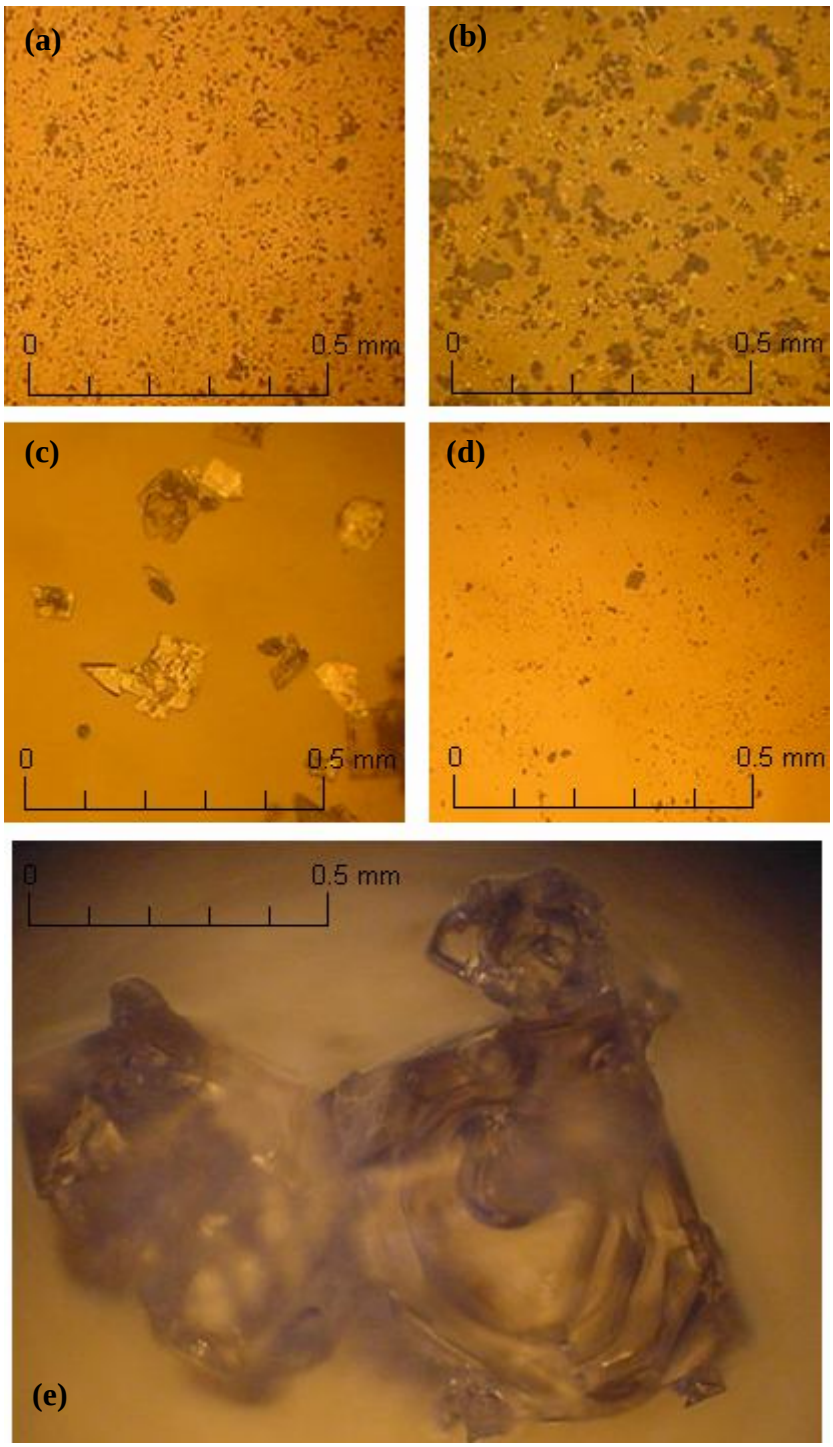

Figure 52: Crystals Viewed Under A Microscope. (a) Aluminium (b) Iron (c) Magnesium (d) Magnesium With Fluorine (e) Pure Phosphoric Acid. Crystal Number Density Is Not A Reflection Of Actual Slurry Characteristics.

4.4 Solubility

4.4.1 Solubility of Metals in Plant Acid

A beaker of as-received phosphoric acid (DAP1) containing a range of impurities was ammoniated and samples taken at various mole ratios, as per section 3.1. The samples were diluted with 50% vol of distilled water and the solids were allowed to settle. The filtrate was then taken with a 0.45µm syringe driven filter and sent for ICPAES analysis. The total solids content at each mole ratio was determined after rinsing with ethanol. The amount of each element in solution, relative to its original concentration, was back calculated and is shown in Figure 53. Since the iron, aluminium and magnesium are nearly completely removed from solution (at high mole ratio) it can be assumed that the compounds formed are predominantly insoluble in water. However, some phosphate and sulphur compounds initially present in the DAP1 solution dissolve during sample dilution and this is reflected by the increase in the calculated concentration after dilution.

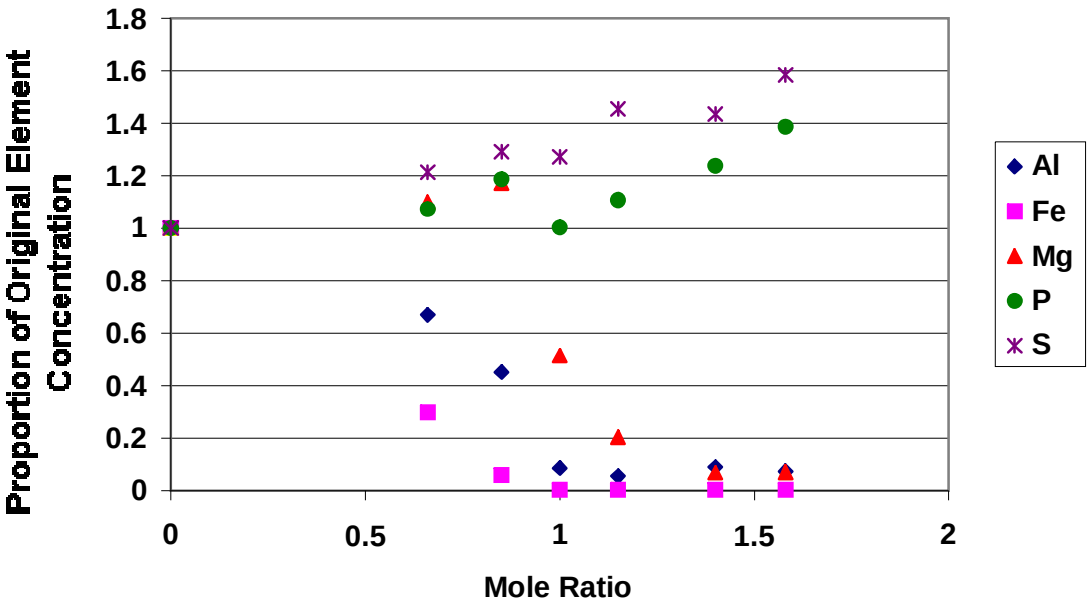

Figure 53: The Concentration of Selected Elements in Solution for Ammoniated Slurries of Various Mole Ratio Relative to the Original Concentration of the Acid.

Figure 53 shows that Mg (II) ions remain completely soluble at a relatively high MR of 0.85 or pH 3.2. The solubility decreases to 50% at MR 1.0 (pH 4.8) and then to 3% at MR 1.6 (pH 7.0). Mg(II) ions are hydrolysed to form $Mg(OH)^{+}$ at pH ~6.7.

Fe(III), Al(III) and Mg(II) metal ions will form hydrolysis products as the pH of the slurry increases with the degree of neutralisation or mole ratio. Figure 54 and Figure 55 show the hydrolysis products formed by Al(III) and Fe(III) over a range of pH and at ambient temperature (Baes and Mesmer 1986). The first hydrolysis product of Fe (III) is formed at a very low pH of 1.0. At pH 2.0 three hydrolysis products; $Fe(OH)^{2+}$, $Fe_2(OH)_2^{4+}$ and $Fe_3(OH)_4^{5+}$ in the following proportion 5%, 50% and 15% by weight of Fe, are formed. Al(III) forms its first hydrolysis product at a higher pH of ~ 2.5. Between pH 2.6 and 5.0, four hydrolysis products, $AlOH^{+}$, $Al_2(OH)_2^{4+}$, $Al_3(OH)_4^{5+}$ and $Al_{13}O_4(OH)_{24}^{7+}$ are formed. In terms of quantity $Al_{13}O_4(OH)_{24}^{7+}$ is most important. Data for the dimeric and trimeric species, $Al_2(OH)_2^{4+}$ and $Al_3(OH)_4^{5+}$, were obtained at elevated temperature; hence these hydrolysis products will also be formed in the ammonium phosphate slurry. Between pH 5.0 and 8.0, $Al_{13}O_4(OH)_{24}^{7+}$ is the only species present. Above pH 8.0, $Al_{13}O_4(OH)_{24}^{7+}$ will undergo further hydrolysis to form $Al(OH)_4^{-}$.

At MR 0.66 (pH 2.0), 70% of all Fe(III) ions are hydrolysed and this result is in good agreement with that in Figure 55, which shows the amount soluble Fe^{3+} ions left is about 30%. At MR of 1.0 (pH 4.8), the remaining 30% have dropped out completely as hydrolysis products. Figure 55 also shows that all Fe(III) ions are hydrolysed at pH 4.0; thus indicating good agreement with solubility results in Figure 53. According to Figure 54 no hydrolysis products of Al(III) ions should be formed at pH 2.0. The solubility results however show a 30% reduction in the Al(III) concentration. At pH 4.8 all Al(III) ions should be hydrolysed according to Figure 54. According to solubility data, the amount of Al(III) present is about 10%, which again indicates good agreement.

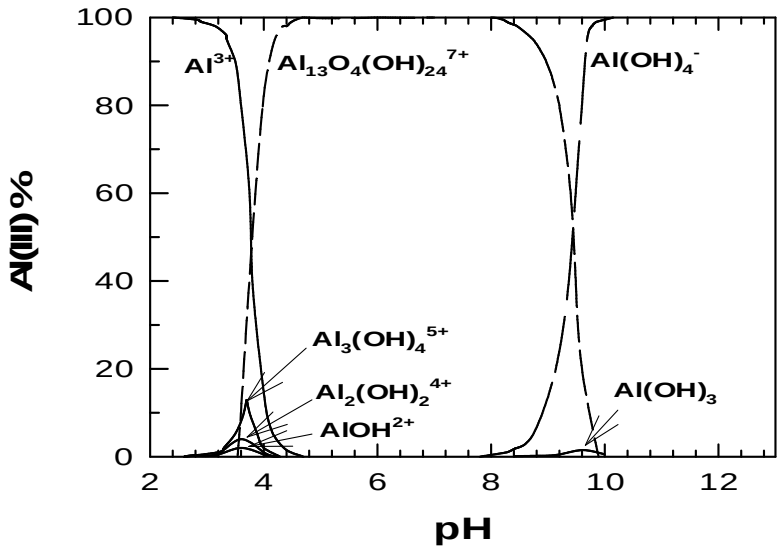

Figure 54: Hydrolysis Products for Aluminium

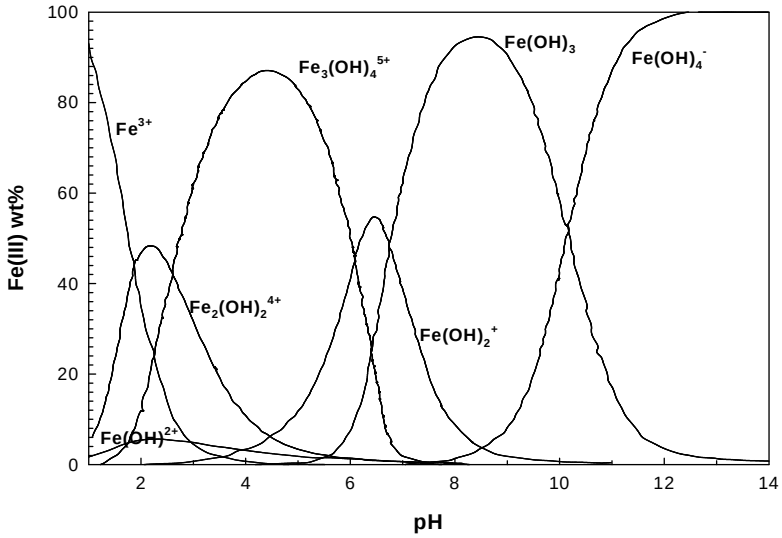

Figure 55: Hydrolysis Products for Iron.

The MR region showing sharp solubility decline increases in the following order of metal ions; Mg>Al>Fe. This trend is consistent with the starting hydrolysis pH of the metal ions; Mg>Al>Fe. Mg(II) forms its first hydrolysis product at pH 6.7. Experiments with pure phosphoric acid with added metal ions have shown that precipitation of solids begins at MR ~0.6 (pH ~2) for Fe(III), 0.85 (pH~3.5) for Al

(III) and 1.3 (pH~7) for Mg(II). This result suggests that hydrolysis products are required to initiate solids formation. The hydrolysis products form very small particles that act as nucleation sites for crystallization. In plant phosphoric acid, hydrolysis products of Fe(III) are formed first at MR 0.6 and these particles will act as sites for ammonium phosphate crystallization. The particles formed induce Al(III) ions to be hydrolysed (James and Healy 1972a). This explains the decrease in solubility of Al(III) ions at MR 0.66 or pH ~ 2.0. In contrast, the delay in hydrolysis of Fe(III) ions at pH~2.0 instead of 1.0 is due to an increase Fe(III) solubility at the elevated temperature of 110°C of the slurry.

4.5 Filtration Experiments with Laboratory Slurry

Samples made of 3% metal impurity (w/w% MgO, Al_2O_3 or Fe_2O_3 for each respective ion) and 40% P_2O_5 (calculated from addition of H_3PO_4) in distilled water were ammoniated. At various mole ratios, two 30ml samples were taken for solids analysis. The first sample was filtered immediately, while hot. The second sample was diluted in ~500ml of distilled water at room temperature in order to dissolve the soluble precipitates. Results from the former filtration may be misleading as the solution experienced cooling and therefore some additional precipitation, due to an expected change in solubility with temperature. In general, precipitates were seen to form in the filtrate, presumably due to such cooling. The results are intended to approximate the total solids content of the solution and the water insoluble content of the solution.

Tests were also carried out on solutions containing 6% metal impurity and 3% metal impurity with 2% by weight of fluorine ion, added in the form of fluosilicic acid. Only the insoluble portion of the slurry was determined in each of these tests.

4.5.1 Solutions Containing Iron

Pure phosphoric acid containing 3% Fe_2O_3 is a slightly pink solution. With ammoniation, the solution begins to darken at a 0.5 mole ratio and precipitates form between 0.55 and 0.6 MR. The solution becomes a homogenous solid white colour between 0.6 and 0.7 MR and stays this way throughout ammoniation before progressively darkening into a yellow colour above 1.4 MR.

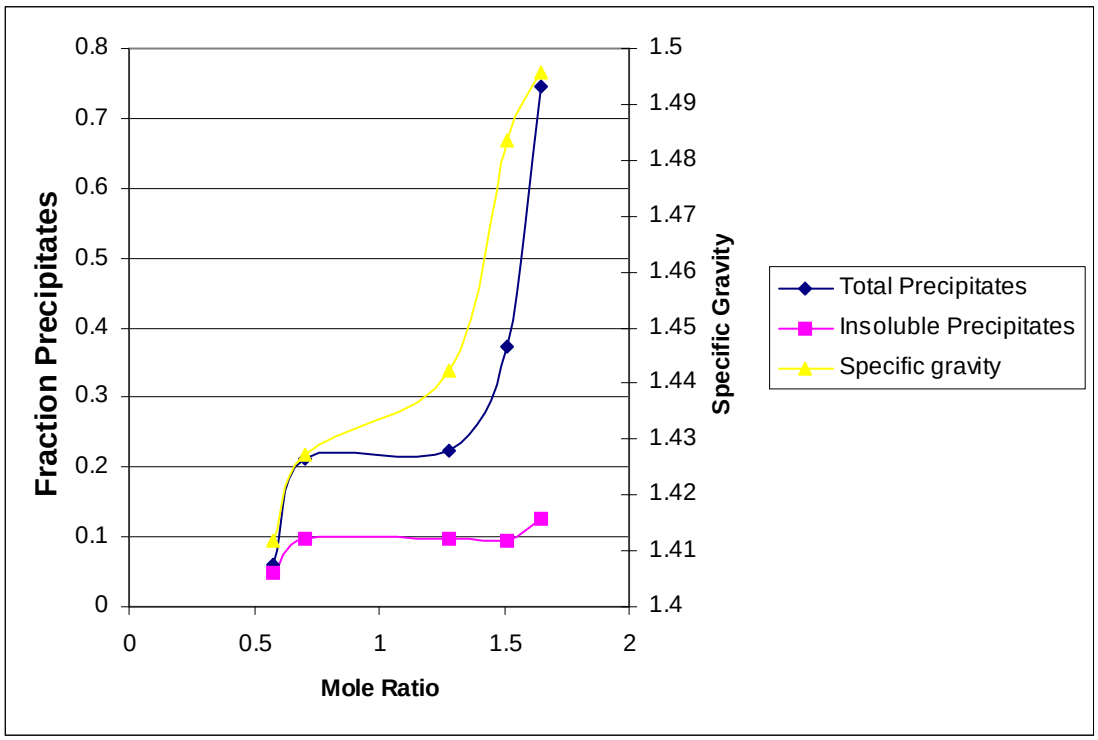

Figure 56: Total And Insoluble Crystal Content Of A Pure Ammonium Phosphate Slurry Containing Iron.

Figure 56 shows that the insoluble content increases between 0.58 MR and 0.70 MR however stays fairly consistent at about 10-wt% across all mole ratios until an increase is observed at MR 1.65. The total crystal content also increased between 0.58 MR to 0.70 MR and again above 1.28 MR. There was no significant change between 0.70MR and 1.28 MR.

Samples were diluted with excess water to dissolve any soluble compounds for the insoluble data. After dilution the 0.58, 0.70 and 1.28 MR samples settled in a fine layer to the base of the beaker. The solutions were easily filtered. The 1.65 MR sample formed a jelly like phase in the solution that barely settled with only a small clear water layer on the surface (about 2% by volume). The flocculated mix was easily moulded and largely held its shape. It took considerable time to filter. The 1.51 MR sample had properties intermediate of the other samples. It formed a settled jelly-like phase that took up about 25% by volume of the liquid in the beaker. The filtration time was also intermediate of the other samples. These observations suggest that the change in colour indicates a change in the suspension characteristics of the solids and further ammoniation leads to flocculation. Figure 57 shows a similar observation from a separate test. Between 1.3-1.5 mole ratio, the slurry becomes progressively yellow and suspended when diluted.

Figure 57: 30ml Of Slurry Settled After Stirring With 500 Ml Of Water At Three Different Mole Ratios. Increasing Mole Ratio Shows Resultant Suspended Solids Layer Increasing In Volume And Progressively Darkening To Yellow.

Testing was also carried out on slurries containing 1.5% and 6% Fe_2O_3, which were ammoniated to about 1 MR. Figure 58 shows that there is a clear linear relationship between the iron content of the acid and the amount of insoluble precipitate formed. In each case the total weight of the insoluble precipitate was higher than the weight of the Fe_2O_3 in solution, indicating that the iron was present in a higher molecular weight precipitate.

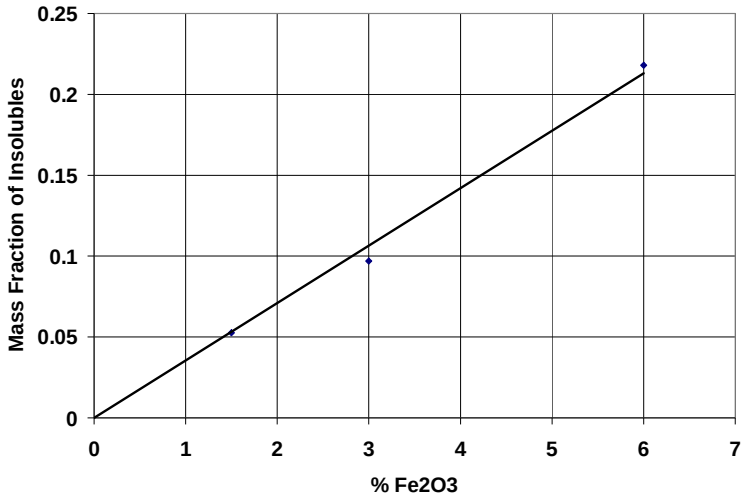

Figure 58: Relationship Between Insoluble Content And Iron Content Of Pure Ammonium Phosphate Slurry Spiked With Fe_2O_3.

Samples containing 6% Fe_2O_3 followed the same colour trend as the 3% Fe_2O_3 acid, although the high mole ratio samples were much brighter in colour. In contrast, the high mole ratio samples containing fluorine did not turn yellow at all, but darkened into a grey colour. Over time, the cooled slurry containing fluorine became a greyish green.

Figure 59 shows that the insoluble crystal content for 6% Fe_2O_3 is just over twice that of the 3% Fe_2O_3 slurry. Precipitates also appear to form sooner, although much of the precipitate gathered at 0.35 MR may have formed in the beaker on addition of water, due to the pH change involved. The slurry with 2% fluorine and 3% Fe_2O_3 showed a slight, but overall negligible increase in the insoluble content (an observed increase of generally less then 1% of the total solution weight). A 2% fluorine:3% Fe_2O_3 by weight ratio in the slurry is equivalent to a 2.8:1 mole ratio of F:Fe. Given this level of saturation of F compared to Fe and the lack of any real increase in the insoluble portion of the precipitate, this could suggest that the fluorine is not present in the insoluble precipitate, or that the new compound formed has a similar molecular weight.

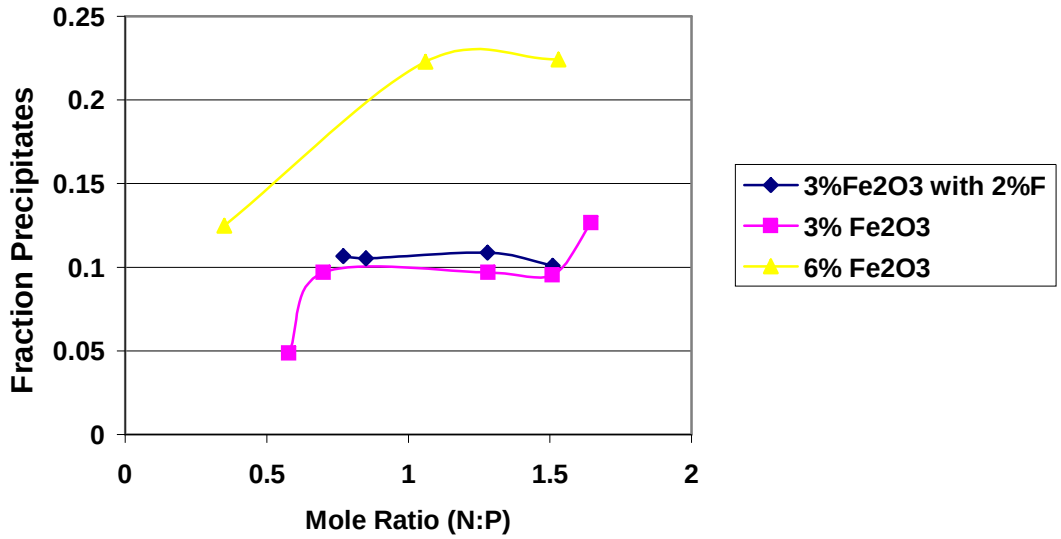

Figure 59: Insoluble Precipitate Content Of Pure Ammonium Phosphate Slurry Dosed With Iron And Fluorine.

4.5.2 Solutions Containing Aluminium

Pure Phosphoric acid containing 3% Al_2O_3 is a pale, syrupy, but clear solution. Upon ammoniation, a pale translucent mixture forms at 0.8-0.9 MR. The solution turns a white colour upon further ammoniation. The white colour became paler again as ammoniation continues above 1.40 MR, but the solution retains its translucent appearance. The colour change is shown in Figure 60. The image does not show the translucent nature of the high mole ratio slurry as effectively as the naked eye.

Figure 60: Pure Ammonium Phosphate Slurry at Low and High Mole Ratio.

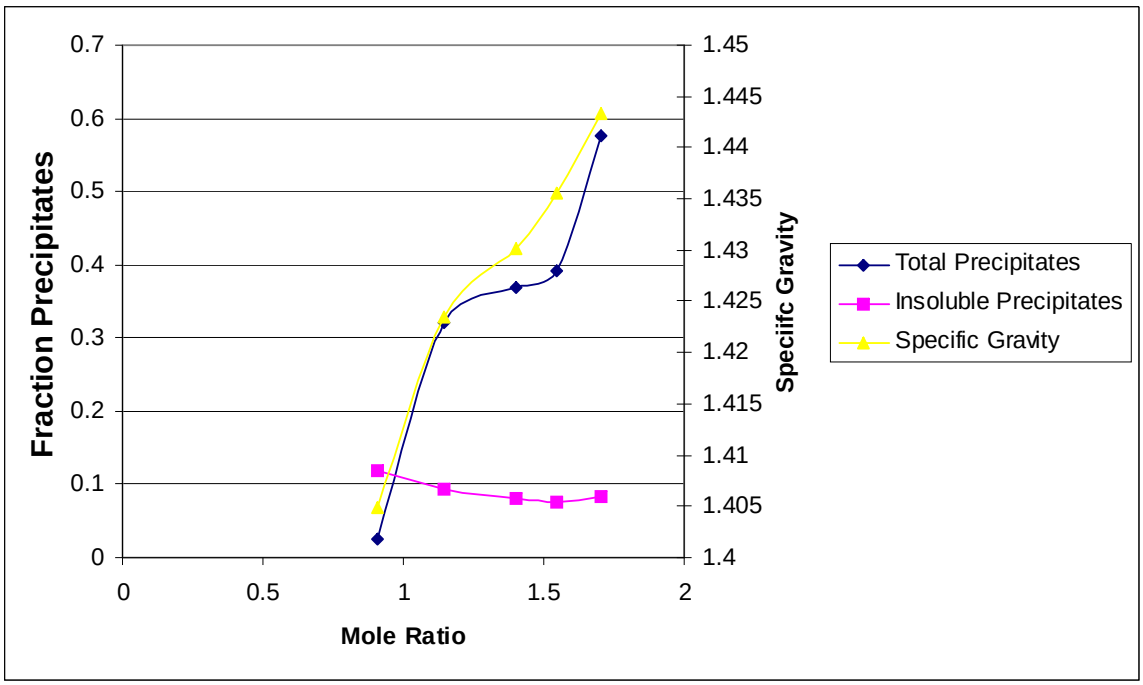

Figure 61: Total And Insoluble Crystal Content Of A Pure Ammonium Phosphate Slurry Containing Aluminium.

Figure 61 shows the total an insoluble portion of precipitates for the DAP1 acid at various mole ratios. The majority of the insoluble portion formed at 0.91 MR formed spontaneously on contact with the water used to dilute it to dissolve any soluble precipitate. This can be seen clearly in the fact that total precipitates were determined

to be much lower than the insoluble portion of such precipitates. Subsequent testing showed that a white precipitate formed instantaneously at around a pH of 3.0 and redissolved when the pH was dropped back below 3.0. Despite this initial spike, the insoluble content remained fairly consistent across all mole ratios. The total precipitates increased dramatically after pH 0.91, mainly because this was when precipitates began to form, and increased again between 1.55 and 1.70 MR.

Upon stirring the diluted samples it was found that the fastest settling occurred for 1.15 and 1.40 MR solutions. The slowest settling was in the 0.91 mole ratio solution. All of the samples settled to form a partially flocculated mix of similar bed height across all mole ratios. The settled layer did not form a stable flocculated mix to the same extent of the high mole ratio iron samples, instead occupying no more than 20-30% of the volume of the beaker. Precipitates formed in the filtrate for all samples, probably due to cooling. The crystals in the 1.40 MR sample appeared finer than the others. Previous tests with lower aluminium content acids have shown that the solution can go relatively clear at this mole ratio, indicating the redissolving of crystals present. When these clear slurries are cooled, the mixture forms a homogenous, single phase translucent gel (no liquid phase remained).

The 6% Al_2O_3 slurry followed the same colour trend as the 3% Al_2O_3 slurry. The slurry became very translucent and gel-like at high MR. In contrast, the slurry containing 2% fluorine and 3% Al_2O_3 appeared to retain the solid white colour across all mole ratios. Figure 62 shows that the 6% slurry contained more than twice the insoluble content of the 3% slurry, with almost triple the insoluble content at higher mole ratio. The crystals formed at roughly the same mole ratio.

The slurry containing fluorine appeared to begin crystallising at the same mole ratio as the 3% Al_2O_3 slurry without fluorine, although a small amount of precipitate was observed to form at mole ratios below 0.85. The insoluble portion of the precipitate was about 2% by total weight of solution higher in the slurry with 2% fluorine, which indicates that the additional precipitate probably contains this fluorine. The fluorine may have substituted another element, such as hydrogen, to bond to the molecule

formed by the aluminium, as has been suggested in the literature review (see section 2.3.6). A 2%F:3%Al_2O_3 by weight ratio is equivalent to a 1.8:1 mole ratio of F:Al.

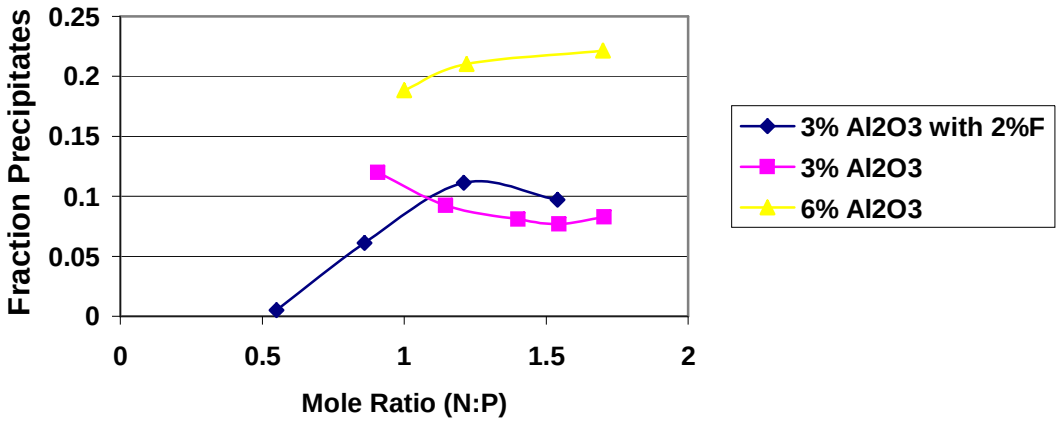

Figure 62: Insoluble Precipitate Content Of Pure Ammonium Phosphate Slurry Dosed With Aluminium And Fluorine.

4.5.3 Solutions Containing Magnesium

Pure phosphoric acid with 3% MgO is a clear solution. With ammoniation, crystallisation begins to appear at 1.25-1.30 MR. The solution becomes progressively more crystalline with increasing ammoniation and there is no apparent colour change. The collected crystals were white in colour.

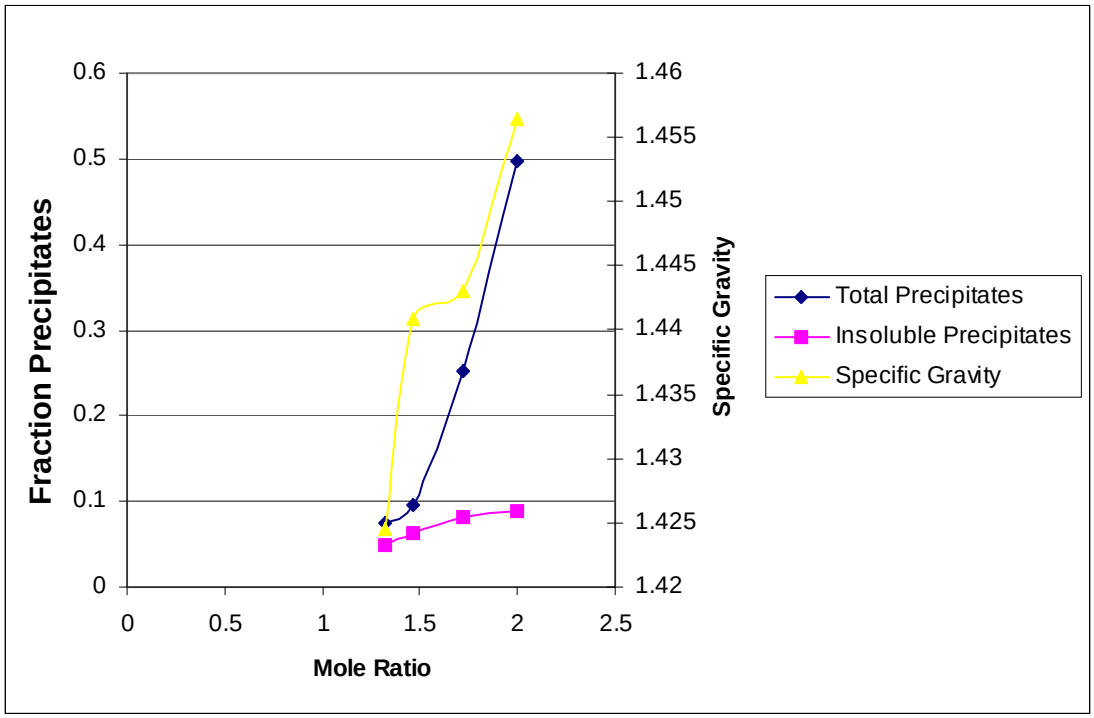

Figure 63: Total And Insoluble Crystal Content Of A Pure Ammonium Phosphate Slurry Containing Magnesium.

Figure 63 shows that the insoluble portion of the washed crystals increases with increasing mole ratio, as does the total crystal content of the slurries. When stirring the diluted samples, the insoluble crystals tended to settle to form a mound in the centre of the beaker.

The 6% MgO slurry contained roughly double the insoluble crystal content than the 3% slurry, as shown in Figure 64. Precipitation of this insoluble content occurred at roughly the same mole ratio. The slurry containing 2% fluorine and 3% MgO precipitated slightly below this mole ratio. Both results show a trend for further precipitation with increasing mole ratio as seen with the 3% MgO slurry. The mass of insoluble for the fluorine containing solution was greater than 2% higher, by total solution weight, than the 3% MgO slurry without fluorine. The results may indicate that all of the fluorine is present in the precipitate. The additional amount may be due to the fluorine causing the magnesium to precipitate at a lower mole ratio. A 3% F: 3% MgO by weight ratio is equivalent to a 1.4:1 mole ratio of F:Mg.

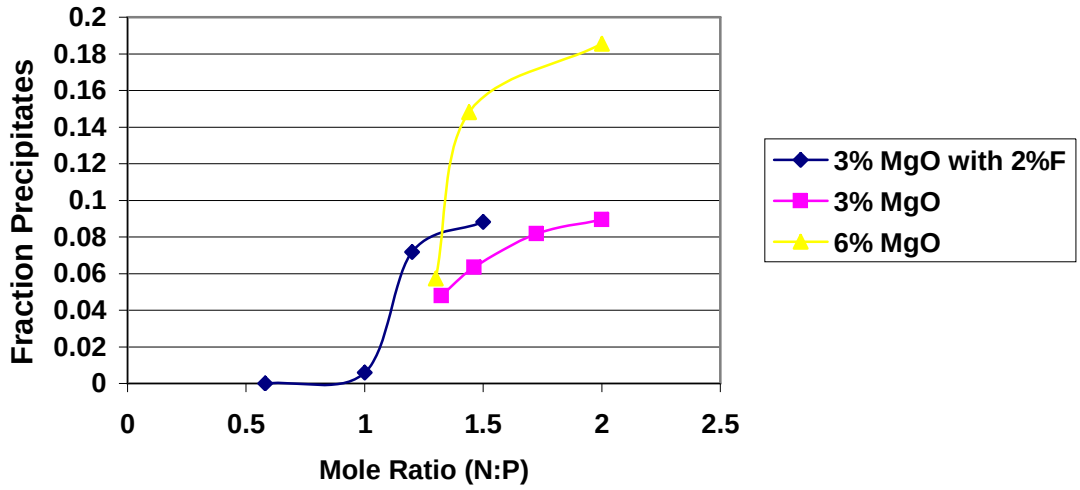

Figure 64: Insoluble Precipitate Content Of Pure Ammonium Phosphate Slurry Dosed With Magnesium And Fluorine.

4.5.4 Solubility of Metals in Laboratory Slurries

Some of the insoluble precipitates in the above experiments were sent for ICP-AES analysis to determine the proportion of the metal ion present in the original solution that forms an insoluble precipitate. The results are summarized in Table 8.

Table 8: Calculated Percentage of Each Impurity in Initial Solution That Precipitates.

Sample	Mole Ratio	wt% Element in Precipitate
6% MgO	1.44	60
	~1.8	81
6% Al_2O_3	1	65
	1.7	70
3% Fe_2O_3	0.58	49
	1.65	86
6% Fe_2O_3	1.06	92
3% MgO, 2%F	1	3
	1.5	62
3% Al_2O_3, 2% F	1.54	71
3% Fe_2O_3, 2% F	0.77	80
	1.51	94

The results show that upwards of 80% of the iron becomes insoluble compared to only 65-70% of aluminium. The proportion of magnesium forming insoluble precipitates increased with increasing mole ratio. This follows the curve seen in Figure 64, where the total insoluble precipitates for pure phosphoric acid with 3% MgO also increases with increasing mole ratio. The addition of fluorine did not appear to alter the percentage of each metal that became insoluble in a significant way.

Solubility tests performed on plant phosphoric acid (Figure 53), suggest that 90% of the aluminium and magnesium precipitates by 1.0 and 1.4 MR respectively. In these tests, the precipitates were diluted with water, therefore if a portion of the precipitate present was soluble, this would have led to a higher value for the dissolved concentration of any element in the soluble precipitate. The dissolved concentrations given by the pure phosphoric acid tests, in contrast, are actually higher, which suggests that the solubility of magnesium and aluminium decreases in plant-acid slurries.

4.6 Mole Ratio Titration

The mole ratio for each experiment was determined via titration, in the method described in section 3.1.3. This method is a suitable means to quickly and accurately determine the mole ratio of a slurry. The alternative method would have been to send a sample away to Phosphate Hill to determine the N and P content via ICP-AES. At the time of testing, the Advanced Analytical Centre (AAC) at JCU did not have the capability to determine the N content. Sending away the sample would have been time consuming and expensive and therefore was not considered feasible. Furthermore, the titration method was routinely used in the laboratory at Phosphate Hill, as a means to determine the mole ratio (with the use of a Metrohm Autotitrator). This meant that by determining the mole ratio in the same way as the industry partner, the results would be more reflective of observations at Phosphate Hill. The titration method was also used in previous studies (Tang, Guo et al. 2004).

Tests were carried out by staff at Phosphate Hill whereby the mole ratio was first determined by titration and then a sample was sent to the laboratory for N, P and S analysis. Results were determined for plant slurry at high and low mole ratio, over a four hour period each. Various ratios based on the N, P and S ratio were calculated and are shown in Table 9. The S content in the as-received acid was significant enough that it affects this titration method. At low pH, S is in the form of H_2SO_4, and as such, the diprotic nature of H_2SO_4 would have a strong effect on lowering the pH of the solution.

Table 9: Mole Ratio Determined By Titration And Various N, P, S Mole Ratios Determined By ICP-AES for High And Low Mole Ratio Plant Slurries

MR (by Titration)	N:P	N:(P+S)	N:(P+2S)
0.73	0.93	0.84	0.78
0.71	0.93	0.83	0.77
0.73	0.88	0.78	0.73
0.73	0.89	0.79	0.73
0.72	0.88	0.79	0.73
1.55	1.70	1.50	1.37
1.52	1.69	1.49	1.36
1.57	1.72	1.52	1.40
1.61	1.86	1.64	1.50
1.59	1.76	1.56	1.43

The mole ratio determined by titration for low mole ratios is closely related to the N:(P+2S) ratio determined by ICP-AES. For high mole ratios, the mole ratio is closely related to the N:(P+S) ratio.

This oversight meant that considerable time was spent attempting to explain the mechanism behind the viscosity reaching a maximum value at 0.9 MR, instead of at 1.0 MR. A review of the literature demonstrates that other studies found the maximum viscosity to be at around 0.9 N:P mole ratio, adding to the misconception that this is a phenomena related to the behaviour of the particles in suspension.

In addition, the magnesium content of the acid appeared to have an affect on the mole ratio titration. When adding the HCl to slurries containing magnesium, it was observed that the crystals present dissolved back into solution approaching a pH of 4 and this in turn raised the pH of the solution. The crystals must therefore contain an ammonium or hydroxide content that is released on dissolution, which acts like a pH buffer. It is possible that this effect leads to an inaccurate evaluation of the mole ratio of the slurry.

4.7 Discussion

4.7.1 Crystal Composition

Previous studies on the viscosity of ammonium phosphate slurry and how it changes with mole ratio and chemical composition have reported that viscosity changes can be attributed to varying crystals being formed during ammoniation. The literature review revealed that many of these studies post conflicting data when it comes to these points. One study may exclaim that high fluorine binds with iron to form a complex which increases the viscosity, whilst a similar study claims high fluorine bonds with iron to form a slightly different compound, lowering the viscosity. The conclusion therefore is that high fluorine and high iron ores should be avoided according to some evidence and welcomed according to others. This focus on the formation of chemical compounds and attributing their presence to changes in the viscosity, led us to believe that a new, more comprehensive study of these compounds was required.

Analysis of the XRD/XRF data for the plant acid tests showed that there was no clear or consistent trend in the formation of any particular chemical compound, with the exception of the major compounds MAP ($NH_4H_2PO_4$) and DAP ($(NH_4)_2HPO_4$). When the washed precipitates (washing removes the soluble MAP and DAP) from laboratory acid tests were examined, the majority of the solids turned out to be amorphous and as such no compound could be determined by XRF/XRD analysis. It soon became apparent that this method was not going to be able to help determine reasons for the changes in viscosity. Furthermore, drying of solids will bring about

crystallization of impurity compounds. Hence, the nature of the chemical species of the metal ion impurities formed in the slurry during neutralization can be different to those obtained by drying solids. There is no evidence to conclusively state the specific water insoluble compounds formed at any particular mole ratio.

4.7.2 Hydrolysis Products and Particle Size

The pH for the precipitation of iron correlates well to the hydrolysis curves shown in the literature review. Aluminium precipitates in the plant-acid based slurry at a lower mole ratio than in a laboratory grade acid based slurry. However, the literature also states that aluminium has a tendency to precipitate at lower mole ratios in the presence of other impurities. The trend for the pH of precipitation of the metal ions is as expected, with iron precipitating before aluminium and lastly magnesium. The crystal content results show that insoluble precipitates are formed at 0.65, 0.98 and 1.25 MR for iron, aluminium and magnesium respectively. These insoluble precipitates contain almost all of the metal impurity from the original solution. Once formed, the insoluble precipitates remain in the solution for all mole ratios up to 2.0 and possibly beyond. There is a linear relationship between the amount of insoluble impurity and the iron content of the acid, for pure acid slurries containing iron. Hydrolysis products initiate crystallization and adsorb readily on particles already present in the slurry. The adsorption of hydrolysis products may hinder crystal size growth. Adsorbed hydrolysis products may give rise to a range of interparticle forces in slurry such as bridging, charged patch and enhanced van der Waals attraction (Leong 2005). These forces will have a significant effect on slurry rheology.

Zeta potential of particles in the slurry give an indication of the nature of the surface charge and strength of the repulsive interactions between particles (Leong and Ong 2003). Zeta potential measurements were conducted on the insoluble solids of the ammonium phosphate slurry. A small amount of the slurry was dispersed in distilled water and the pH was adjusted with pure phosphoric acid. The result showed that the zeta potential of the particles produced at MR of 1.0 from pure phosphoric acid with added Fe(III) is very low, -0.2mV at pH 2.6 obtained at a relatively low ionic strength

of 6.05mS/cm. At higher pH the zeta potential is more negative, ~-10mV, but is still low. The zeta potential indicates that the particles are negatively charged. The low zeta potential even at such low ionic strength compared to actual slurry ionic strength of ~100mS/cm suggests that particles are strongly flocculated. Hydrolysis products may be regarded as unstable nanoparticles with a very high surface energy. Their adsorption will reduce this energy. Hydrolysis products are also known to absorb readily on net charged neutral particles (Leong 2005).

Phosphate ions have been reported to adsorb readily onto oxide particles (Leong, Scales et al. 1993). It is plausible that phosphate ions are adsorbed onto the layer of hydrolysis products coating the particle surface and this explains the negative zeta potential of the particles.

Particle number concentration has a very significant effect on flocculated slurry rheology (Leong, Scales et al. 1995). A larger number concentration of particles means a higher concentration of particle-particle bonds. This will require a greater expenditure of shear energy to disrupt these bonds. The higher energy dissipation is reflected by a higher viscosity and yield stress. If these bonds are very strong, even more energy is required to break them. Adsorbed hydrolysis products may increase the bond strength as they give rise to a range of other attractive forces such as bridging and charged patch attraction (Leong 2005). The adsorbed phosphate ions may also act as a binding agent between hydrolysis products adsorbed on two interacting particles at close contact. Each phosphate ions has three negative charges and hence it is possible to bind the two positively charged hydrolysis product layers. (Leong 2005) has reported an enhancement in the particle-particle bond strength of a few orders of magnitude by particle bridging with hydrolysis products. At complete surface coverage, the adsorbed hydrolysis product layer may even enhance the van der Waals attraction by increasing the effective Hamaker constant of the particles. The increased attraction is normally reflected by a large increase in slurry yield stress and viscosity. Fe(III) and Al(III) ions are commonly used as coagulants in water treatment to bridge suspended particles.

The effect of the interactions between hydrolysis products formed by Fe(III) and Al(III), adsorbed on particle surfaces, on the slurry viscosity and yield stress is not clear. Since the hydrolysis products of Fe(III) ions are formed first, these products will initiate crystallisation and the excess will adsorb onto the growing crystal particles. The hydrolysis products of Al(III) being formed later may adsorb onto particles already containing adsorbed Fe(III) hydrolysis products. The presence of $(Fe,Al)NH_4H_2(PO_4)_2.½H_2O$ crystalline compound reported by Ando and Akiyama (1972) suggests the possibility of the hydrolysis product of Al(III) ions adsorbing onto the hydrolysis product of Fe(III) ions. When the Fe(III) ions are exhausted in solution at pH of 4.0, the hydrolysis products of Al(III) ions formed above this pH may act as nucleation sites for further crystallization. The adsorption of phosphate ions will minimise any differences in the surface properties between particles containing predominantly adsorbed Fe(III) hydrolysis products and those containing Al(III) hydrolysis products.

Experiments on the particle size of plant acid slurries showed that there was no significant change in particle size distribution with increasing mole ratio. However, it was discovered that pure ammonium phosphate dissolved readily in water. This meant that only the insoluble particles could be analysed with the particle size analyser available. Whilst the distribution did not change, observations on slurries made from pure phosphoric acid with a single metal ion impurity showed that the impurities lead to a decrease in particle size. Aluminium based acids had the smallest particle size, followed by iron and magnesium. Aluminium and iron based slurries did not have any large inter-dispersed ammonium phosphate crystals. However, magnesium based slurries did have inter-dispersed ammonium phosphate crystals that were larger than the largest particle size that could be determined by the Malvern analyser. They are not detected in the Malvern particle size analyser as the analysis requires the sample to be diluted in a large volume of water, causing all of the soluble crystals to dissolve. The presence of these large particles lends weight to the hypothesis that hydrolysis products seed the formation of fine particles as magnesium does not form hydrolysis products below 1.25 MR. The large crystals would have formed before the hydrolysis of the magnesium, as a result of the decreasing solubility of ammonium phosphate approaching 1.0 MR.

4.7.3 General Trends in Viscosity

All of the plant acid slurries experienced a spike in the viscosity at 0.85-0.9 mole ratio. This is noteworthy, because the minimum solubility point, and hence the point whereby the viscosity should be the highest due to the solids to liquid ratio, occurs at 1.0 MR. The mined phosphate rock is contacted with sulphuric acid to produce phosphoric acid and calcium sulphate bi-product. Some sulphuric acid is left over after the reaction. This acid reduces the pH of the slurry. A titration is performed when testing for the mole ratio, making the result dependant on the initial pH of the slurry. The sulphuric acid therefore returns a lower (N:P) mole ratio than is in fact the reality. The titration method appears to determine the N: (P+2S) ratio for low mole ratios and the N: (P+S) for higher mole ratios. The reason for the difference is that the sulphuric acid is not bonded to the ammonia at lower mole ratio and therefore the diprotic nature of the acid has an increased effect on lowering the pH of the solution for its equivalent concentration. Therefore, the peak in the viscosity that appears at 0.85-0.9 MR (determined by titration), actually occurs at closer to 1.0 true N:P mole ratio (determined by ICP-AES). Any mole ratio listed throughout this document is the mole ratio determined by titration, unless specified as the *true* mole ratio. The peak in the viscosity at the minimum solubility point of MAP occurs at a slightly lower mole ratio in the literature than in the experimental for this work. At the same time, the concentration of S in the acid used in the literature was higher.

The viscosities of the plant acid slurries were more erratic at higher mole ratios. Ammonium phosphate solubility reaches a maximum (between 1.0 MR and 2.0 MR) at about 1.5 MR. From 1.0 MR to 1.5 MR, some of the mono ammonium phosphate that has crystallised dissolves back into solution, whilst some begins to turn into di-ammonium phosphate. Above 1.5 MR, additional mono ammonium phosphate crystallises out and begins to turn into di-ammonium phosphate. This process is very temperature dependant and the crystal size of the ammonium phosphates may differ as a result of inconsistencies in the temperature at which the slurry was being

ammoniated. This will in turn affect the viscosity and could explain why the viscosity is very sensitive at high mole ratios.

The difference in interaction between the impurities in predominantly MAP slurry or predominately DAP slurry is distinctive, as will be explained below. Therefore, we can make conclusions about the preferred processing route of the incoming acid stream, based on its impurity content.

4.7.4 Low Mole Ratio Slurries

Iron begins to precipitate out of solution at 0.5 MR. The peak in the viscosity occurs at 0.9 MR, which is likely to be close to the true N:P mole ratio of 1.0. This peak correlates well to the solubility of mono-ammonium phosphate, indicating that viscosity change is directly related to the amount of solids in solution. Increasing the amount of iron also increases the magnitude of this peak. Iron has been shown to reduce the particle size of the slurry. Therefore, the addition of iron increases the viscosity in ammonium phosphate slurry for low mole ratios by increasing the proportion of insoluble fine particles in the slurry. The trend in the viscosity change for different mole ratios (for low mole ratio slurries) at a fixed iron composition is governed by the solubility of ammonium phosphate.

Aluminium begins to precipitate out of solution at a mole ratio of 0.8. The precipitation of the aluminium based compounds can be observed by altering the pH of the solution either side of approximately 3.0 pH. A white cloudy solution develops when the pH is increased beyond ~3.0 and the solution goes clear when the pH is changed to less than ~3.0pH. When the aluminium based compounds precipitate, they form very fine particles. These particles are even smaller than those formed in iron based solutions and lead to an increase in the viscosity. At higher mole ratio, the solids have been observed to redissolve back into the solution. The increase in the viscosity should form a peak at 0.9 MR (1.0 true N:P mole ratio), relative to the solubility of MAP, however it is skewed to one side of the 0.9 mole ratio mark, since

the aluminium does not come out of solution below 0.8 MR. Also, the peak for aluminium is wider than for iron.

4.7.5 High Mole Ratio Slurries

For higher mole ratios, the mono-ammonium phosphate begins to dissolve and turn into di-ammonium phosphate. When iron is in the solution, interparticle forces begin to dominate and the system forms particles with high interparticle attractive forces, increasing the viscosity. This change is brought about by the conversion of the principal hydrolysis products of iron from $Fe_3(OH)_4^{5+}$ to $Fe(OH)_3$ between pH 6-7. The evidence for this is clear, in that between 1.3 to 1.5 MR, the mixture begins to change colour from white to yellow, whilst the bed height of a 30ml sample of slurry diluted in 500ml of water changes from complete settling below 1.3 MR to forming a flocculated suspension occupying almost all of the volume of the fluid, above 1.5 MR. The colour change across this mole ratio range is indicative of a change in the chemistry within the system. This change occurs over the mole ratio range that mono-ammonium phosphate is dissolving, while di-ammonium phosphate is precipitating. Further precipitation of di-ammonium phosphate occurs after 1.5 MR, but by this time most of the iron in the solution would have already formed higher mole ratio complexes. Evidence shows that the amount of insoluble particles stays relatively constant from 0.5 to 1.5 mole ratio, indicating that the iron in solution remains precipitated in some form, since pure di-ammonium phosphate and mono-ammonium phosphate are both soluble. The viscosity in laboratory slurry was, in fact, higher than the DAP 3 Acid viscosity at the same point. DAP 3 acid contained 60% more Fe ions in terms of a Fe:P weight ratio, as well as a variety of other impurities.

The large increase in viscosity for slurries containing iron at high mole ratios, coupled with a colour change, may explain high viscosities at low mole ratios that were observed for laboratory slurries in particular. In these cases a sharp increase in the viscosity was observed together, with a colour change during ammoniation. Slurries became yellow in colour, but reverted to the expected white colour upon standing.

The increase in viscosity is due to the particles obtaining the characteristics that cause high viscosities at higher mole ratios (attractive interparticle forces). It is possible that DAP is being produced during ammoniation and interacting with the iron in solution. Upon standing, the di-ammonium phosphate dissolves to form more stable mono-ammonium phosphate due to the ammonia to phosphoric acid mole ratio. The interaction between iron and the di-ammonium phosphate leads to a higher viscosity, despite the eventual reversion to mono-ammonium phosphate for the bulk of the solution.

At higher mole ratios, aluminium forms a translucent gel. This gel dissolves at higher temperatures and lower Al concentrations. Cooled slurry, containing only aluminium impurity at high mole ratio, will form a single phase gelatinous substance. The viscosity of this slurry remains low and the solids do not form a flocculated suspension as with iron containing slurries.

4.7.6 Magnesium and Fluorine

Magnesium has little effect on the viscosity of the slurry. The viscosity does increase slightly after precipitates are observed to have formed but the overall increase in viscosity between the highest and lowest values determined is less than 1 order of magnitude. The increase in viscosity appears to correspond with the increase in the proportion of insoluble precipitates. These precipitates are of small particle size and could lead to an increase in viscosity. Di-ammonium phosphate is also being produced as the slurry is ammoniated and this could be responsible for the increasing viscosity trend. What magnesium might do is inhibit the formation of mono-ammonium phosphate compounds. When pure phosphoric acid slurry is ammoniated without the presence of any impurities, it tends to crystallise between 0.9 and 1.1 MR, where MAP is least soluble. Magnesium based slurries do not appear to do this, or at least the extent of crystallisation appears to be lower. Also, the mole ratio determination has shown that some crystals that form increase the pH of the mixture when they dissolve back into solution. This dissolution, on acidulation, occurs at roughly the same pH of when crystals are first observed to form during ammoniation.

Fluorine has a dramatic affect on the properties of the slurry. Fluorine was found to increase the viscosity, at high mole ratio, when added to any of the three metal ion impurities. Aluminium experienced the greatest change in viscosity, while magnesium was affected the least. This is interesting in the case of magnesium as fluorine was found to greatly decrease the particle size whilst also increasing the insoluble crystal portion of the slurry. Despite these changes, the viscosity of magnesium with added fluorine did not approach the viscosities seen in aluminium and iron with or without fluorine, indicating that particle size and insoluble crystal content were not the major factors involved in the viscosity changes seen. The changes must have something to do with the interactions involving the metal impurities themselves. Fluorine had no effect on the viscosity of any of the metal ions at low mole ratio.

Aluminium and iron have often been thought to form metal complexes where the metal ion is interchangeable, such as (Al,Fe) $NH_4HF_2PO_4$. The fact that the addition of fluorine led to an increase in the insoluble portion of aluminium based slurries, whilst not exhibiting any appreciable increase in the iron based slurries puts this in doubt. Add to this the evidence that aluminium and iron containing slurries behave differently across all mole ratios.

5.0 CONCLUSIONS AND RECOMMENDATIONS

In general terms, at low specific gravity, the flow behaviour of slurries is Newtonian in the range of shear rate characterised. Slurries display non-Newtonian shear thinning behaviour at higher specific gravity and at higher specific gravity. The viscosity increases exponentially with increasing slurry specific gravity (or decreasing water content of the slurry). The specific gravity of slurry is directly related to the free moisture content in the slurry at given mole ratio, MR.

A typical trend for the viscosity of plant slurry with mole ratio is shown in Figure 65. The first peak, A, occurs at 0.9 MR. This mole ratio is determined by titration, but this titration is affected by the SO_4 in solution and the true mole ratio is closer to 1.0 N:P. The peak at A is principally due to the precipitation and dissolution of mono-ammonium phosphate, whilst the onset of the increase in viscosity that occurs at C is affected by the conversion of mono-ammonium phosphate to di-ammonium phosphate and a change in the principle hydrolysis products formed by iron. The shape of the graph is altered by the differing concentration of impurities in the incoming acid stream to the slurry reaction vessel. The mechanisms for these changes are described below.

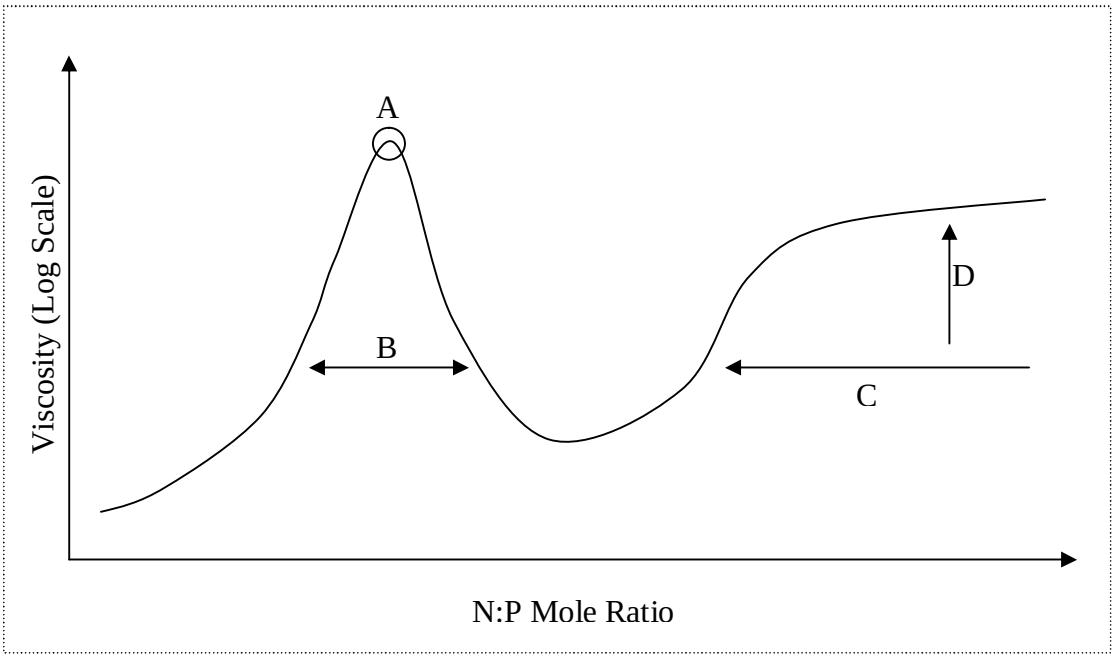

Figure 65: Typical Viscosity Vs Mole Ratio Trend for Plant Acid.

Increasing the iron content of a slurry will increase the peak at A and the height at D. Also, the point of onset for increased viscosity, C, will occur at lower mole ratio (the length of C will increase). The peak, A, is increased through the formation of fine particle size crystals. The iron hydrolysis products precipitate at very low mole ratio (0.5MR) and form the seed for the precipitation of fine crystal size ammonium phosphate crystals. The bulk of the hydrolysis products of the iron in solution change between 1.2 to 1.5 MR (from $Fe_3(OH)_4^{5+}$ to $Fe(OH)_3$ between pH 6-7). This change, combined with the conversion of MAP to DAP leads to the formation of particles with attractive inter-particle forces. These form a flocculated dispersion, which is visually apparent when the slurry changes from a solid white to a yellow colouration. This flocculated dispersion increases the viscosity across the range of C.

Increasing the aluminium content of the slurry will increase the width of the peak, B. However, the aluminium does not form the hydrolysis products necessary to affect the viscosity at mole ratios below about 0.8 MR (this value is affected by other impurities in solution) and as such, the width of the peak, B, expands more to the right of the peak, A, than to the left. The hydrolysis products of aluminium cause the precipitation of a much finer ammonium phosphate crystal size than those of iron. Aluminium does not affect the onset of C as this viscosity increase is solely due to the iron present. If enough aluminium is added, the increase in viscosity at C is not seen, as the width of B effectively cancels it out. The hydrolysis products of aluminium essentially do not change across the range of mole ratios that have been examined. The conversion of MAP to DAP from 1.3-1.5 MR leads to a visual change in the way that the aluminium interacts with the solution. However, this change does not have any significant impact on the viscosity and is therefore not examined further.

Changes in the viscosity with increased magnesium content could not be established. It is assumed that the magnesium has little to no effect on the viscosity at low mole ratios, since the hydrolysis products of magnesium only form above 1.2 MR. However, the viscosity results for magnesium were erratic. The amount of magnesium in the as-received acid was insignificant compared to the amount of aluminium and iron, although the acid dosed with magnesium had 20 times the

magnesium content of the as-received acid. Essentially, the iron and aluminium are the dominant impurities that will govern changes in the viscosity of a slurry.

Fluorine was shown to increase the viscosity of slurries containing iron or aluminium, at high mole ratios only. The investigation into the effect of varying the fluorine concentration was carried out with laboratory produced phosphoric acid only and the results should be treated with caution before applying to an industrial situation.

5.1 Recommendations and Further Work

When producing DAP, acids containing high iron or high fluorine should be avoided. When producing MAP, acids containing high aluminium should be avoided. The viscosity results displayed in this thesis should be examined to determine the most appropriate processing method for any given acid.

Slurries high in iron content were shown to exhibit strong interparticle forces above 1.4 mole ratio, corresponding with a colour change, leading to an increase in the viscosity of the slurry. The effect has also been unexpectedly observed at lower mole ratios on rare occasions. Establishing the precise mechanism that leads to the increased interparticle attractive forces could help develop methods to inhibit their onset and ultimately reduce the viscosity of the slurry.

This work focused primarily on the three metal ion impurities of magnesium, iron and aluminium. Some work was conducted on fluorine, although it was limited in scope. A more comprehensive analysis of the effect of fluorine would be beneficial to the fertiliser industry, as it is a major impurity. Furthermore, the viscosity work using plant based slurries was conducted with acid that was dominated by iron. Repeating this work using acid with greatly reduced iron content would assist in confirming the observations seen with respect to the effect of aluminium and magnesium on the viscosity of slurry.

Computational Fluid Dynamics (CFD) modelling was conducted on the mixing dynamics of the PN vessel and appears in APPENDIX I - CFD MODELLING. The CFD model showed that the upper region of the vessel was the least well mixed. The potential for stagnation of the flow field and subsequent solidification increases when the viscosity of the slurry also increases. To counteract this threat, the volume of slurry in the reactor must be decreased, or the agitation speed increased. The most effective method to ensure proper mixing dynamics in the vessel was to lower the viscosity, by preferentially processing each slurry by its impurity content. Further CFD modelling could be conducted to investigate changes in the reactor geometry on the fluid mixing dynamics.

REFERENCES

Mono Ammonium Phosphate 2005 www.chemicalland21.com.

pH Curves (Titration Curves) 2002 www.chemguide.co.uk.

Product Detail (Product: 466123) 2005, www.sigmaaldrich.com.

Achorn, F. P., E. F. Dillard, et al. (1980). Effect of Impurities in Wet-Process Phosphoric acids on DAP Grades. IFA Technical Conference, Vienna, Austria, Ta/80/11, 31pp.

Akhtar, M. S., T. S. Steenhuis, et al. (2003b). "Chloride and Lithium Transport in Large Arrays of Undisturbed Silt Loam and Sandy Loam Soil Columns." Vadose Zone J **2**(4): 715-727.

Ando, J. and T. Akiyama (1972). Ammoniation Reactions of Wet Phosphoric Acid. IFA Tech Conf, Lte/72/12.

Baes, C. F. and R. E. Mesmer (1986). The Hydrolysis of Cations. Malabar, Florida, Krieger.

Barbera, A. (1988). Effect of Raw Materials, Process Operation and Conditions on Physical Characteristics, Chemical Properties and Behaviour of N.P.K. Fertilisers. IFA Tech Conf, Ta/88/3.

Barbera, A. and R. Monaldi (1980). Use of Chemical and Physical Data to Improve the Quality of Granular Fertiliser Production. IFA Tech Conf, Ta/80/12.

Brouckaert, C. J. and C. A. Buckley (2003). The application of Computational Fluid Dynamics to Water and Wastewater Treatment Plants. Natal, University of Natal.

Bui, A. and M. Rudman (2003). Modelling of Viscous Resuspension using a One-Field Description of Multiphase Flows. The 3rd International Conference on CFD in the Minerals and Process Industries, Melbourne, Australia.

Bujalski, J. M., Z. Jaworski, et al. (2002). The influence of the addition position of a tracer on CFD simulated mixing times in a vessel agitated by a Rushton Turbine. 7th UK COnference on Mixing, University of Bradford.

Datsun, A. (2002). Gelling Behaviour of Ammonium Phosphate Slurries Spiked With Phosphoric Acid Sludge, WMC.

Dinsdale, A. and F. Moore (1962). Viscosity and its Measurement. London, Chapman and Hall Limited.

Everett, D. H. (1988). Basic Principles of Colloid Science. London, Royal Society of Chemistry.

Frazier. *Year and Title Unknown.*

Fuerstenau, M. C., D. A. Rice, et al. (1965). "Metal Ion Hydrolysis and Surface Charge in Beryl Flotation." Institute of Mining and Metallurgy Transaction **74**: 381-391.

Garner, D. (2003). G. Campbell**:** Email communication.

Gobby, D., I. S. Hamill, et al. (2002). Application of CFD to Multi-Phase Mixing. 7th UK COnference on Mixing, University of Bradford.

Handley, M. (1984). Effects of Impurities on Production of Diammonium Phosphate. IFA Tech Conf, Ta/84/6.

Hensel, F. and U. Rohde (1998). "Measurement and simulation of the turbulent dispersion of a radioactive tracer in a two-phase flow system." Advanced Fluid Mechanics **21**: 283-292.

Hunter, R. J. (1993). Introduction to Modern Colloid Science. New York, Oxford University Press.

James, R. O. and T. W. Healy (1972). "Adsorption of Hydrolyzable Metal Ions at the Oxide-Water Interface, I. Co(II) Adsorption on SiO_2 and TiO_2 Model Systems." Journal of Colloid Interface Science **40**: 42-52.

James, R. O. and T. W. Healy (1972a). "Adsorption of Hydrolyzable Metal Ions at the Oxide-Water Interface, I. Co(II) Adsorption on SiO_2 and TiO_2 Model Systems." Journal of Colloid Interface Science **40**: 42-52.

James, R. O. and T. W. Healy (1972b). "Adsorption of Hydrolyzable Metal Ions at the Oxide-Water Interface, II. Charge Reversal of SiO_2 and TiO_2 Colloids by Adsorbed Co(II), La(III) and Th(IV) as model systems." Journal of Colloid Interface Science **40**: 53-64.

Khoo, K. Y., K. R. Davey, et al. (2003). "Numerical Simulation and Experimental Visualization of the Isothermal Flow of Liquid Containing a Headspace Bubble Inside a Closed Cylinder During off-Axis Rotation." Food and Biopruducts Processing **81**(C2): 119-128.

Leong, Y. (2005). "Yield stress and zeta potential of nanoparticulate silica dispersions under the influence of adsorbed hydrolysis products of metal ions - Cu(II), Al(III) and Th(IV)." Journal of Colloid Interface Science **292**: 557-566.

Leong, Y. and B. C. Ong (2003). "Critical Zeta Potential and the Hamaker Constant of Oxides in Water." Powder Technology **134**: 249-254.

Leong, Y. K. (2000). Ammonium Phosphate Slurry (or Melt) Rheology, WMC.

Leong, Y. K. (2002). Viscosity-Shear Rate Behaviour of Ammonium Phosphate Slurries Prepared From 40% Phosphoric Acids Containing a Range of Ferric Ions Concentration, WMC.

Leong, Y. K. (2005). "Yeild Stress and zeta potential of nanoparticulate silica dispersions under the influence of adsorbed hydrolysis productd of metal ions - Cu(II), Al(III) and Th(IV)." Journal of Colloid Interface Science **292**: 557-566.

Leong, Y. K., P. J. Scales, et al. (1995). "Effect of Particle Size on Colloidal ZrO2 Rheology at the Isoelectric Point." Journal of American Ceramic Society **78**: 2209-2212.

Leong, Y. K., P. J. Scales, et al. (1993). "Rheological Evidence of Adsorbate Mediated Short Range Steric Forces in Concentrated Dispersions." Journal of Chemical Society, Faraday Transaction **89**: 2473-2478.

Levenspeil, O. (1999). Chemical Reaction Engineering, John Wiley.

Lide, D. R. (1996). Handbook of Chemistry and Physics. Boca Raton, FL, CRC Press.

López, L. A. G., M. C. Veiga, et al. (2003). "A technique using a membrane flow cell to determine average mass transfer coefficients and tortuosity factors in biofilms." Water Science and Technology **47**(5): 61-67.

Matijevic, E., M. B. Abramson, et al. (1960). "Detection of Metal Ion Hydrolysis by Coagulation: II Thorium'." Journal of Physical Chemistry **64**: 1157-1161.

Matijevic, E. and G. E. Janauer (1966). "Coagulation and Reversal of Charge of Lyophobic Colloids by Hydrolysed Metal Ions. II. Ferric Nitrate." Journal of Colloid Science **21**: 197-223.

Montante, G. and F. Magelli (2005). "Modelling of Solids Ditribution in Sitrred Tanks: Analysis of Simulation Strategies and Comparison with Experimental Data." International Journal of Computational Fluid Dynamics **19**(3): 253-262.

Mpofu, P., J. Addai-Mensah, et al. (2003). "Influence of hydrolyzable metal ions on the interfacial chemistry, particle interactions, and dewatering behavior of kaolinite dispersions." Journal of Colloid Interface Science **261**: 349-359.

Nyvlt, J. (1972). The Effect of Periodic Temperature Changes on the Shape of Crystals. Symposium on Particle Growth in Suspensions, Brunel University, Academic Press.

Online Source (2005b). Di-ammonium Phosphate (DAP), www.chemicalland21.com.

Rohde, U., T. Höhne, et al. (2005). Fluid mixing and flow distribution in the reactor circuit (FLOMIX-R). The 4-th International Conference "SAFETY ASSURANCE OF NUCLEAR POWER PLANTS", FSUE EDO Gidropress, 23.-25.05.2005, Podolsk, Russian Federation.

Schnetler, F. (2003). Personal Communication.

Shekhar, S. M. and S. Jayanti (2002). "CFD Study of Power and Mixing Time for Paddle Mixing in Unbaffled Vessels." Chemical Engineering Research and Design **80**(A5 Special issue: Materials Processing): 482-498.

Shekhar, S. M. and S. Jayanti (2003). "Mixing of power-law fluids using anchors: Metzner-Otto concept revisited." AIChE Journal **49**(1): 30-40.

Shengwei, T., G. Hui, et al. (2004). "Physiochemical Properties of Acidic Ammonium Phospahte Slurries." Ind. Eng. Chem. Res. **43**: 3194-3199.

Tang, S., H. Guo, et al. (2004). "Physicochemical Preoperties of Acidic Ammonium Phosphate Slurries." Industrial Engineering Chemical Research **43**: 3194-3199.

Ternik, P., J. Marn, et al. (2002). "Electrostatic Ash and Water Flow Mixture Modeling." PAMM **1**(1): 369-370.

White, R. and C. Doblin (2003). An Investigation of Sparged Mixing Tanks Using Electrical Impedance Tomography and Computational Fluid Dynamics. Third International Conference on CFD in the Mineral and Process Industries, Melbourne, Australia.

White, R. and C. Doblin (2003a). Measurement and simulation of the turbulent dispersion of a radioactive tracer in a two-phase flow system. The 3rd International Conference on CFD in the Minerals and Process Industries, Melbourne, Australia.

WMC (1999). DAP/MAP Plant Training Manual. QLD Fertilizer Project. Lakelands, Florida, Jacobs Engineering Inc.

WMC (2000). Pre-Neutraliser Datasheet. P&ID. Phosphate Hill.

WMC (2001). Site Induction Presentation. Phosphate Hill.

APPENDIX I - CFD MODELLING

Background

Computational fluid dynamics (CFD) is an increasingly utilized research tool for chemical engineers. There have been a number of studies that identify areas of research for and the effectiveness of CFD in a variety of applications. Some major commercial packages include CFX, FLUENT, FlowER and FIDAP. CFD packages claim to be able to solve complex engineering situations such as multiphase flow, reacting flows, suspended particles, free surface flows and non-Newtonian flows.

Many publications have found CFD to be effective in areas such as in a sparged mixing tank (White and Doblin 2003), on modeling particles in suspension (Bui and Rudman 2003) and even on mixing in nuclear reactors (Rohde, Höhne et al. 2005). The CFX package itself comes with several tutorial lessons that detail how to conduct simulations with the use of a tracer, modeling multiphase flow, using non-Newtonian fluids, free surface flow and also modeling flow in stirred, baffled tanks. A number of these tutorials ideally replicate the type of simulation we intend to perform and therefore make the modeling much easier to apply. CFD has also been shown to be effective in modeling Non-Newtonian fluids (Khoo, Davey et al. 2003), particularly power law fluids (Ternik, Marn et al. 2002; Shekhar and Jayanti 2003), baffled (Montante and Magelli 2005) and un-baffled (Shekhar and Jayanti 2002) stirred vessels and multiphase flow (Hensel and Rohde 1998; Gobby, Hamill et al. 2002).

In this thesis CFX 5.7 was chosen as the CFD package for modeling the flow field inside the pre-neutraliser reactor. The CFX model needs to be validated with plant base measurements to ensure its accuracy. As velocity measurements are not feasible, a standard method of comparing simulated and experimental residence time distribution will be used (Hensel and Rohde 1998; White and Doblin 2003a). An experimental tracer test will be undertaken (Levenspeil 1999) and the same process will be simulated in the CFX model. The RTD results of the field test and the simulation will be compared, in order to validate the model. It has also been shown

that the addition point of a tracer can have an effect on the simulation results (Bujalski, Jaworski et al. 2002). Bujalski demonstrated that simulated RTD results were much more sensitive to the addition point of the tracer than for experimental results. He claimed that the greater discrepancies between the results were manifested closer to the wall of the vessel.

The tracer that will be used for this study is Lithium Chloride. Lithium chloride has been shown to be a fairly inert substance and has been used as a tracer in medical applications on biofilms (López, Veiga et al. 2003), as a tracer in soils (Akhtar, Steenhuis et al. 2003b) and in wastewater treatment plants (Brouckaert and Buckley 2003). The diffusion co-efficient of lithium in water is $1.03x10^{-9}$ m^2 s^{-1} (Lide 1996).

Experimental Testing

Plant Data

Tracer tests were performed at phosphate hill on 30/07/2005. Control system data was gathered at the time of these tests and was used to specify the following process parameters:

- Slurry specific gravity
- Ammonia input flow rate
- Phosphoric acid input rate
- Output flow rate
- PN Level

The values used for these parameters may not be precise, as the instrumentation used to determine them is under industrial conditions. In particular, the PN level may be out as the calculation appears to be based on a fixed specific gravity. The level indicator for 0% level is also not at the base of the tank. There is some confusion

about how to determine the PN level, however a spreadsheet developed by staff at Phosphate Hill was selected as the most confident method.

In addition to this, a sample of the PN slurry was taken for viscosity analysis. The slurry may have cooled between the sample point and the analysis point, however the results were fairly consistent and stable during the analysis time, indicating accurate results. The viscosity vs shear rate behaviour of the slurry was characterised and the relationship inputted into the CFD model describing reactor fluid properties. The viscosity-shear rate behaviour of the slurry is shown in Figure 66. It can be represented by a power law equation:

$$\text{Viscosity} = 2.23 \times (\text{Shear Rate})^{-0.270}$$

This equation has an R^2 correlation with the data of 0.998.

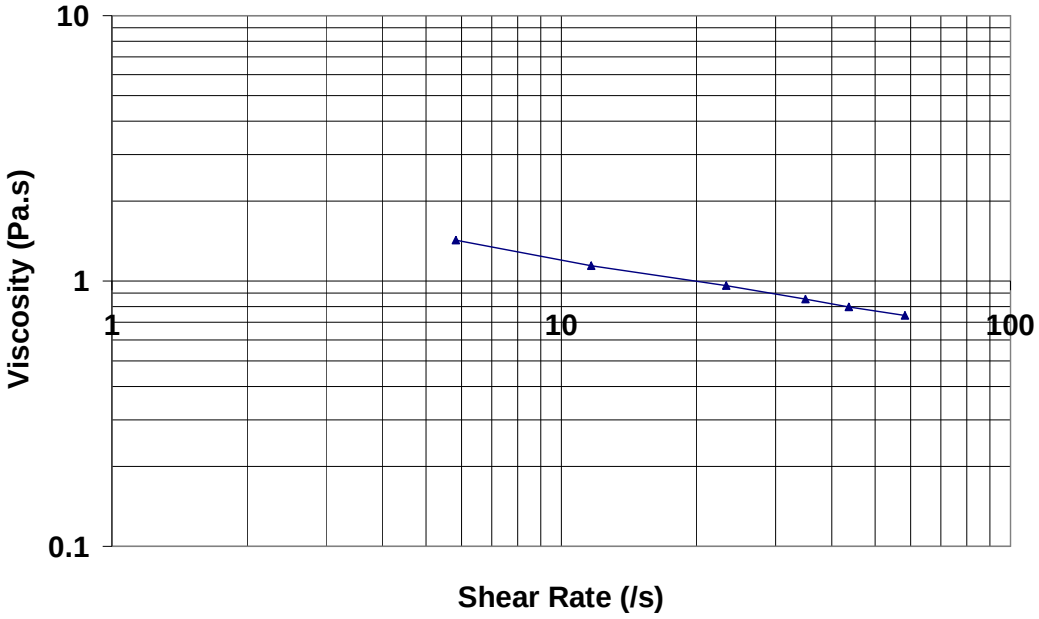

Figure 66: Viscosity Vs Shear Rate For PN Slurry Measured During Tracer Testing.

Tracer Test

The tracer was gravity fed into the PN through the cleanout inlets at the top of the tank. In the laboratory, 10kg of LiCl was slowly dissolved in water and allowed to

cool (the dissolution of LiCl is highly exothermic). This saturated solution was poured into a fabricated holding tank, blocked by a ball valve, attached to the cleanout inlets. The ball valve was opened and the time for the holding tank to empty was recorded for use in the CFD model (8 seconds). Samples of slurry were periodically taken from the sample point at the feed of the granulator (the next unit operation after the PN). The samples underwent ICP-AES analysis to determine their Lithium content. The concentration of lithium at the sample point over time is shown in Figure 67. The distribution strongly resembles the expected RTD curve from a CSTR reactor. The data also appears to show that there is some lithium present in the acid feed stream at a concentration of 3.0-3.5 ppm.

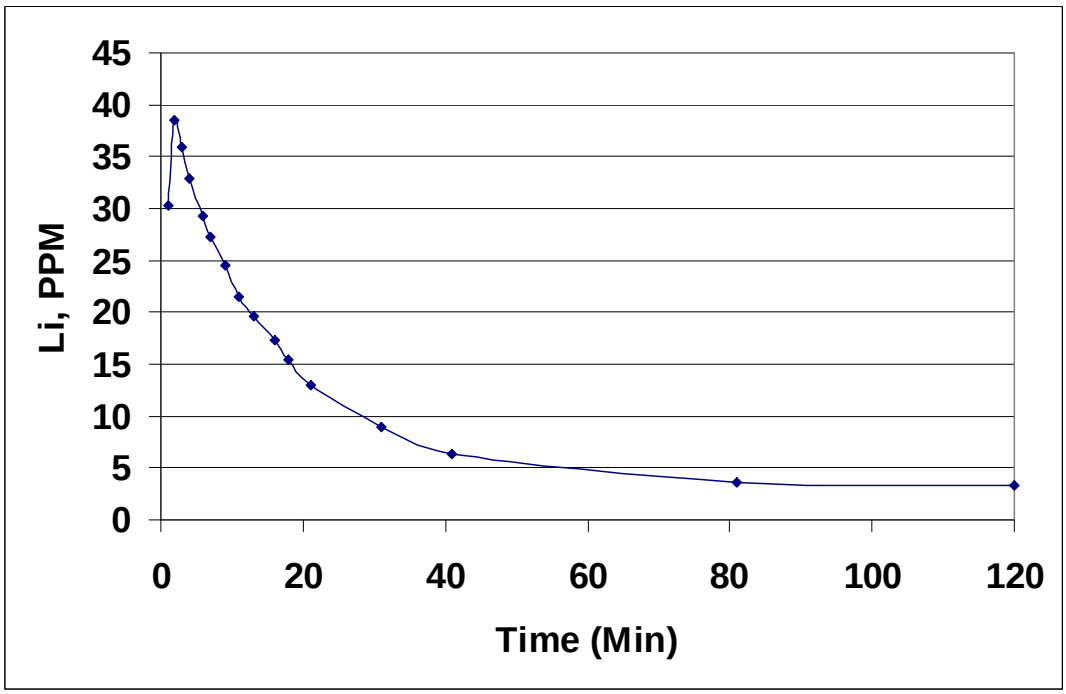

Figure 67: Concentration of Lithium over Time at Granulation Sample Point.

CFX Model Development

Model Geometry

The tank was split into two domain assemblies. The bulk of the tank, including the surface, base, walls, baffles and ammonia inlet pipes were part of the domain referred to as "tank" (Figure 68). The second domain consisted of a cylinder cut from the tank

domain around the impeller blades, designated as “impeller’ (Figure 69). The entirety of the tank was created, as no symmetry existed. If the model could be split into symmetrical segments, the entire vessel could be modelled from a single segment, using repeating interfaces, to decrease computation time. The PN vessel consisted of one output pipe on the side of the vessel and seven non-equally spaced ammonia inlet pipes, making it not symmetrical. In addition, the PN had the following characteristics:

- Stirred tank
- Free surface
- Baffles
- Non-Newtonian flow (slurry)
- Multiphase, reacting flow.

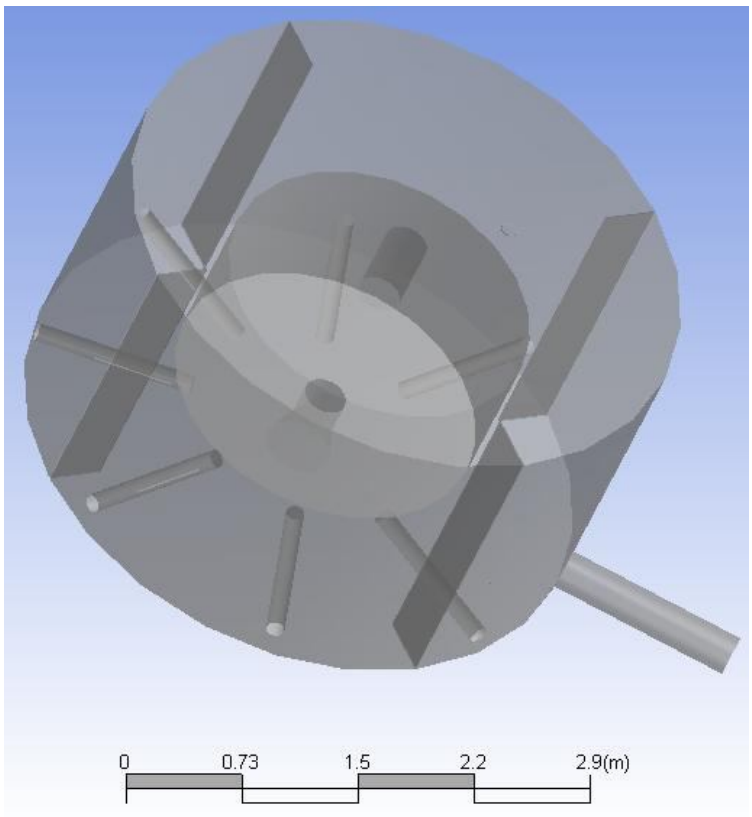

Figure 68: ‘Tank’ Domain for CFX Model

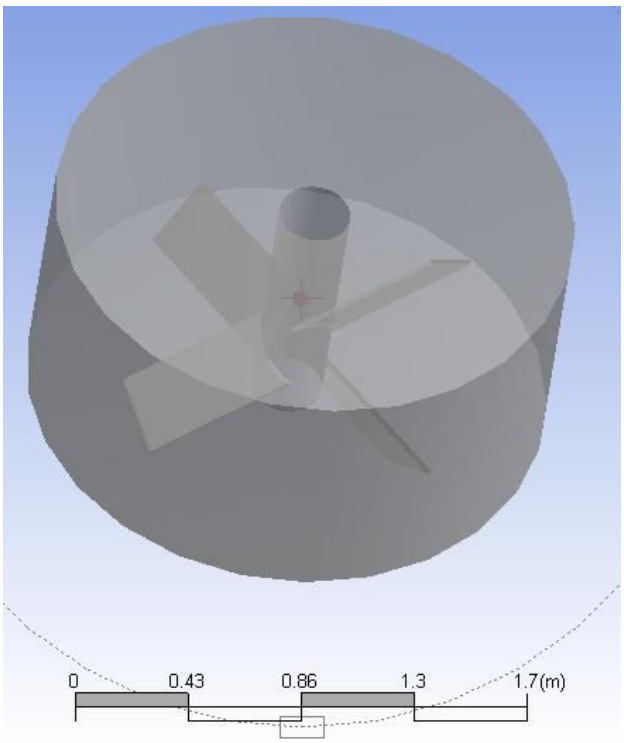

Figure 69: 'Impeller' Domain for CFX Model

The CFD model had several simplifications in comparison to the actual equipment in order to reduce modelling and solver time and complexity. These include:

- Removal of gaps between baffle and wall and base of the tank
- Removal of supports that hold baffles
- Ammonia inlet consisted of 15 holes spaced out evenly along the base of an inlet pipe. This was replaced with one continuous opening.
- Removal of ammonia pipe supports
- The central impeller shaft was modelled as one continuous vertical cylinder and the blades of the impeller were modelled as four rectangular prisms extruding from the shaft (i.e. nuts and bolts etc were not modelled).
- Assumption (based on experimental observations) that ammonia rapidly reacts in the slurry. This enables us to model a homogenous slurry, rather than three-phase reacting system near the ammonia inlet (slurry, acid and ammonia). This may have an effect on the results at the ammonia inlets but a three-phase system is too complicated to model and introduces several additional indeterminate variables.

- The outlet is modelled as a short pipe extending from the base of the tank. For tracer injection the actual outlet sample point is located a significant distance along this pipe and contains several bends. It is reasonable to consider the pipe to be plug flow. Essentially this just leads to an offset in the RTD data.

The resolution of a CFD model is dependent largely on the mesh size of the model. A coarse mesh decreases computation time but reduces the accuracy. A fine mesh is ideal, but requires more memory to run. It is important to find a balance between the resolution of the model and both the computational and time limitations to run the model.

For the 'Tank' domain, the maximum default body spacing was specified as 0.15m. The small opening for the ammonia inlet meant that a local mesh size at this point was set at 0.02. The baffle edges were left unspecified. The tank outlet surface had a local maximum face spacing set at 0.1m. The minimum edge length for all surfaces was set at 0.001m. An inflation boundary was also used on the tank walls, base, impeller shaft and the outlet pipe walls. This boundary set at maximum thickness of 0.3m with 5 inflation layers and an expansion factor of 1.2. All other parameters were left at their default values. Surface meshing was then conducted using Delaunay method, followed by volume meshing using advancing front method. The mesh program displayed warnings about the model containing faces with small angles. The small angles are located where the outlet pipe emerges from the tank wall, as it is flush with the base of the tank, as shown in Figure 70. Mesh quality may be poor in this area, but it is not a great concern for the overall model quality.

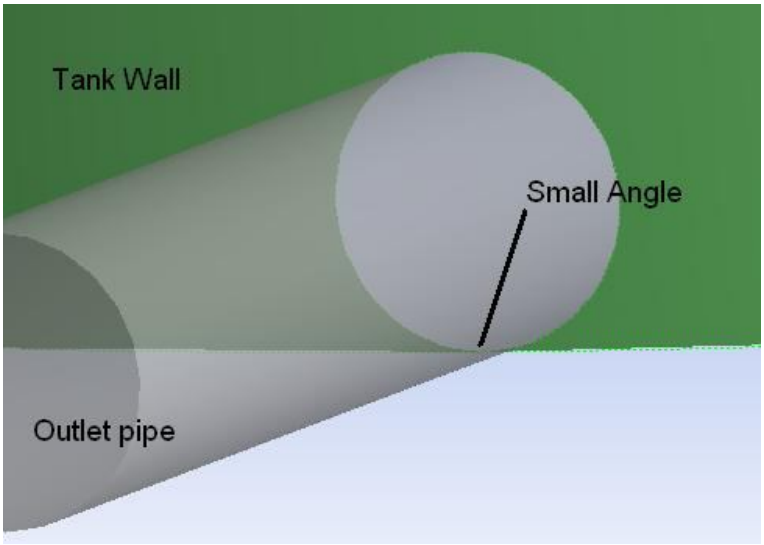

Figure 70: Occurrence of Small Angle on PN Wall Surface near the Outlet Pipe.

For the 'impeller' domain, the default body and face spacing were set at a slightly smaller 0.1m. Local mesh sizing was not set for any particular part of the domain and no inflated boundary was used. The meshing methods were the same as for the tank domain.

An inspection of the mesh for both domains appeared to show that there were no abnormalities. The mesh sizing meant that the upper part of the impeller shaft and some parts of the ammonia inlet tubes near the wall did not appear cylindrical, but this is not considered to have an appreciable effect on the model outcome.

Model Solving

The model was solved in two ways. Firstly, the unsteady state Navier Stokes equations with a standard k-Epsilon turbulence model was solved to steady state with a rotating impeller and input/output flow rates, in order to determine the flow fields within the tank. Subsequent to this, the model was solved in transient mode, with flow solving turned off, whilst the tracer was injected into the tank, in order to create

a tracer concentration over time plot to validate the model. The model was run as an isothermal system.

In order to test the validity of the model, it was first solved with water as the fluid inside the tank. Tracer injection was then used to determine if the model behaved essentially like a CSTR, as expected. Once this was successful, the fluid was changed to slurry and two separate viscosities were solved so as to see the effect of Newtonian viscosity changes on the fluid. Finally a non-Newtonian formula was entered for the viscosity.

CFX Pre Setup

A material called 'Slurry' was created to represent the fluid inside the tank. This material had the following specifications:

- Density = 1.60 g/cm^3
- Transport properties were set for dynamic viscosity, either as specified value (Newtonian fluids) or as an equation (non-Newtonian Fluids)

Each domain was specified in CFX-Pre and transformed to the appropriate position. The domain 'impeller' was specified as rotating at –68 rev/min, about the z axis. The 'tank' domain was specified as stationary. The only fluid specified for the problem as the user created material 'Slurry', or in early model runs 'water' was used. The heat transfer Model was set to 'none.' The turbulence model was changed from k-epsilon to Shear stress transport as the non-Newtonian fluid viscosity depends on the shear stress of the fluid.

The default boundary condition was set as 'wall' with 'No Slip.' The shaft section of the tank domain was set as a rotating wall at the same speed as the impeller. Three separate interfaces were created for the surfaces between the two domains. The Mass and Momentum option for each inlet and outlet was set at 'mass flow rate', with all other options left at their default settings. Turbulence eddy dissipation was checked in the global initialisation settings.

Non-Newtonian Fluid

When solving using a non-Newtonian fluid, the dynamic viscosity of the material must be set to an equation. This equation relates the viscosity to the shear stress, in this case it was using a power law formula. Upper and lower limits were also set for the shear stress, to ensure that the viscosity value returned remained physically meaningful.

Tracer Set Up

The following steps were performed so as to perform a tracer analysis on the results:

- An additional Variable, known as 'Tracer' was created of type Volumetric with Units kg/m^3
- The 'Tracer' was selected in the domain and was not given a kinematic diffusivity.
- A source point was created at the point of tracer injection. In equation sources, 'Tracer' was selected with option 'Total Source' which was specified by an equation 'TracerIn'.
- The equation 'TracerIn' specified the input rate of the tracer in kg/s and the length of time the tracer was injected into the vessel.
- All inlets were defined as having no tracer input and the initial conditions for the tracer in the PN was set at 0.
- The model simulation type was changed from steady state to transient and time steps were set accordingly.
- Two methods were used to determine the output of tracer from the tank. The first used an equation to average the tracer concentration across the outlet of the tank, whilst the second determined the concentration of tracer at a single point on the outlet.
- A monitor point or expression was set up for these two equations and the results were plotted by CFX-Solve during computation.

Model Validation

The tracer test data taken from plant trials are shown in Figure 71. After 2 hours, the lithium content had flattened out but still had not reached a zero value. The non-zero value was due to the slurry containing a residual amount of Lithium that was being introduced within the plant acid. Therefore the 'Tracer Test – Residual' data is the tracer concentration resulting from the addition of Lithium Chloride and is the trend we hope to see in the simulated data. It should be noted that the sample point for these values is along a long pipe. Therefore, the time between the addition of LiCl to the reactor, to when the given concentration of Lithium leaves the reactor may be different to that shown, but this should be a simple offset rather than affect the slope of the curve.

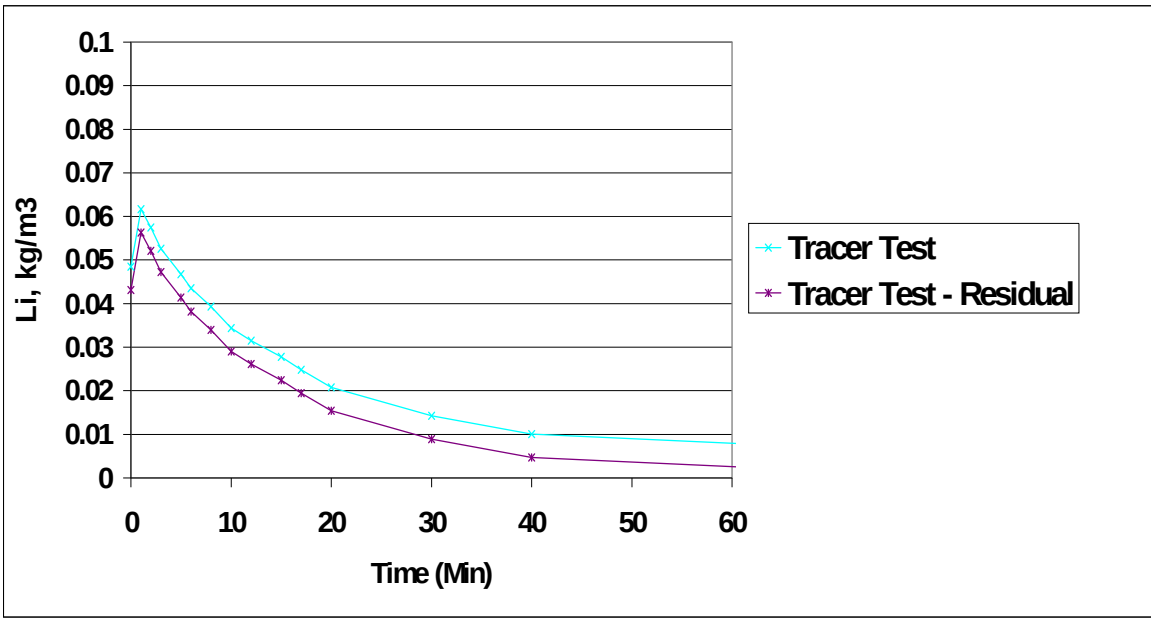

Figure 71: Experimental Results from Tracer Injection into the PN

The water simulation was performed with the same mass flow rates as recorded during actual tracer testing. The results for the simulated tracer test are shown in Figure 72. The residence time is observed to be much lower for the water simulation compared to the actual tracer test residence time. This is due to the water having a much lower specific gravity, as all the flow rates were specified in mass per unit time.

The simulated initial concentrations for the Lithium were much higher than for the experimental, however the experimental lacks the same resolution as the simulation. The trend of a CSTR reactor can clearly be seen by these results, therefore the geometry and mesh had achieved a reasonably convergence with respect to steady state flow.

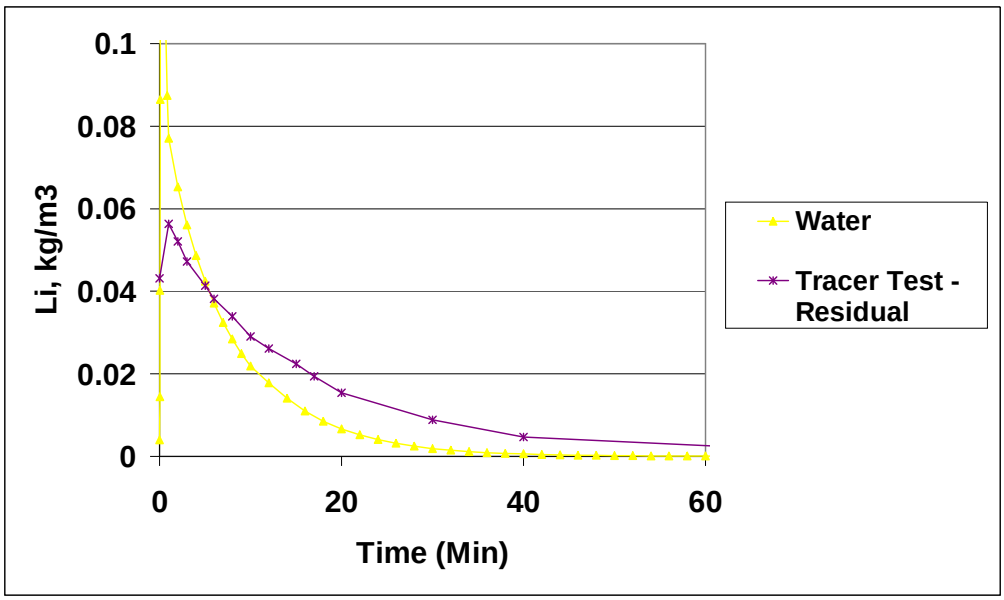

Figure 72: Water Simulation of Tracer Injection Compared To Experimental Results

Tests on the effect of viscosity of the PN slurry were carried out in conjunction with the tracer tests. From this data it was decided to simulate two Newtonian slurries, one at 0.5 Pa.s and the other at 5 Pa.s, as the typical PN slurry viscosity generally lies between these two values. The simulated tracer tests are shown in Figure 73. As with the water-based tests, the initial concentration of lithium in the slurry is higher than the experimental. Also, at around 20-30 minutes, both simulated results dip below the experimental. These combined observations indicate that the volume of the slurry in the PN during the experimental may be greater than the simulated value. An example of this is shown in Figure 74. This graph shows a purely numerical result (calculated in excel), assuming a perfectly stirred mixer. The effect of doubling the vessel size or halving the vessel throughput is clearly seen, with the reduced flowrate compared to unchanged (PN) results showing similar characteristics to the experimental compared

to simulated results. Observation of the simulated Newtonian compared to the experimental results appear to show that the experimental tank volume is about 40% greater than the simulated volume.

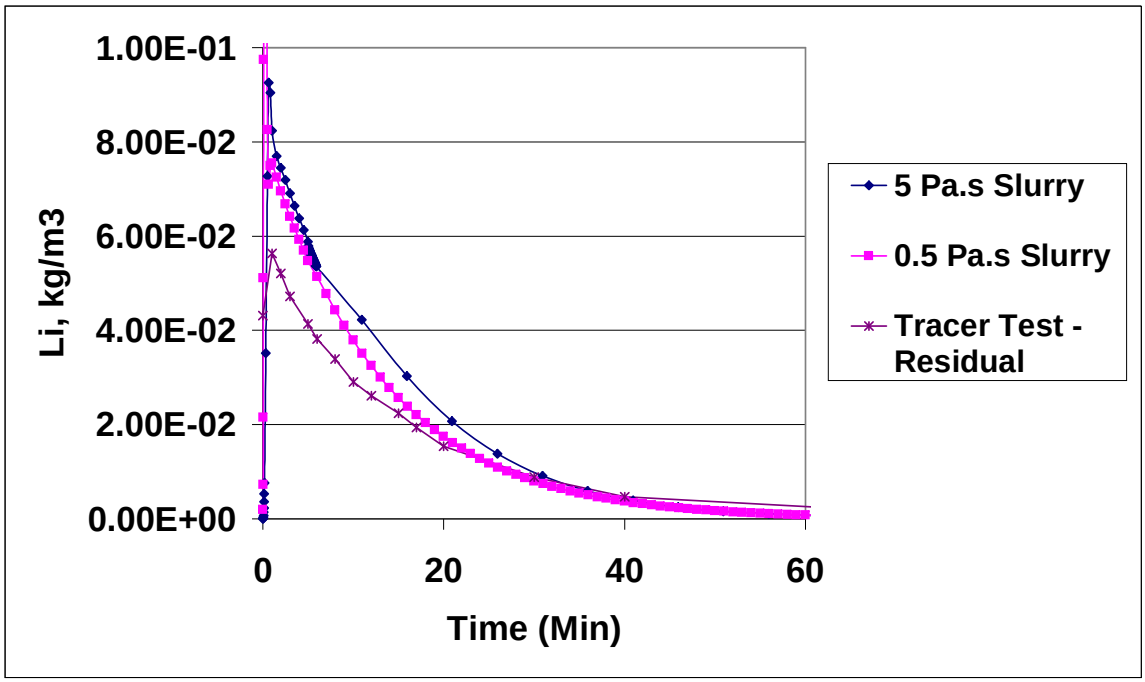

Figure 73: Simulated Newtonian Slurry Tracer Injection Compared To Experimental.

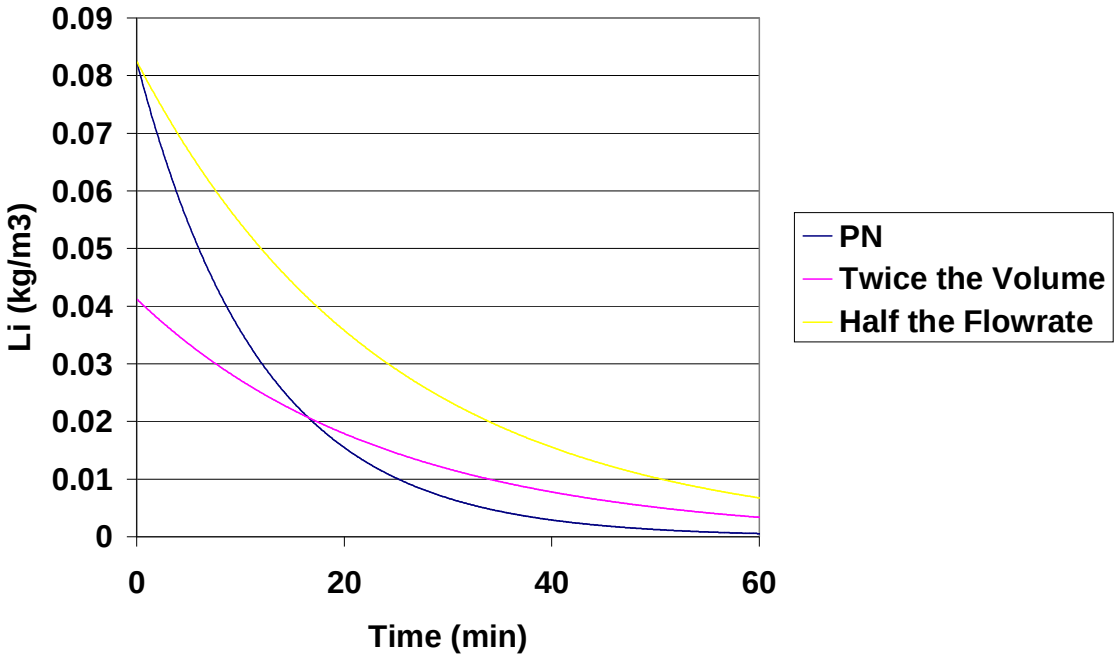

Figure 74: Effect of Changing Volume Size or Flowrate on the Residence Time Distribution for a Perfectly Mixed Vessel.

As there was some conjecture as to the actual height of the slurry in the PN, a second set of values was used to determine the height. The original values placed the height of slurry in the tank at 2m. The alternative values increased this to 3.27m. The RTD of this new model compared to the experimental results is shown in Figure 75. This time it appears that the values given overestimate the height of the slurry in the vessel.

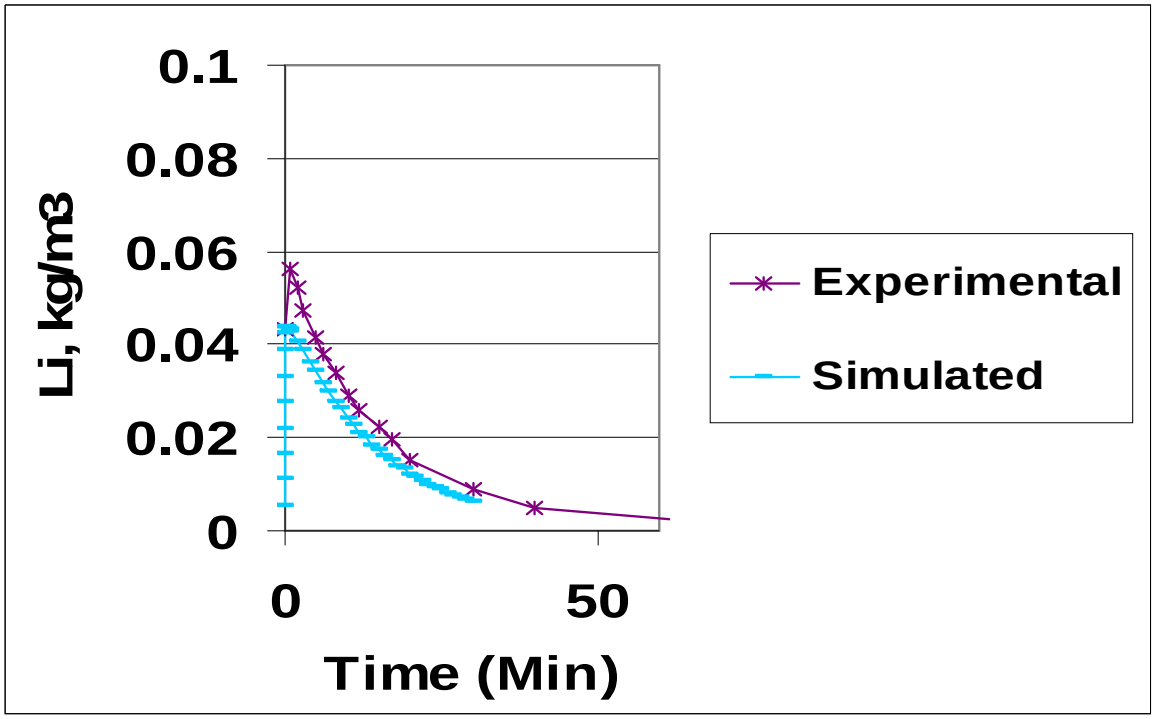

Figure 75: Simulated Results For Alternative Slurry Height Compared To Experimental Results.

Further enquiry to the industry partner was not able to ascertain a confirmed height of the slurry in the reactor. Analysis of our experimental data was presumed to be the most effective way of determining the height. If the reactor is well mixed, the concentration of lithium at the outlet soon after time zero should relate linearly to the volume of slurry in the vessel. By interpolating between the simulated results for the two alternative heights, it has been determined that a height of 2.7m is the likely slurry level for the PN during tracer testing. This height correlates well to an analysis of the peak lithium concentration found during the tracer experiment. If we assume that the maximum reading occurs when there is an equal distribution of Lithium throughout the PN, then this translates into a PN slurry volume of about 28 m^3, which in turn correlates to a slurry height of about 2.7m. This height was used in the final simulations, in lieu of a height being confirmed by the industry partner.

Simulation Results and Discussion

The flow characteristics (velocity field) for the PN vessel simulations are shown in Figure 76. Five separate simulations are shown: (i) the Pre-neutraliser under standard conditions (those at the time of the residence time distribution test); (ii) standard conditions with all flow rates doubled; (iii) standard conditions with increased impeller rotational speed; (iv) standard conditions with lower viscosity slurry; and (v) standard conditions with reversed impeller rotation. Each simulation is represented by a horizontal plane at the level of the impeller blades, and a vertical plane through the centre of the PN vessel and outlet pipe.

The results for the simulation based on conditions at the time of the tracer test (Figure 76(i)) show that the slurry within the PN is propelled down and outwards by the impeller blades. The flow subsequently rises at the walls of the vessel. By the time the flow has recirculated to the top of the PN, the velocity has slowed considerably. Interestingly, the bottom corners of the vessel appear to be remarkably well mixed. There are no obvious stagnation points behind the baffles. The primary concern for 'dead' areas, where the flow of the slurry has stagnated, is in the upper corner of the vessel, where the shape of the vessel is no longer cylindrical. The surface of the vessel was modelled as a solid, rather than free surface, which would have contributed to the stagnation seen in this region. However, the velocity profile clearly shows that the flow field of the fluid begins to separate from the wall of the vessel before reaching the surface.

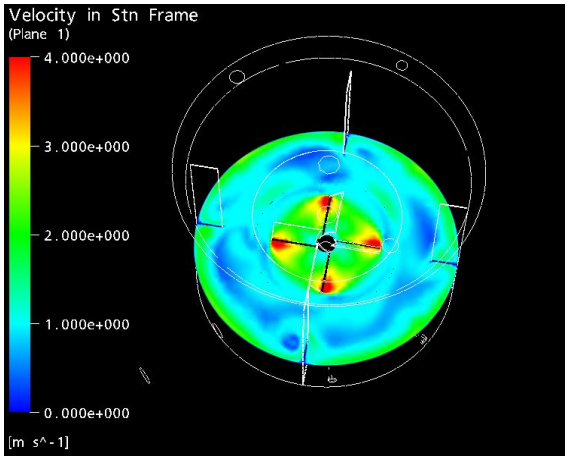

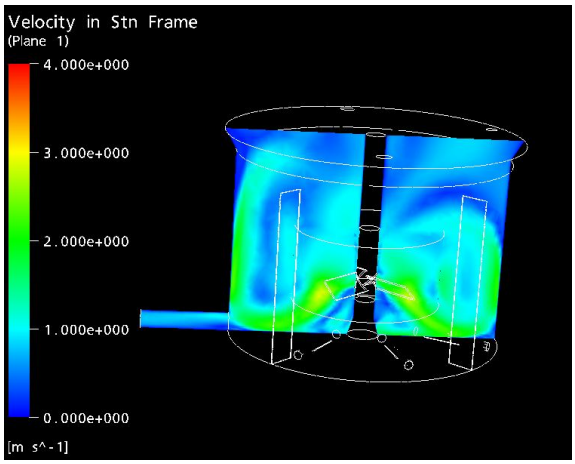

(i) Standard Conditions

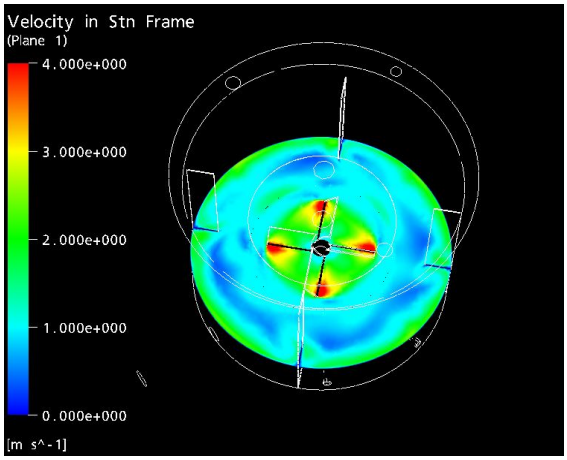

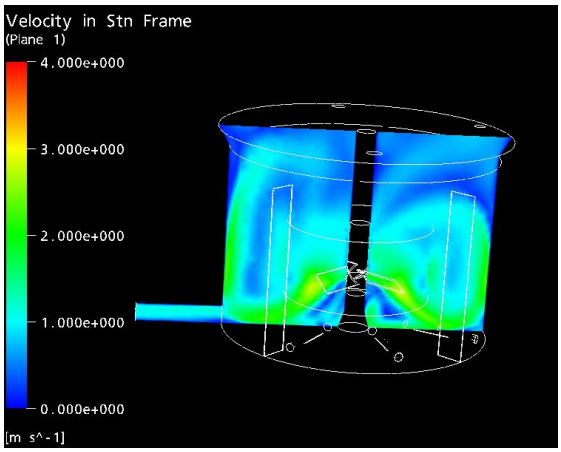

(ii) Double Flow Rates

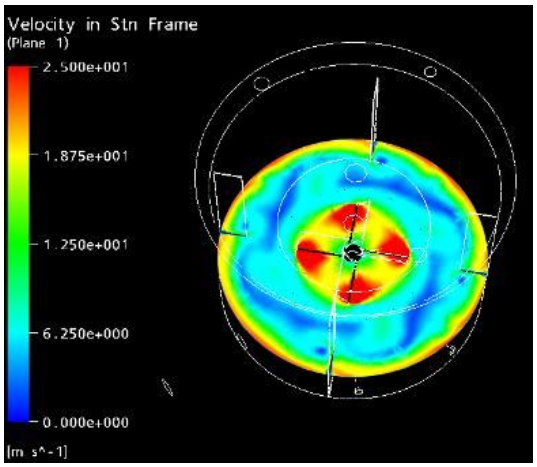

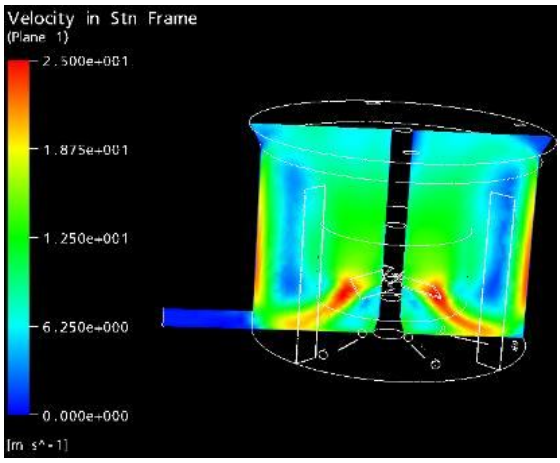

(iii) Increased Agitation Speed

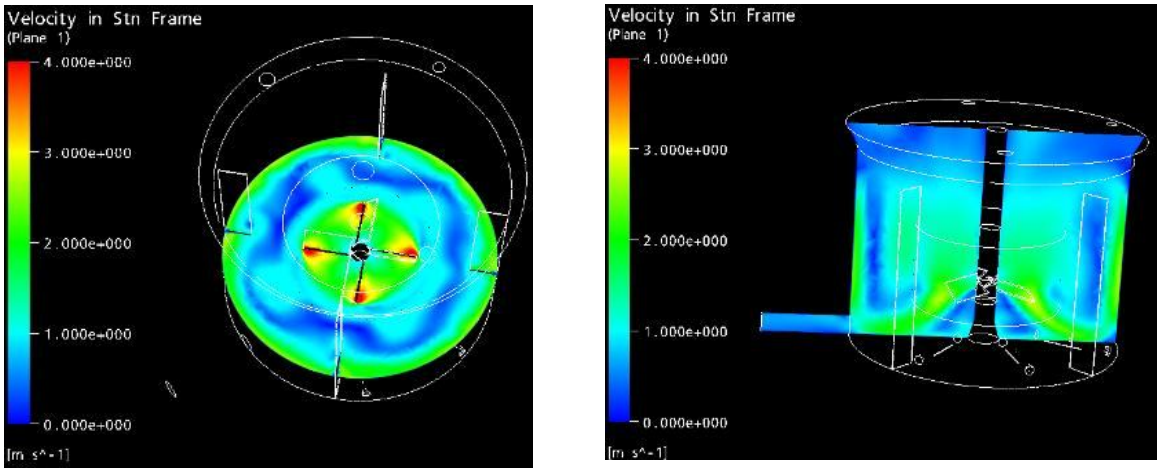

(iv) Low Viscosity Slurry

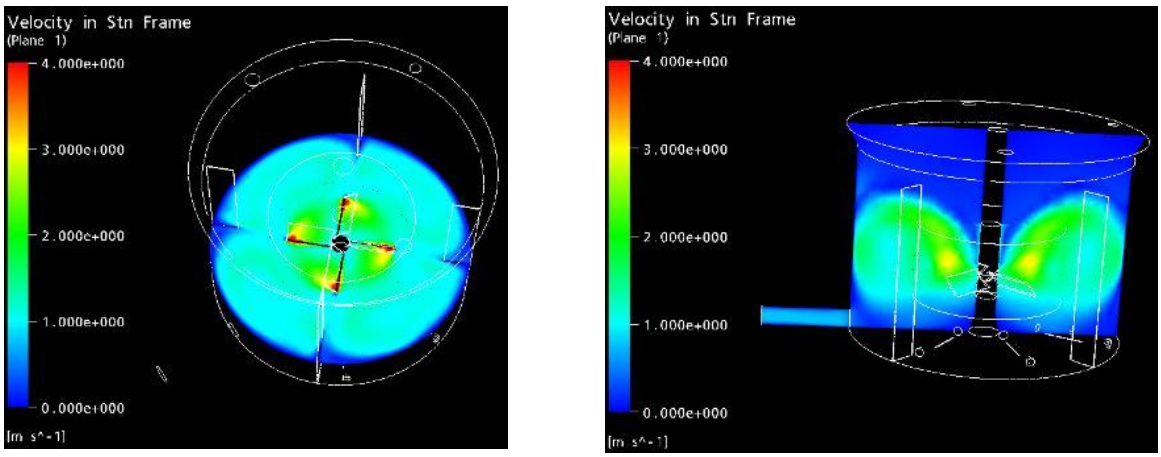

(v) Reversed Impeller Rotation

Figure 76: Simulation Results for Pre-Neutraliser Vessel.

During the laboratory viscosity experiments with slurry, similar situations were found, in that the lower part of the beaker was well mixed, whilst the upper section began to stagnate. This occasionally led to the solidification of slurry at the surface of the beaker. Whilst ambient air in the laboratory experiments would have contributed to the solidification, there is still a concern that the process can occur in the reactor. The simulated slurry level, of 40% (according to DCS display), appears to be close to the maximum level the PN should be subjected to.

The experimental simulation was repeated at double flow rates of all input and output flows, as shown in Figure 76(ii). There is only a minor effect to the flow patterns of the slurry inside the PN, besides the noticeable flow increase through the outlet pipe. This indicates that the volume of slurry in the PN is sufficient enough to handle fluctuations in flow rate without adverse effect on the flow pattern. The rotational speed of the impeller blades and the reactor volume, therefore, govern the flow dynamics of the PN slurry within the reactor.

Figure 76(iii) shows the flow pattern when the impeller rotational speed is increased significantly. The approximate increase in this case is 60-fold. By changing the velocity scale it can be seen that the majority of the slurry is well mixed, with dead-spots only occurring in the upper conical sections of the vessel. The modelling of a solid surface would have been the main cause for these dead spots. The low flow (dark blue) regions a short distance from the wall in the vertical plane, are temporary and are a result of the blade positioning as shown by observing the flow pattern in the horizontal plane. This simulation demonstrates how significant the up-flow of slurry is on the vessel walls, indicating that there is little to no chance of stagnation at this rotational speed. Increasing the impeller speed is therefore likely to result in better mixing characteristics and would be necessary if the volume of slurry in the PN is increased.

Figure 76(iv) shows the flow field of a slurry with a viscosity that is 10% of the slurry viscosity simulated in Figure 76(i). The flow field for the low viscosity slurry is well dispersed compared to the flow field for the standard slurry, which has clear streamlines and fluid flow patterns. The standard slurry is very dependant on the rate

of shear, leading to sharp velocity gradients perpendicular to the flow field. Lower viscosity slurries, therefore, are more effectively dispersed in the PN vessel, reducing the chance of stagnation and blockages.

Finally, the effect of reversing the rotational direction of the impeller blades is shown in Figure 76(v). The results show that major short circuiting of the flow field will occur in this configuration. Stagnation and slurry solidification would almost certainly occur at the surface of the fluid. It is very important to maintain the impeller direction in the current configuration, so that the fluid is drawn downwards in the centre of the vessel and propelled down and outwards along the base and up the walls.

The present design of the PN vessel is effective in mixing the reacting ammonium phosphate slurry. There are no obvious stagnation points in the lower portions of the vessel. The two opportunities for improvement that relate to operational characteristics of the PN are fairly intuitive and include increasing the rotational speed of the impeller and keeping the slurry volume to a level that ensures proper mixing in the upper regions of the tank. The current structural configuration of the tank is acceptable. The principle means of obtaining better mixing dynamics in the PN is to control the slurry viscosity. To achieve this, knowledge of the impurity content of the incoming acid and its most appropriate processing strategy is essential.

Conclusions

Validation of the computational fluid dynamics model of the pre-neutraliser was not able to be achieved due to the absence of industry recorded critical information. However, analysis of the residence time distribution curve and data gathered during the tracer experiments has enabled us to conclude that the model results will be at least indicative of conditions within the reactor.

The model shows that the pre-neutraliser reactor provides excellent mixing dynamics in the lower portion of the vessel. The upper region of the reactor is the least well mixed. The potential for stagnation of the flow field and subsequent slurry

solidification increases when the viscosity of the slurry also increases. To counteract this threat, the volume of slurry within the reactor must be decreased, or the agitation speed increased. Correspondingly, the level may be increased when producing slurries of low viscosity. The most effective method of increasing the mixing dynamics within the pre-neutraliser is to lower the viscosity of the solution. This can best be accomplished by processing each slurry according to how the impurity content is likely to have an effect on the viscosity.

The level of slurry in the pre-neutraliser must be controlled to ensure proper mixing is achieved. The conditions at the time of the tracer experiments (40% slurry level by DCS display) are adequate for processing most slurries, though this level should not be exceeded. Ideally, the slurry level should be kept as low as practicably possible. Additionally, the level sensor on the PN reactor should be recalibrated to obtain more reliable process data.

APPENDIX II – VISCOSITY GRAPHS

Viscosity vs. Shear Rate Graphs

Interpretation:

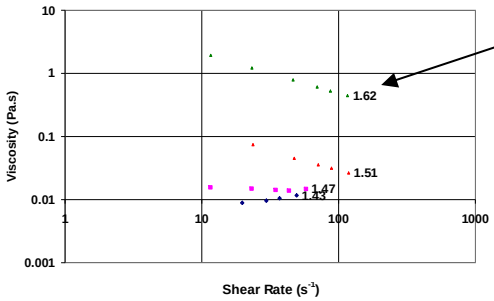

Specific gravity of test

2% Fe_2O_3 0.74MR

Plant acid used (DAP#) or amount and type of impurity added for laboratory grade acids.

Mole ratio of experiment

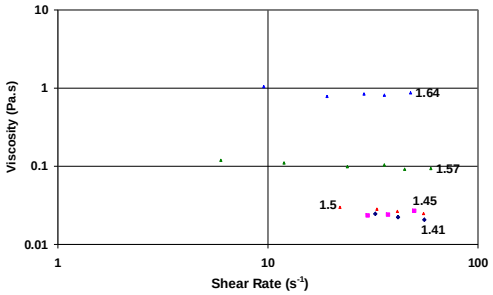

DAP1 0.8MR

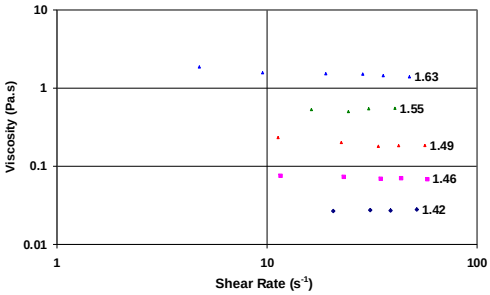

DAP1 1.2MR

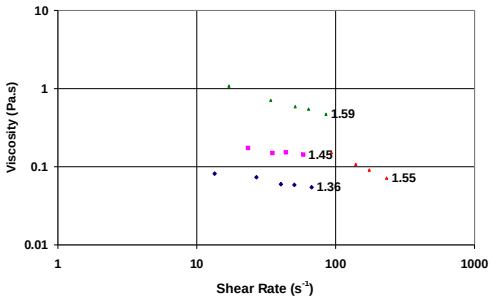

DAP1 0.9MR

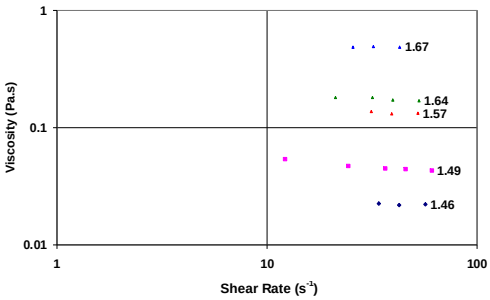

DAP1 1.2MR

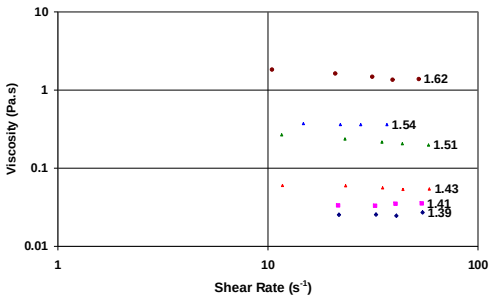

DAP1 1MR

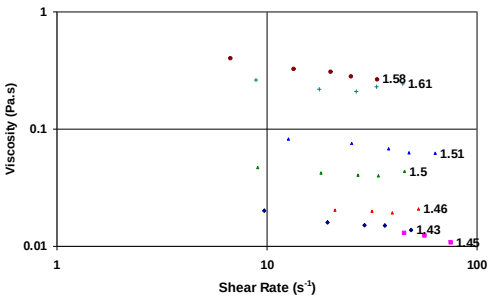

DAP1 1.3MR

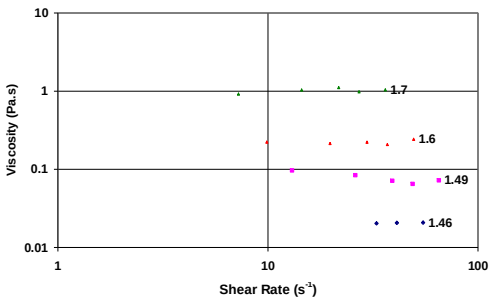

DAP1 1.1MR

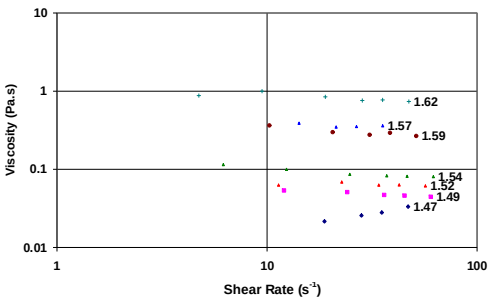

DAP1 1.3MR

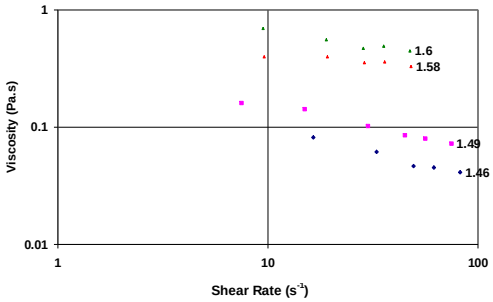

DAP1 1.4MR

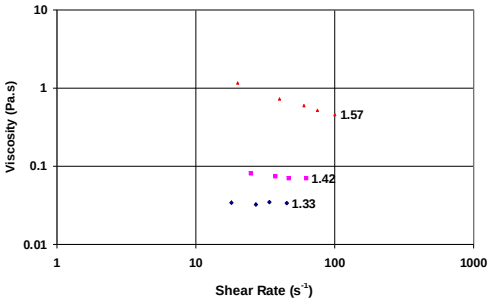

DAP1 0.9MR

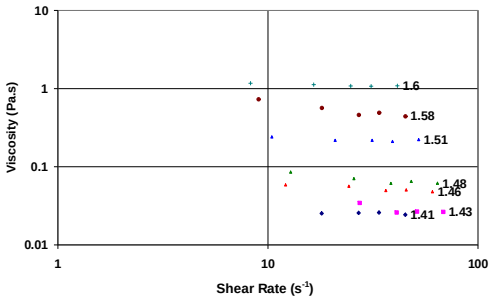

DAP1 1.5MR

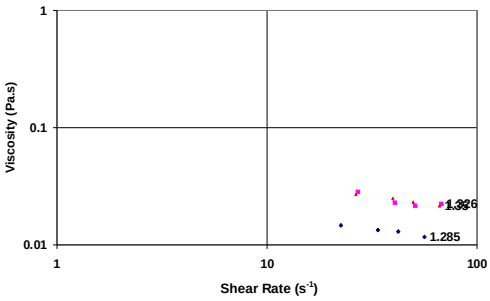

DAP1 1.6MR

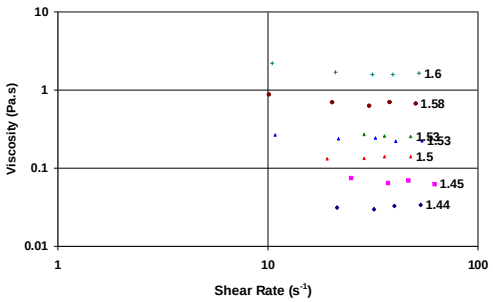

DAP1 1.6MR

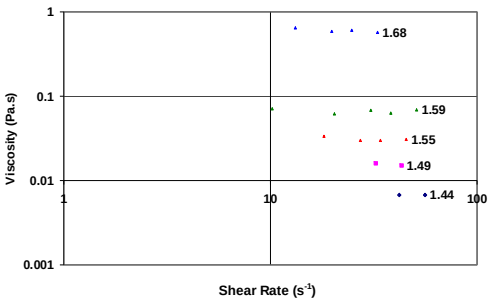

DAP2 0.7MR

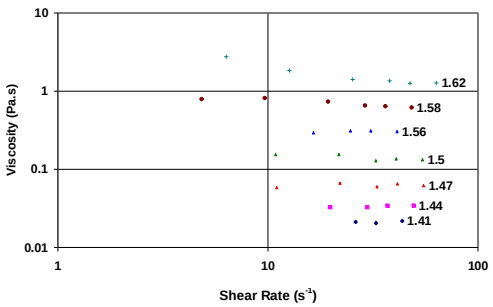

DAP1 1.7MR

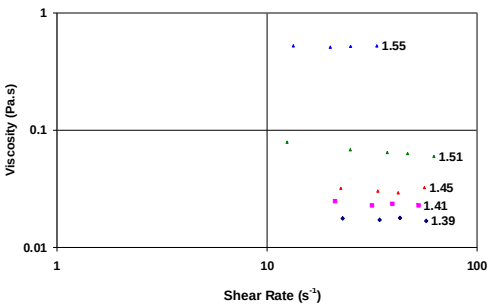

DAP2 0.8MR

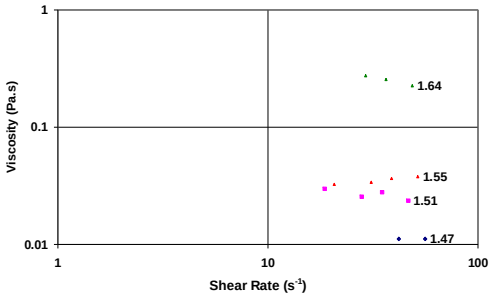

DAP2 0.9MR

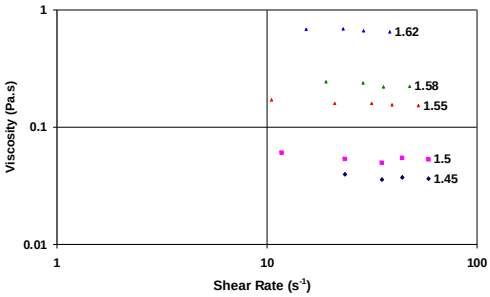

DAP2 1.2MR

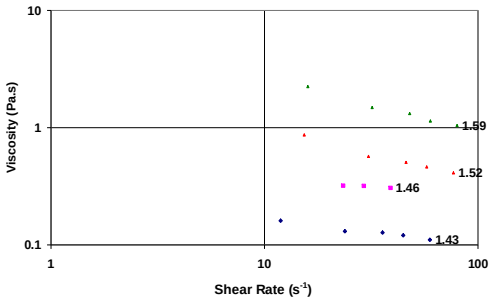

DAP2 0.9MR

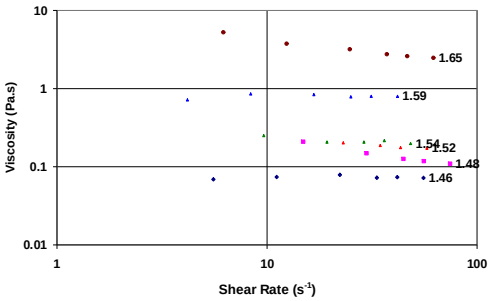

DAP2 1.3MR

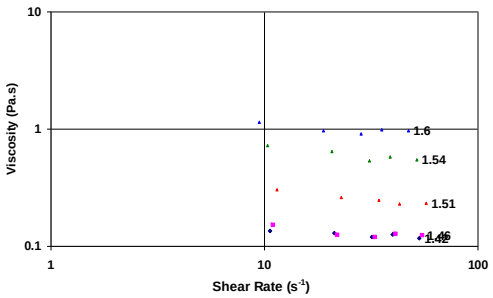

DAP2 1MR

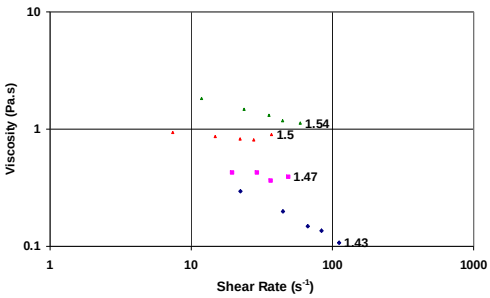

DAP2 1.4MR

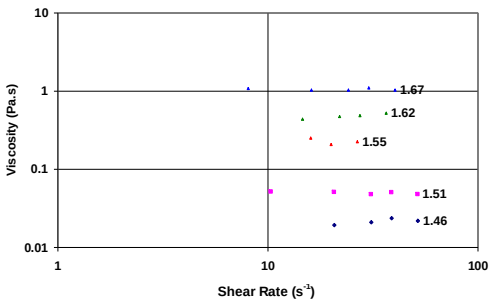

DAP2 1.1MR

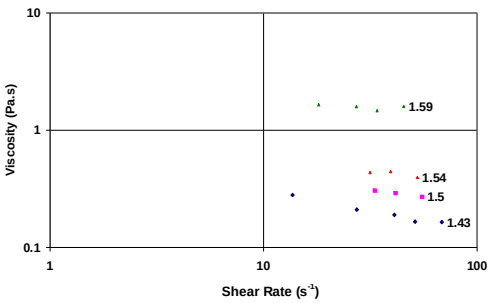

DAP2 1.4MR

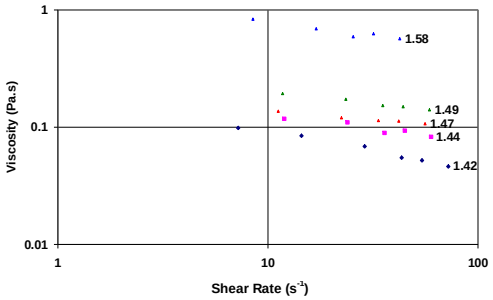

DAP2 1.5MR

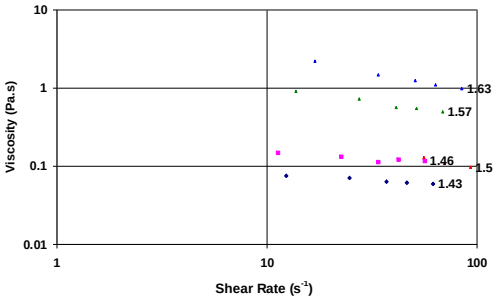

DAP3 0.8MR

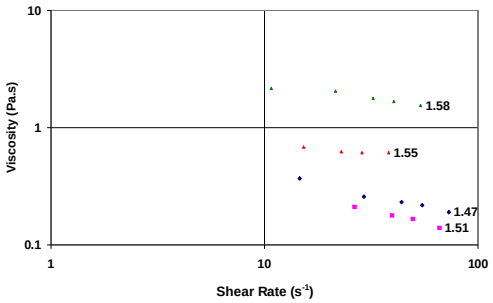

DAP2 1.6MR

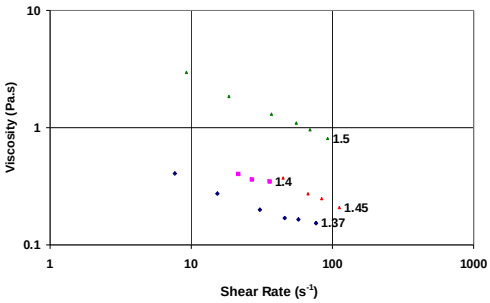

DAP3 0.9MR

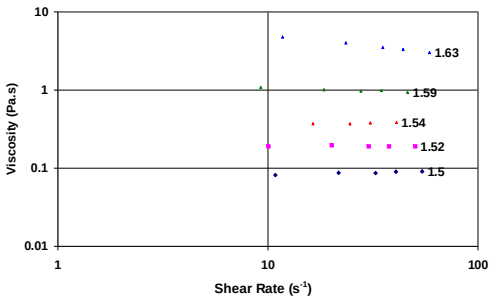

DAP2 1.7MR

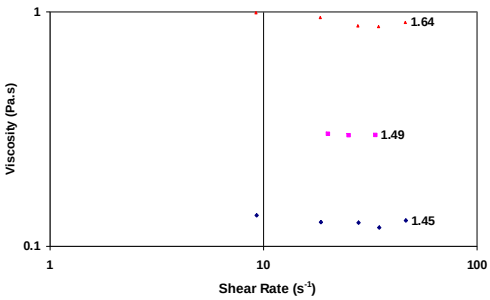

DAP3 1MR

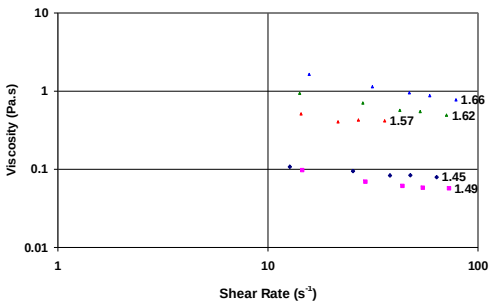

DAP3 0.7MR

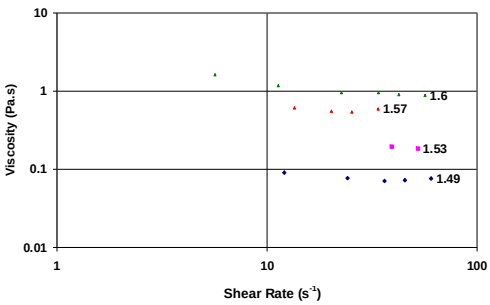

DAP3 1.1MR

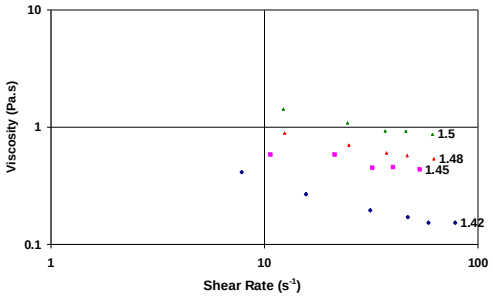

DAP3 1.2MR

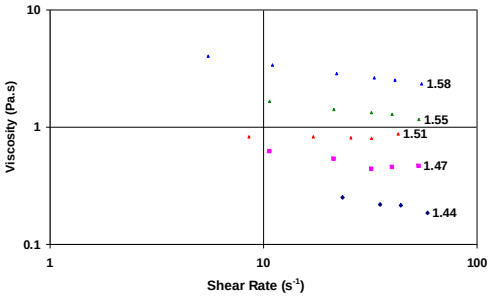

DAP3 1.5MR

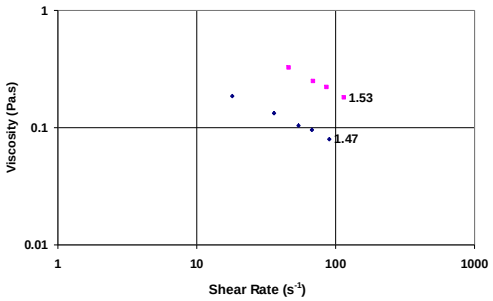

DAP3 1.2MR

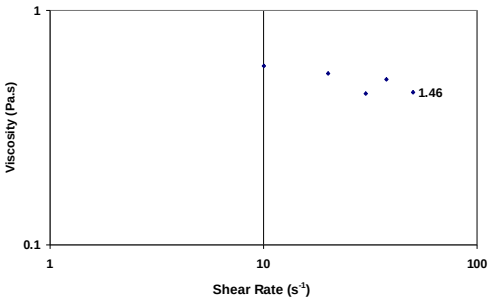

DAP3 1.6MR

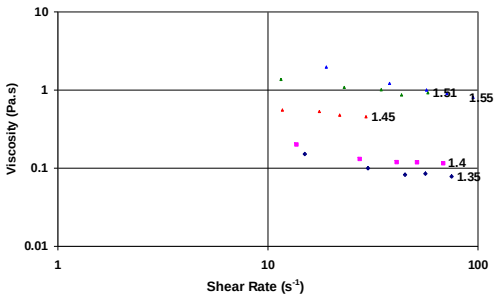

DAP3 1.3MR

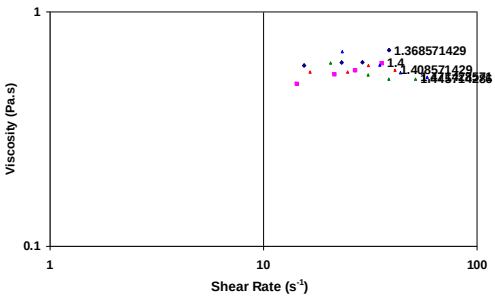

DAP5 0.9MR

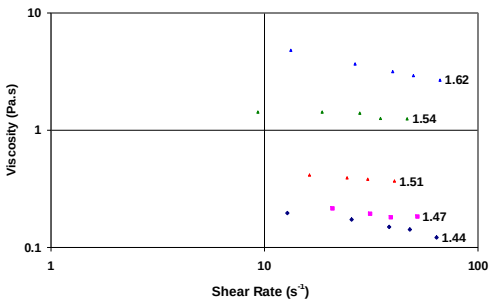

DAP3 1.4MR

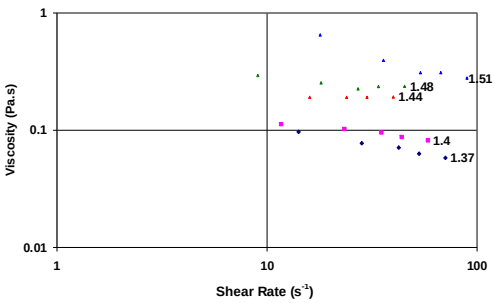

DAP5 0.7MR

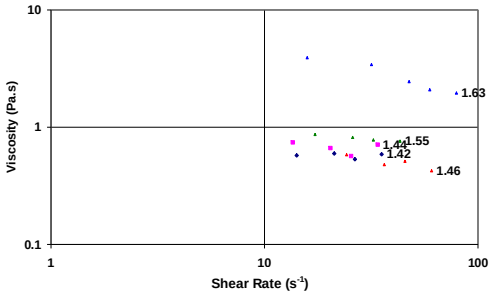

DAP5 0.8MR

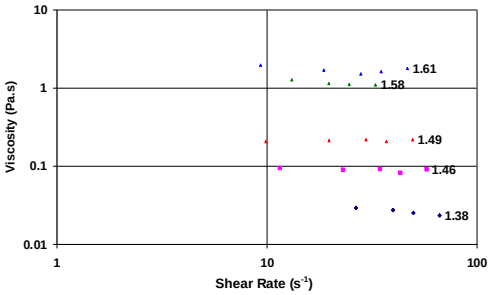

DAP5 1.3MR

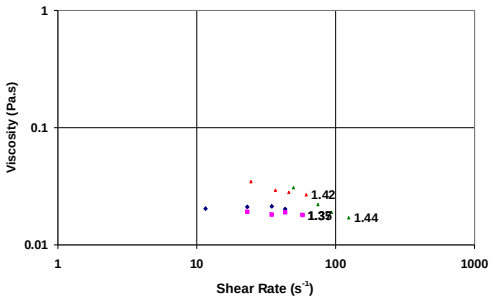

DAP5 1MR

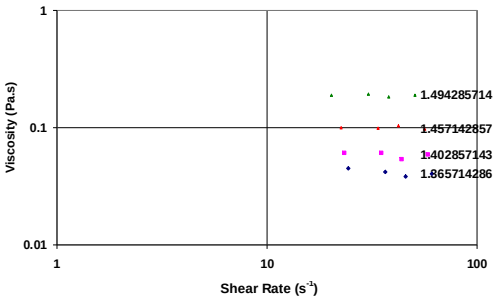

DAP5 1.4MR

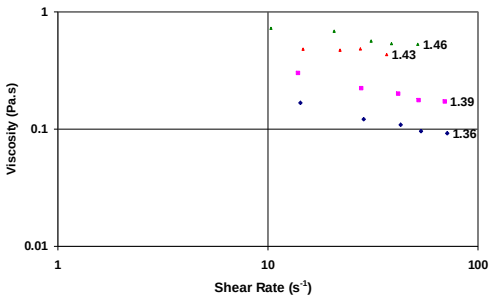

DAP5 1.1MR

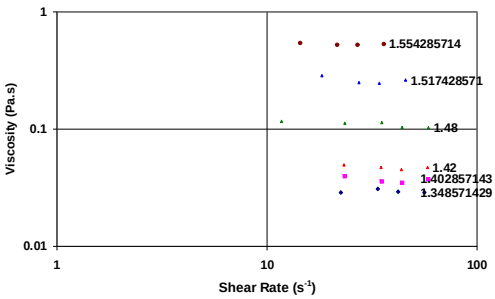

DAP5 1.5MR

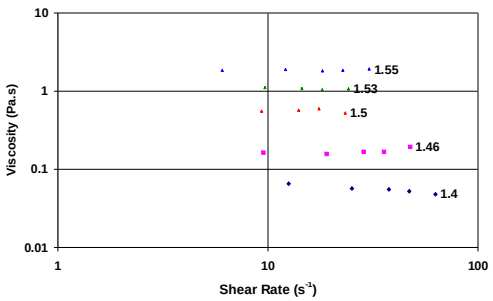

DAP5 1.2MR

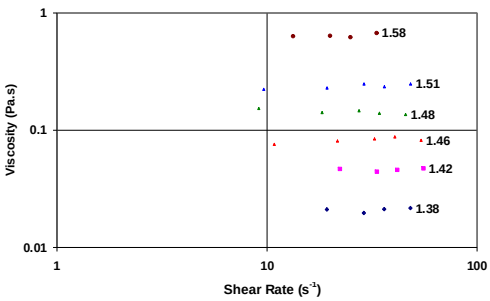

DAP5 1.6MR

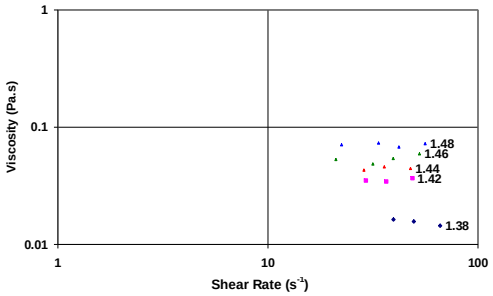

DAP5 1.7MR

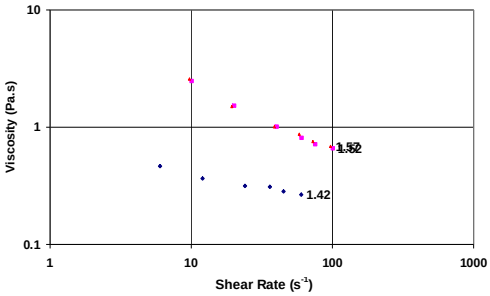

DAP7 1.11MR

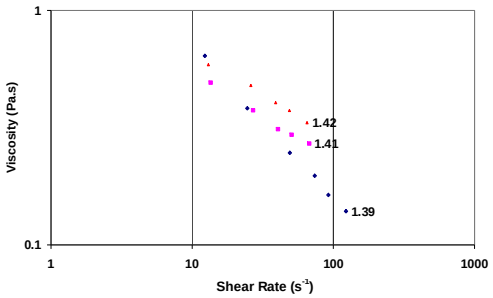

DAP7 0.8MR

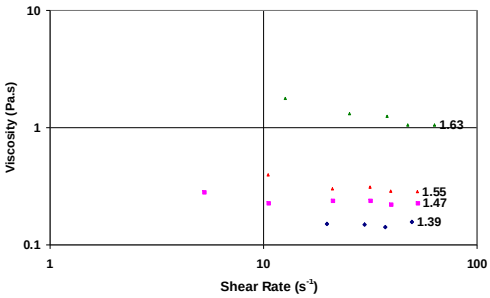

DAP7 1.35MR

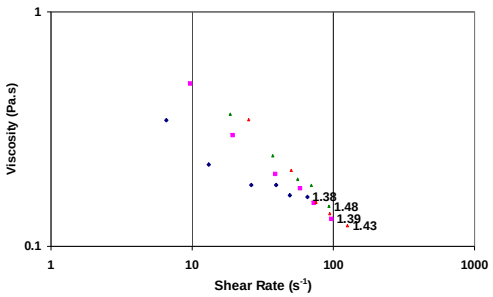

DAP7 0.95MR

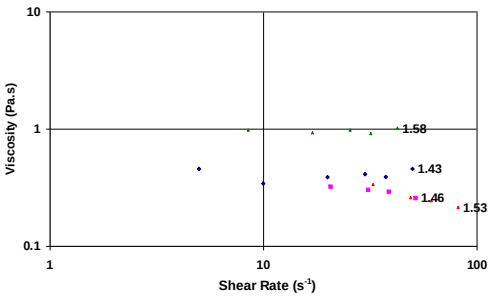

DAP7 1.56MR

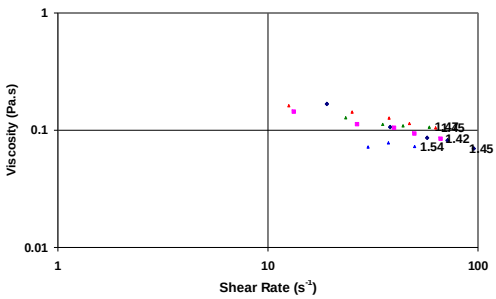

DAP7 1.05MR

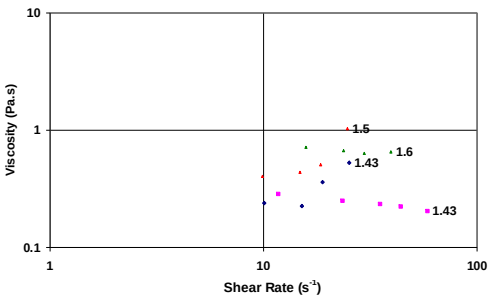

DAP7 1.4MR

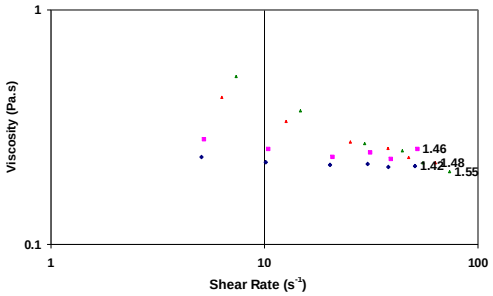

DAP7 1.44MR

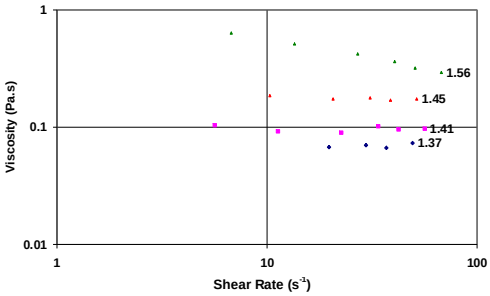

DAP8 1.12MR

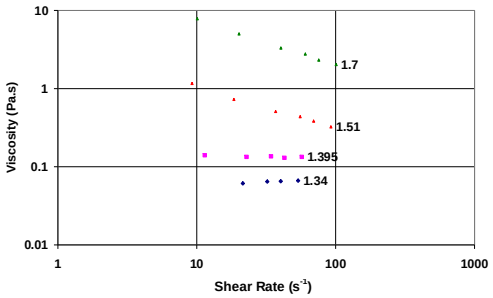

DAP8 0.75MR

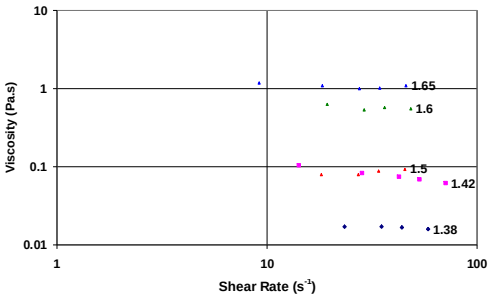

DAP8 1.22MR

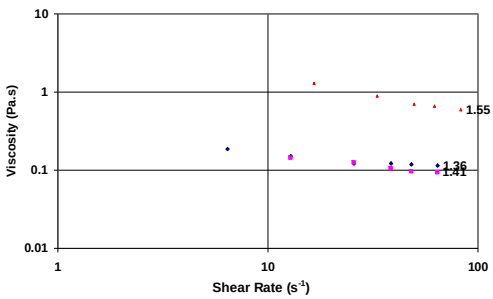

DAP8 0.89MR

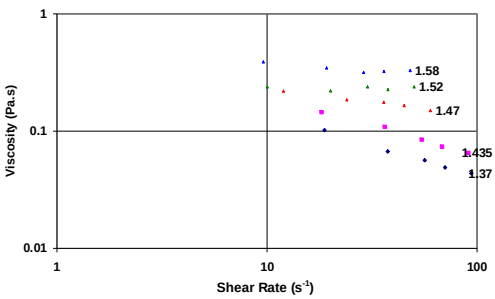

DAP8 1.32MR

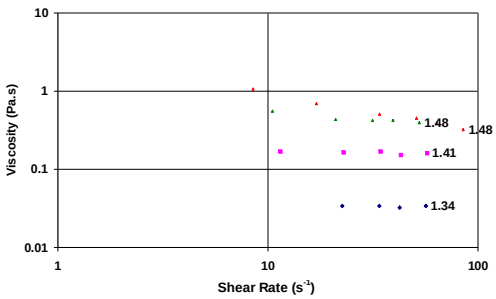

DAP8 1.02MR

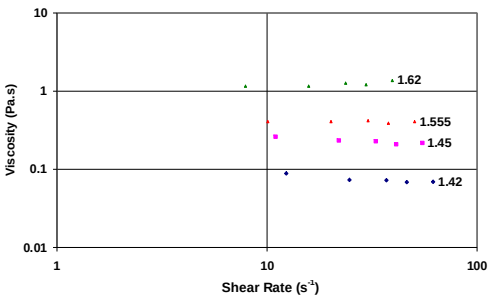

DAP8 1.43MR

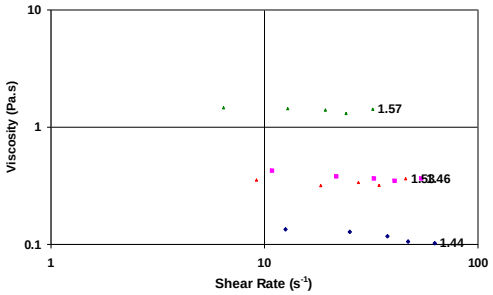

DAP8 1.55MR

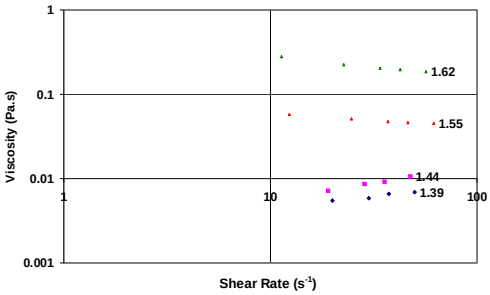

2% $Fe_2O_3$0.99MR

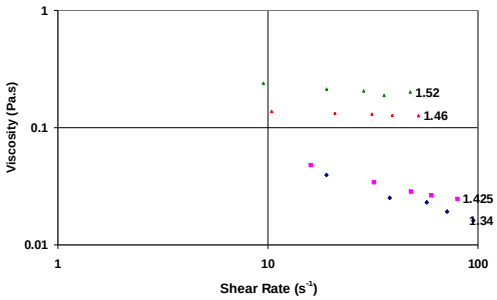

DAP8 1.62MR

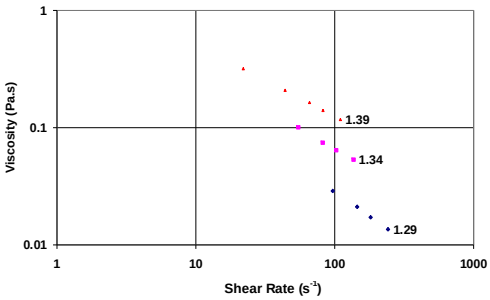

2% Fe_2O_3 1.13MR

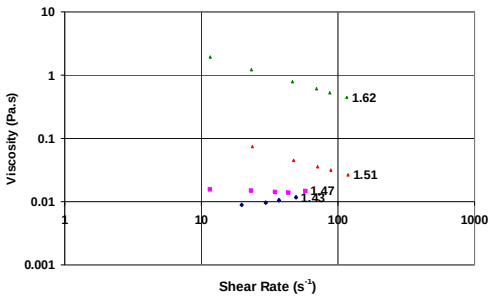

2% Fe_2O_3 0.74MR

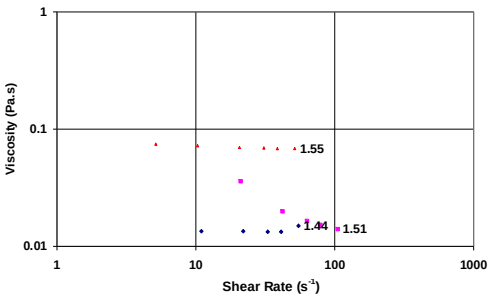

2% Fe_2O_3 1.3MR

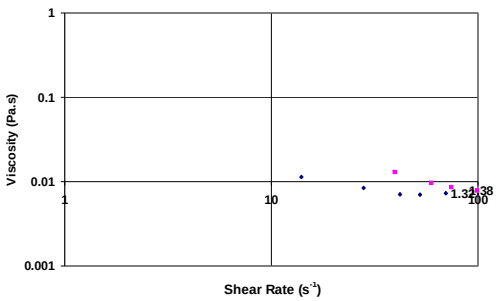

2% Fe_2O_3 0.92MR

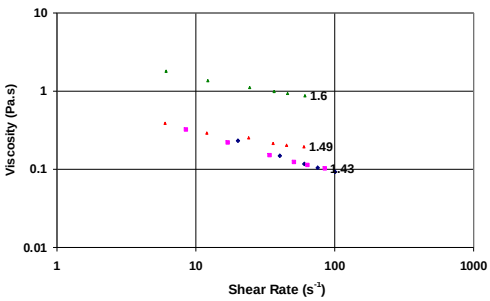

2% Fe_2O_3 1.48MR

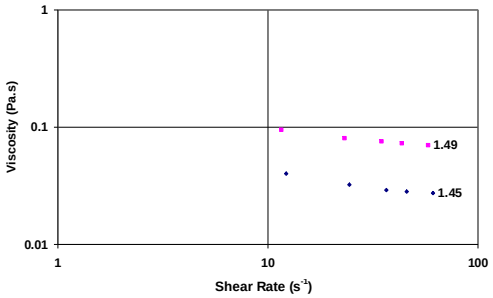

2% Fe_2O_3 1.58MR

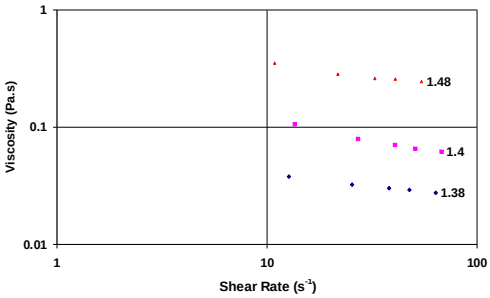

2% Al_2O_3 1.35MR

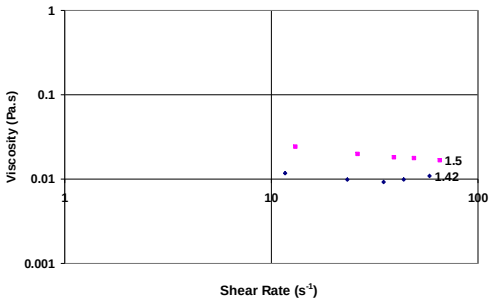

2% Al_2O_3 0.94MR

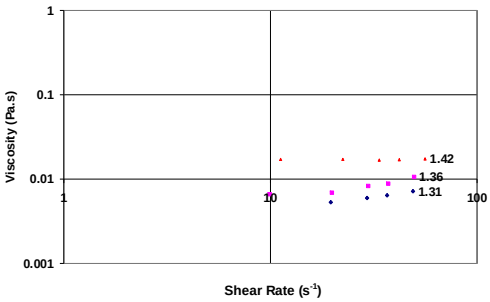

2% Al_2O_3 1.5MR

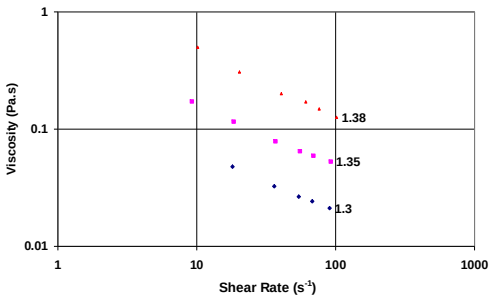

2% Al_2O_3 1.03MR

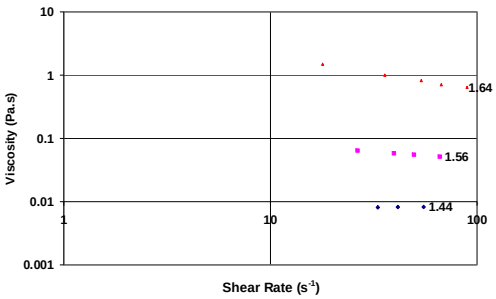

3% Al_2O_3 1.26MR

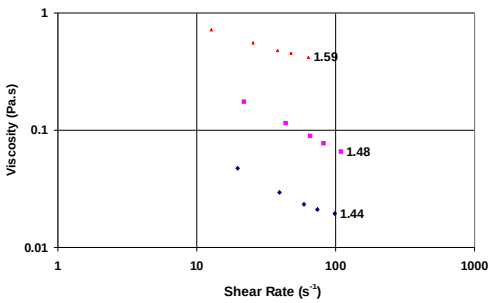

2% Al_2O_3 1.22MR

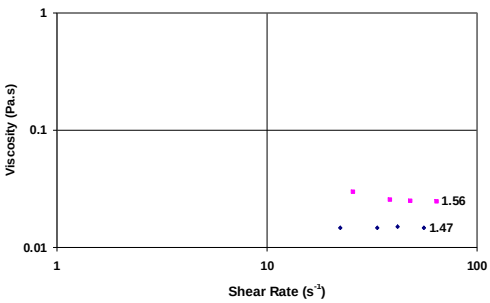

3% MgO 1.12MR

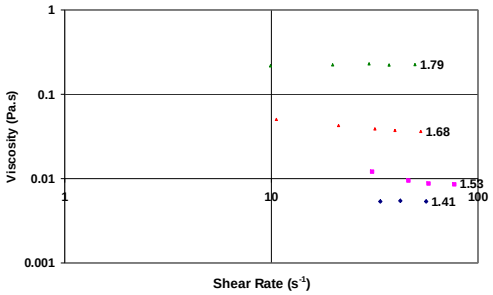

3% MgO 0.81MR

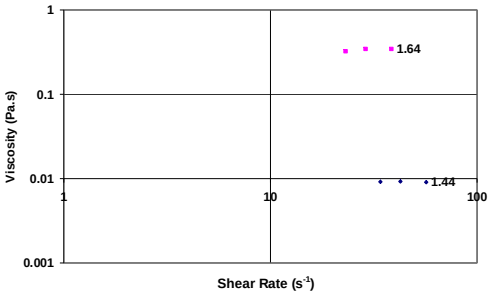

3% MgO 1.36MR

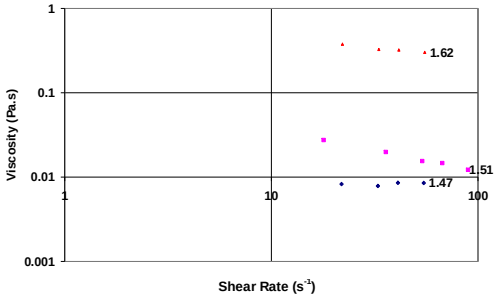

3% MgO 1.5MR

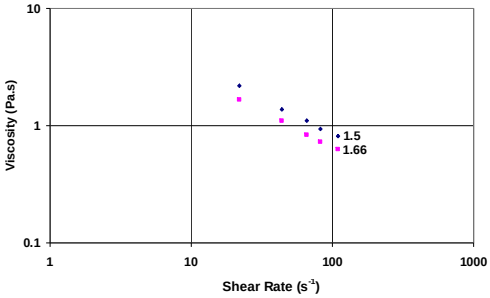

3% Fe_2O_3 1.63MR

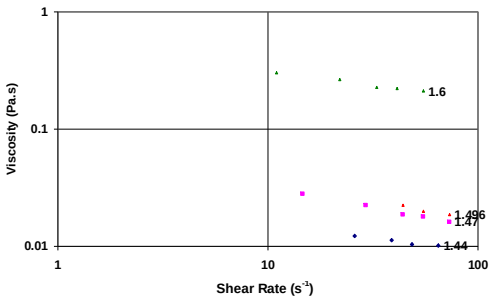

3% MgO 1.81MR

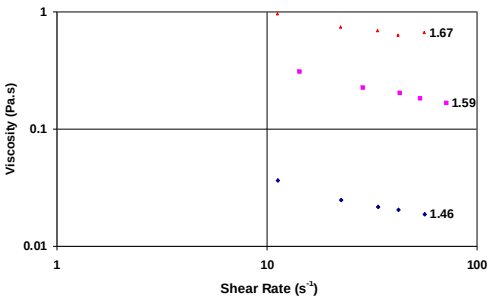

3% Fe_2O_3 0.91MR

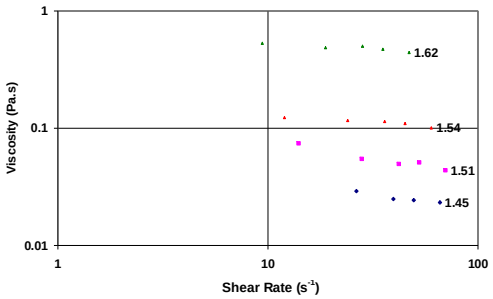

3% MgO 1.6MR

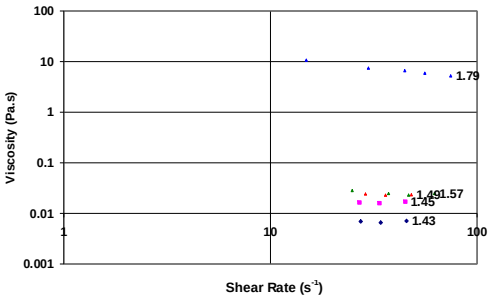

3% Fe_2O_3 0.78MR

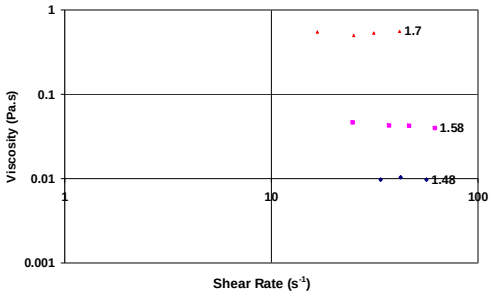

3% Fe_2O_3 1.2MR

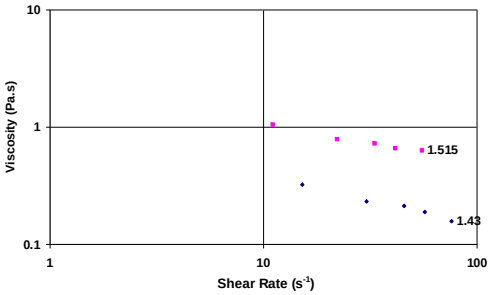

3% Fe_2O_3 1.5MR

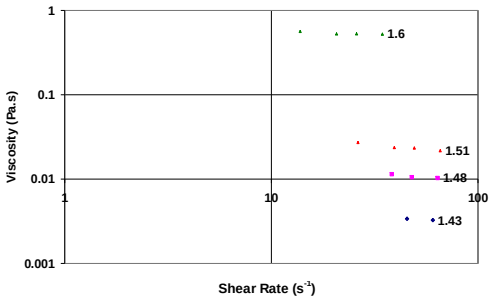

3% Fe_2O_3 1.04MR

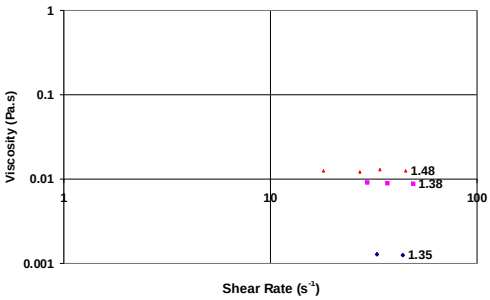

3% Fe_2O_3 1.34MR

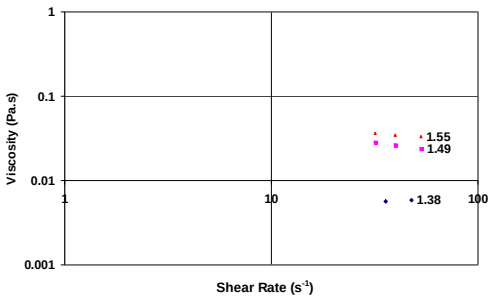

3% Fe_2O_3 1.38MR

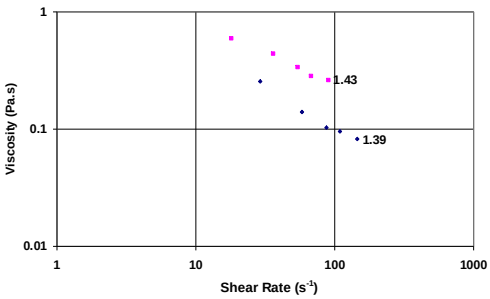

3% Fe_2O_3 1.51MR

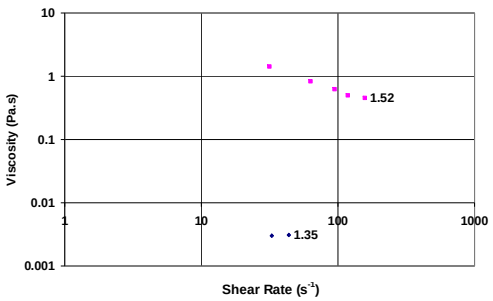

3% Fe_2O_3 0.77MR

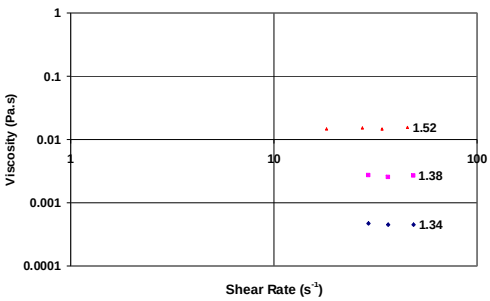

3% Fe_2O_3 0.9MR

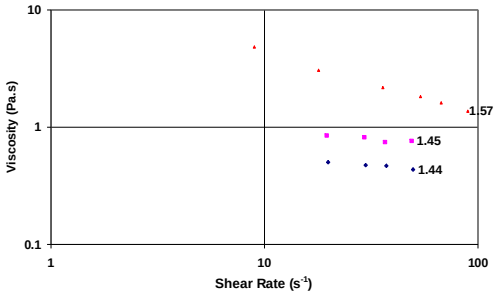

3% Al_2O_3 1.17MR

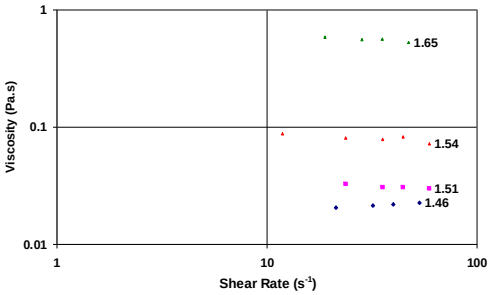

3% Al_2O_3 1.43MR

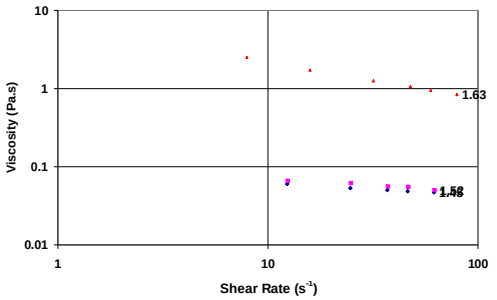

3% Al_2O_3 0.8MR

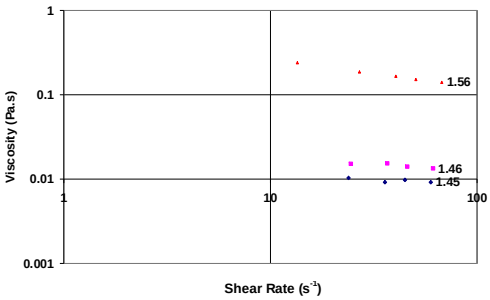

3% Al_2O_3 0.98MR

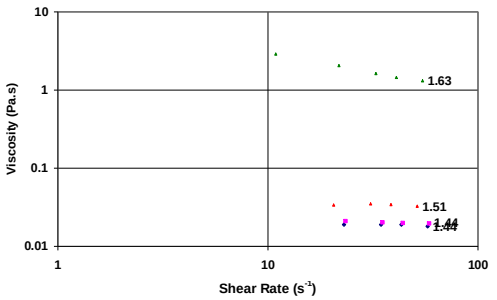

3% Al_2O_3 1.74MR

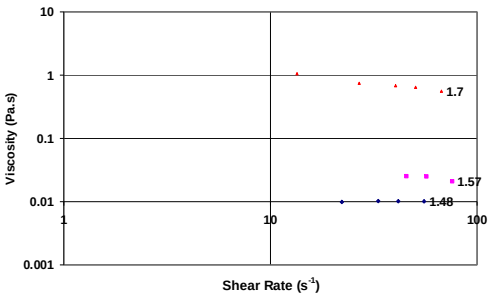

3% Al_2O_3 1.27MR

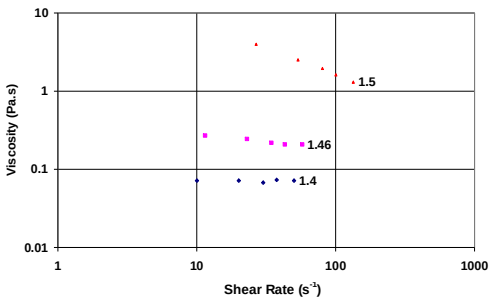

3% Al_2O_3 0.85MR

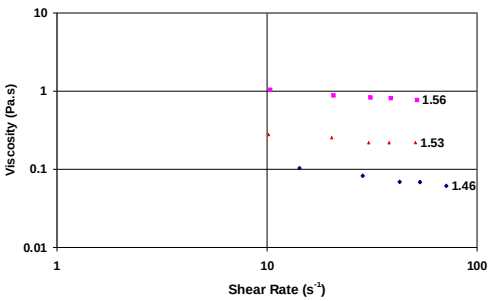

3% Al_2O_3 1.5MR

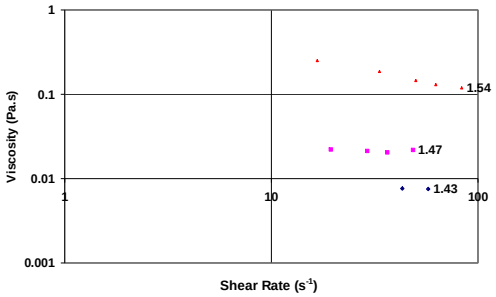

3% Al_2O_3 0.96MR